

UNCLASSIFIED

AD 268 378

*Reproduced
by the*

**ARMED SERVICES TECHNICAL INFORMATION AGENCY
ARLINGTON HALL STATION
ARLINGTON 12, VIRGINIA**



UNCLASSIFIED

NOTICE: When government or other drawings, specifications or other data are used for any purpose other than in connection with a definitely related government procurement operation, the U. S. Government thereby incurs no responsibility, nor any obligation whatsoever; and the fact that the Government may have formulated, furnished, or in any way supplied the said drawings, specifications, or other data is not to be regarded by implication or otherwise as in any manner licensing the holder or any other person or corporation, or conveying any rights or permission to manufacture, use or sell any patented invention that may in any way be related thereto.

CATALOGED BY ASTIA
AS AD NO. 268 378
268378

62-1-5-
XEROX

AN INVESTIGATION OF TWO METHODS OF ARRESTMENT OF HIGH-SPEED AIRCRAFT

DONALD F. HAUSKNECHT
RAMOJUS P. VAITYS

AMERICAN MACHINE & FOUNDRY COMPANY
MECHANICS RESEARCH DIVISION
NILES, ILLINOIS

SEPTEMBER 1961

100-1-5-
XEROX
E

AERONAUTICAL SYSTEMS DIVISION

NOTICES

When Government drawings, specifications, or other data are used for any purpose other than in connection with a definitely related Government procurement operation, the United States Government thereby incurs no responsibility nor any obligation whatsoever; and the fact that the Government may have formulated, furnished, or in any way supplied the said drawings, specifications, or other data, is not to be regarded by implication or otherwise as in any manner licensing the holder or any other person or corporation, or conveying any rights or permission to manufacture, use, or sell any patented invention that may in any way be related thereto.

Qualified requesters may obtain copies of this report from the Armed Services Technical Information Agency, (ASTIA), Arlington Hall Station, Arlington 12, Virginia.

This report has been released to the Office of Technical Services, U. S. Department of Commerce, Washington 25, D. C., for sale to the general public.

Copies of ASD Technical Reports and Technical Notes should not be returned to the Aeronautical Systems Division unless return is required by security considerations, contractual obligations, or notice on a specific document.

AN INVESTIGATION OF TWO METHODS OF ARRESTMENT OF HIGH-SPEED AIRCRAFT

*DONALD F. HAUSKNECHT
RAMOJUS P. VAITYS*

*AMERICAN MACHINE & FOUNDRY COMPANY
MECHANICS RESEARCH DIVISION*

SEPTEMBER 1961

**DIRECTORATE OF AEROSPACE GROUND EQUIPMENT ENGINEERING
CONTRACT No. AF 33(616)-7152
PROJECT No. MR 1135-90**

**AERONAUTICAL SYSTEMS DIVISION
AIR FORCE SYSTEMS COMMAND
UNITED STATES AIR FORCE
WRIGHT-PATTERSON AIR FORCE BASE, OHIO**

FOREWORD

This Technical Note is the second and final of two Technical Notes submitted in accordance with Air Force Contract No. AF 33(616)-7152, under which the work was performed by the American Machine & Foundry Company, Mechanics Research Division, Niles, Illinois. The first Technical Note which was submitted under this contract is entitled "An Analysis of the Materials and Constructions of Tension Members for Use in Aircraft Arrestment Equipment."

Acknowledgement is made to Dale H. Duel who did much of the analysis and computation. Recognition is also due Norman F. Eslinger, Michael F. Darienzo, and Richard Kessler of the Mechanics Research Division and V. Vary and A. Barbato of Aeronautical Systems Division for their helpful comments, suggestions, and guidance.

PREPARED BY:

Donald F. Hausknecht
Donald F. Hausknecht

Ramojus P. Vaitys
Ramojus P. Vaitys

REVIEWED BY:

Glen L. Neidhardt
Glen L. Neidhardt, Group Leader
Engineering Mathematics Group

APPROVED BY:

D. L. Arenson
D. L. Arenson, Assistant General Manager
Mechanics Research Division

ABSTRACT

Two methods of aircraft arrestment are investigated to determine their suitability for aircraft landing speeds far above the capabilities of present arresting systems.

One method is preacceleration of components of a present arresting system in order to reduce the relative impact velocity between the aircraft and the preaccelerated components. Energy requirements and tolerances affecting timing of the preacceleration are investigated and illustrated with numerical examples.

The other method is the use of an energy-absorbing material in the cable of an arresting system in order to obviate a separate arresting engine. Basic formulas for interactions of waves in a yielding cable are developed. The formulas are applied in numerical examples for specific arrangements of the cable.

Results indicate that both methods offer sufficient promise of success to be worthy of development.

PUBLICATION REVIEW

This report has been reviewed and is approved.

FOR THE COMMANDER



VERYL V. VARY
Asst Chief, Base Equipment Division
Directorate of Aerospace Ground Eqp Engr
Deputy for Engineering

TABLE OF CONTENTS

<u>SECTION</u>	<u>Page</u>
1 INTRODUCTION, PURPOSE AND SCOPE	1
2 PREACCELERATION TECHNIQUES	3
2.1 Purpose and Primary Requirements	3
2.2 General Methods of Solution	4
2.2.1 Adaptation of Method I to Different Energy Absorbers ..	5
2.2.2 Adaptation of Method II to Different Energy Absorbers .	7
2.3 Conclusion	10
Notation for Section 3	11
3 ANALYSIS OF DETECTION AND TIMING PROBLEM	13
3.1 Purpose and Scope	13
3.2 Problem Defined	16
3.3 Extent and Limitations	16
3.4 System Analyzed	18
3.5 Mathematical Analysis of the Timing Problem	19
3.5.1 Equations of Motion	20
3.5.1.1 General Discussion	20
3.5.1.2 Particular Example	26
3.6 Tolerance Requirements	33
3.6.1 Motivation for the Tolerance Problem	33
3.6.2 Problem Defined	33
3.6.3 Effect of an Error in τ	33
3.6.3.1 Conditions for Interception	35
3.6.3.2 Range of L and Location of Aim Point	37
3.6.3.3 Meaning of L and Aim Point	37
3.6.4 Method of Approach to Solution	37
3.6.5 Evaluation of the Actual Timing Error $\Delta\tau$	40
3.6.6 Formula for Evaluation of Tolerances	42

TABLE OF CONTENTS (Continued)

3.6.7	Particular Example.	43
3.7	Discussion of the Side Drift Tolerance	46
3.8	Summary of Procedure Followed in Obtaining the Computed Results. . .	46
3.9	Modification of the Computational Procedure.	47
3.10	Explanation of the Curves.	48
3.11	Conclusion	49
	Notation for Section 4.	64
4	USE OF ENERGY-ABSORBING MATERIALS	66
4.1	Wave Interactions in the Plastic Region.	68
4.1.1	Propagation of Singularities.	69
4.1.2.1	Transverse Impact (Kink Lags Wave Front)	74
4.1.2.2	Transverse Impact (Kink Travels with Wave Front) . . .	77
4.1.3.1	Kink Impact Against Sheave (Reflected Kink Lags Wave Front).	80
4.1.3.2	Kink Impact Against Sheave (Reflected Kink with Wave Front).	84
4.1.3.3	Kink Impact Against Sheave (Original Kink with Wave Front).	86
4.1.4	Kink Impact Against Sheave with Disengagement	90
4.1.5	Meeting of Kink and Tension Loading Wave.	92
4.1.6	Kink Overtaken by Tension Jump.	97
4.1.7.1	Cable End Catapulted with Simultaneous Arrival of Kink and Tension Wave (Reflected Kink Travels with Wave Front).	99
4.1.7.2	Cable End Catapulted with Simultaneous Arrival of Kink and Tension Wave (Resultant Unloading Wave) . . .	102
4.1.8	Interaction of Two Kinks and Two Waves.	104
4.1.9	Plastic Loading Wave Overtaken by Unloading Wave.	108
4.2	Practicability of Specific Aircraft-Arresting Concepts	111
4.2.1	Case I: Energy-Absorbing Cable with Fixed Ends	111
4.2.2	Case II: Energy-Absorbing Rope Using a Series of Sheaves . .	120
4.2.3	Case III: Energy-Absorbing Cable in Water Trough.	124
4.3	Conclusion	130
	REFERENCES.	131

LIST OF ILLUSTRATIONS

<u>Figure No.</u>		<u>Page</u>
1	Coordinate System and Initial Position	17
2	Aircraft and Deck Pendant Trajectories Before Interception (Vertical Scale Exaggerated)	21
3	Time Vs. Position Plots of the Deck Pendant Alone (Effect of Aircraft Not Shown).....	22
4	Time History of X - Displacements	23
5	Time History of Z - Displacements	24
6	Positions of Aircraft and Deck Pendant For $\tau_x < \tau_z$ (This Condition Exists When the Cable is Fired too Late).....	27
7	Positions of Aircraft and Deck Pendant For $\tau_x > \tau_z$ (This Condition Exists When the Cable is Fired too Early).....	28
8	Space and Velocity Relations Between Aircraft and The Deck Pendant Just Before Impact	34
9	Definition of Terms ($\Delta x, \Delta \tau$) Used in The Timing Tolerance Problem	39
10	Velocity Difference at Time of Impact	50
11	Time of Impact	51
12	Target Delay Time	52
13	Maximum Tolerance on Delay Time	53
14	Maximum Tolerance on Horizontal Component of Average Aircraft Deceleration	54
15	Maximum Tolerance on Horizontal Component of Average Cable Deceleration	55
16	Maximum Tolerance on Horizontal Component of Aircraft Velocity	56
17	Maximum Tolerance on Horizontal Component of Cable Velocity .	57
18	Maximum Tolerance on Horizontal Position of Aircraft.....	58
19	Maximum Tolerance on Vertical Component of Average Aircraft Deceleration	59
20	Maximum Tolerance on Vertical Component of Average Cable Deceleration	60
21	Maximum Tolerance on Vertical Component of Aircraft Velocity	61
22	Maximum Tolerance on Vertical Component of Cable Velocity .	62
23	Maximum Tolerance on Vertical Position of Aircraft	63

LIST OF ILLUSTRATIONS (Continued)

<u>Figure No.</u>		<u>Page</u>
24	Tension Vs. Strain	71
25	7 x 19 Stainless Steel Wire Rope Velocity Vs. Strain	72
26	7 x 19 Stainless Steel Wire Rope The Function U Vs. Strain	73
27	Velocity Diagram for Transverse Impact	75
28	Kink Travels With Wave Front	78
29	Kink Impact Against Sheave (Kink Lags Wave Front).....	81
30	Kink Impact Against Sheave (Original Kink With Wave Front).....	85
31	Kink Impact Against Sheave (Original Kink With Wave Front).....	87
32	Kink Impact At Sheave With Disengagement	91
33	Kink Encountering a Tension Loading Wave	93
34	Schematic Stress-Strain Diagram Illustrating An Unloading Strain Condition	95
35	Kink Overtaken By Wave	98
36	Cable End Catapulted With Simultaneous Arrival of Kink and Tension Wave	100
37	Cable End Catapulted With Simultaneous Arrival of Kink and Tension Wave (Resultant Unloading Wave).....	103
38	Interaction of Two Kinks and Two Waves	105
39	Loading Wave Overtaken by Unloading Wave	109
40	Energy-absorbing Cable with Fixed Ends	112
41	Energy Absorbing Rope Using a Series of Sheaves	121
42	Sequence of Interactions for Case II	123
43	System Using Water Troughs	126

SECTION 1

INTRODUCTION, PURPOSE AND SCOPE

The introduction of high-speed aircraft with high stalling speeds requires the aircraft to land at speeds in excess of those permissible with the present length runways and arresting systems. Inasmuch as the length of runway is subject to space and cost limitations, a logical area to which improvement may be directed is that of developing superior aircraft-arrestment techniques.

This improvement may be accomplished in either of two ways:

1. By increasing the aircraft engaging velocity that can be tolerated.
2. By reducing the initial impact velocity by preacceleration of components of the arresting system.

The scope of the present report is comprised of certain problems in the application of these two ways to arresting systems which employ a deck pendant connected, possibly through a purchase cable, to an energy absorber.

To increase tolerable engaging velocity may require an increase in initial-impact tolerance as well as an improvement in ability to tolerate subsequent tension jumps governed by the constraints of the arresting system. Initial-impact tolerances for deck pendants of superior materials were investigated in Reference 1. Subsequent tension jumps may be combatted not only by various sheaving arrangements and end conditions but also by the use of an energy-absorbing material in the tension member of the arresting system. An analytical study of the effectiveness of various energy-absorbing materials in this role

Manuscript released by authors for publication as an ASD Technical Note, August 1961.

comprises the scope of Section 4 of this report.

Preacceleration of various components of an arresting system can be identified with specific features of improvement. Preacceleration of the deck pendant alone reduces the relative velocity of initial impact, but the maximum subsequent tension level is virtually unaffected. (A vertical component of preacceleration of the deck pendant is for the sole purpose of engaging aircraft which do not have a tail hook that is dragging on the runway). Preacceleration of the purchase cable and energy absorber reduces all subsequent tension levels but not the initial-impact tension. A study of methods of preaccelerating various existing arresting systems or their components comprises the scope of Section 2 of this report. Preacceleration must be suitably timed with respect to the arrival of the aircraft, and requires accurate detection of the aircraft approach path and velocity to control the instant at which preacceleration is begun. Allowable tolerances for all design parameters which affect successful timing are determined in Section 3 of this report.

SECTION 2

PREACCELERATION TECHNIQUES

2.1 Purpose and Primary Requirements

The purpose of this study of preacceleration is to determine the problems which will be encountered in preacceleration techniques and the extent of necessary modifications of present systems before practical preacceleration of them can be achieved.

The basic requirement of any practical mechanical system with respect to its working load is translated to a form amenable to the analysis of a preaccelerated arresting system. Two general methods of satisfying this overall requirement are set forth and subsequently applied to the arresting systems examined.

Preacceleration of aircraft-arresting systems has the explicit function of preventing the impact velocity of the hook against the deck pendant from producing a strain level which will either immediately or after subsequent wave interactions exceed a tolerable limit. But preacceleration itself may generate strains in the deck pendant. Therefore a primary requirement of any arresting system which makes use of a preacceleration technique is, for all time,

$$\epsilon_p(t) + \epsilon_a(t) \leq \epsilon_w \quad (2.1)$$

where:

- t = time
- $\epsilon_p(t)$ = strain due to preacceleration
- $\epsilon_a(t)$ = additional strain due to aircraft arrestment
- ϵ_w = working strain of the load carrying material

In consideration of the above inequalities, a large number of otherwise favorable methods for preacceleration need not be considered at all.

2.2 General Methods of Solution

Method I

One way to satisfy inequality 2.1 is to preaccelerate the system in such a way that no tension in the cable is generated. This means that the entire system must have the same acceleration and velocity. The entire system includes specifically:

1. All the cable (purchase and deck pendant)
2. All sheaves (including the deck sheave)
3. Energy absorber(s)
4. Carriage(s)

Thus, the necessary and sufficient condition that $\epsilon_p(t) \equiv 0$ is that all components must be accelerated equally, simultaneously, and symmetrically. A straightforward manner of achieving this situation is to mount the entire system on carriages and accelerate them equally.

Method II

If only certain members of the arresting system are brought up to speed (such as the deck pendant), there will be strains introduced into the

load-carrying members due to relative velocities, and ϵ_p will not be zero. At the time of impact, the strain due to preacceleration must be at a sufficiently low level that the impact tolerance will be greater than the closing velocity between hook and deck pendant and that no subsequent wave interaction will produce an $\epsilon > \epsilon_w$. In order to offer full benefit, preacceleration must be complete prior to the first critical wave interaction in the deck pendant or purchase cable. An unloading of ϵ_p is initiated upon termination of the preaccelerating force. Thus it appears feasible that one could design a system in which ϵ_p has decreased to a small value by the time ϵ_a nears its maximum.

Because the determination of the strains produced during the wave interactions subsequent to impact is a complex and extensive calculation and not within the scope of the present study, the impact tolerance of the arresting system will be used as the criterion for a successful preacceleration in the cases for which such a criterion is necessary. Although a complete design study would require an evaluation of the strains due to wave interactions, the impact tolerance is considered to be a suitable criterion for determining a successful preacceleration of the various energy-absorbing systems by either method.

Application of Method I to several energy absorbers of current interest is considered separately from the application of Method II because the masses and velocities encountered in applying each are distinct.

2.2.1 Adaptation of Method I to Different Energy Absorbers

Values of the amount of work necessary to preaccelerate the system to 200 kt (338 ft/sec) are shown in Table I for the approximate total

weights of each of the systems. Table I also shows the quantities of propellants necessary to provide the momentum or work requirements of the several energy-absorbers.

TABLE I

Comparative Preacceleration Data for Method I
(Based on a Preaccelerated Velocity of 200 Knots)

System	Estimated Mass (Slugs)	Momentum (lb-sec)	Energy (10^6 ft-lb)	**Jato (lb) Equivalent	TNT (lb)*** Equivalent
E. W. Bliss	275	93,000	15.7	465	131
Navy Mark VII	2,800	946,000	160.6	4730	1338
Water Squeezer	6,020	2,035,000	343.8	10175	2865
Van Zelm Metal Bender*	266-1050	90,000-355,000	15.2 to 60	450-1775	127-500

* Range of values shown is due to the range of models available.

** Based on a yield of 200 lb-sec of momentum per lb. of Jato fuel.

*** Based on a yield of 120,000 ft-lb of useful energy per lb. of TNT

If this method were to be used, a means for programmed braking of the carriages on the tracks would be necessary. However, this is not a serious problem, since the braking system could be part of the tracks rather than the carriages and thereby would contribute no additional weight to be accelerated.

The desirable feature of this method is that the length of the preacceleration run could be made as short as desired, limited only by the power available. This method would allow the arrestment to be accomplished in the shortest possible distance.

This method of preacceleration produces essentially no strains in the system which would affect the impact tolerance. The feasibility comparison thus reduces to merely a comparison of the work inputs necessary to accelerate the various energy-absorbers.

2.2.2 Adaptation of Method II to Different Energy Absorbers

The strain ϵ_p was assumed to reduce the effective impact tolerance of the system by 50 knots. The results in Table II are therefore based on preaccelerating to a velocity of 250 kt (475 ft/sec). Inasmuch as the components of each energy absorbing system are in motion with respect to each other under preacceleration by Method II (a factor not present under preacceleration by Method I) it is necessary to evaluate the behavior of each energy absorbing system individually rather than just determine total masses. The calculations of these results take proper account of the mechanical ratios inherent in each system. Each component mass was assigned its proper velocity. In cases where accurate values of the masses were not available, estimates were made for the sake of comparison. Except for the second line, the results of Table II do not reflect the effects of friction and aerodynamic losses, as these effects are relatively unimportant. Some of the systems have special energy losses which were also neglected. These losses will be mentioned in the following discussions under the system in which they occur. Also, except for the second line, the elimination of deck-sheave and deck-pendant preacceleration for each system will reduce the energy requirement given in Table II by about 6 million ft-lbs.

TABLE II

Comparative Data for Method II Preacceleration
(Based on a Preaccelerated Velocity of 250 Knots)

Type of System	Components to be Preaccelerated	Energy Required (10 ⁶ ft-lb)	Equivalent Energy in Pounds of T.N.T*
E. W. Bliss	Deck Sheaves with Carriages Deck Pendant Cable Drum and Cable (rotation)	13.0	108
E. W. Bliss	Purchase Cable and Drum (rotation)	2.58	21.5
Navy Mark VII	Oil Pistons Piston Rods Sheaves Purchase Cable Deck Sheaves Deck Pendant Cable	7.42	62
Water Squeezer	Deck Sheaves with Carriage Deck Pendant Cable Purchase Cable	18.52	154
VanZelm Metal Bender	Deck Sheaves Deck Pendant	6.36	53

* Calculated on the basis that 1 lb of TNT yields 120,000 ft-lb of useful energy.

E. W. Bliss - The figures given in line 1 are based on a greater moment of inertia than the figures given on line 2. The figures given on line 2 of Table II take into account (as upper bounds) the effects of aerodynamic and friction losses.

Navy Mark VII - When the piston moves down the cylinder during pre-acceleration, it must force some of the oil through an orifice. The energy required to do this has been neglected.

Water Squeezer - If the cable is accelerated dry and suddenly immersed, strains will arise in a manner similar to those caused by an impact. Avoiding this impact can be accomplished in one of three ways. The first is to preaccelerate the cable and water as one body. Another way is to accelerate the cable through the water. The third method is to accelerate the cable through the water and partially accelerate the water to reduce the drag force by reducing their relative velocity. The additional energy required by the use of any of these three methods was not considered when the energy requirement was calculated.

VanZelm Metal Bender - During preacceleration the rollers of the Metal Bender are separated so that they exert no retarding force on the strap. Once the aircraft has been engaged, the rollers would be closed in a programmed manner by a hydraulic or other device. If the Van Zelm Lo Inertia Reel is used, virtually all the energy requirement shown in Table II consists of the work needed to bring the deck pendant and sheaves up to speed. On this basis it would be possible to reduce the energy requirement to a value low enough to be supplied by a properly designed cable pop-up device. This cable pop-up device would set in motion only the deck pendant plus a small amount of steel strap (the deck sheaves and carriages having been eliminated) and would preclude the use of a separate preaccelerator. For this particular system the advantages of a cable pop-up device are therefore overwhelming.

2.3 Conclusion

Consideration of the discussions of the particular energy absorbers in Section 2.2 and inspection of Tables I and II will show that, for either method of preacceleration, the E. W. Bliss and the Van Zelm Metal Bender have significantly lower energy requirements than do the other systems. Since these energy requirements are well within the capabilities of present-day catapult systems, preacceleration of either energy absorber appears feasible.

Notation for Section 3

Coordinates

- X - a horizontal axis, coincident with the centerline of runway, positive in the direction of aircraft motion.
- Y - a horizontal axis at right angles with the centerline of runway.
- Z - the vertical axis, perpendicular to the plane of the runway, positive in the upward direction.
- t - time variable, measured from the instant of last detection (= measurement) of the aircraft.
- T - delay time. $t = T$ is called the firing (or ejection, or pop-up) instant, at which the preacceleration of the deck pendant is completed, and at which the deck pendant begins its coasting flight (trajectory).
- τ - predicted (or "extrapolated") trajectory time. $t = \tau$ is called the interception instant, at which the coasting deck pendant strikes the underside of the aircraft fuselage.

Aircraft Trajectory Parameters:

- \ddot{x}_m = horizontal acceleration of the aircraft - an average value for the duration $0 < t < \tau$
- \ddot{z}_m = vertical acceleration of the aircraft - an average value for the duration $0 < t < \tau$
- \dot{x}_0 = horizontal component of aircraft velocity (ground speed) at $t = 0$.
- \dot{x}_τ = horizontal component of aircraft velocity at $t = \tau$
- \dot{z}_0 = vertical component of aircraft velocity at $t = 0$.
- \dot{z}_τ = vertical component of aircraft velocity at $t = \tau$
- x_0 = horizontal distance between the position of aircraft at $t = 0$ and the deck pendant at $t = T$.
- z_0 = altitude of aircraft above the runway level, at $t = 0$.

Deck Pendant Trajectory Parameters:

(Referred to the center of span of the deck pendant)

$\ddot{\xi}_m$ = horizontal acceleration - an average value for the duration $T < t < \tau$

$\ddot{\zeta}_m$ = vertical acceleration - an average value for the duration $T < t < \tau$

$\dot{\xi}_0$ = horizontal velocity component at $t = T$.

$\dot{\xi}_\tau$ = horizontal velocity component at $t = \tau$

$\dot{\zeta}_0$ = vertical velocity component at $t = T$.

$\dot{\zeta}_\tau$ = vertical velocity component at $t = \tau$

SECTION 3

ANALYSIS OF DETECTION AND TIMING PROBLEM

3.1 Purpose and Scope

The purpose of this section is to investigate the detection and timing problem in an aircraft arresting system employing a preaccelerated arresting cable where the preacceleration is accomplished by firing ("popping up") into the air of the deck pendant portion of the cable: to determine the relationship that exists between the instant of firing, the instant of interception and the aircraft and cable trajectory parameters such as to render interception (i.e. the engagement of the preaccelerated cable by the arresting hook of the aircraft) possible, and to study the effect of variations in those trajectory parameters and from these the problem of parameter tolerance requirements.

Preacceleration of the purchase cable and energy absorbing apparatus, forward preacceleration of the deck pendant, and pop-up of the deck pendant conceivably can be accomplished by separate mechanisms and so may occur in any desired sequence.

The case treated here is that in which the purchase cable and energy absorber are preaccelerated first, followed by preacceleration of the deck pendant in a direction having both forward and upward components (that is, pop-up and forward preacceleration of the deck pendant occur simultaneously).

To preaccelerate the deck pendant forward after pop-up would be impractical from the standpoint of control over the position of the pendant. Forward preacceleration of the deck pendant prior to pop-up might be practical if the forward preacceleration is simultaneous with that of the purchase cable and

energy absorber, as in the case where all these components are preaccelerated by the same mechanism; this case can be analyzed in the same manner as the case actually treated. Vertical pop-up with no forward preacceleration of the deck pendant is clearly a special case of the one treated.

If preacceleration of the purchase cable occurs during or after that of the deck pendant, the purpose of preaccelerating the deck pendant would be defeated by the tensions generated during purchase-cable acceleration. While this scheme might be used to control the maximum height of the deck pendant in the case of purely vertical pop-up, it is regarded as an unnecessary complication in view of the simple, reliable device already available for this purpose. Conceivably there are arrangements of sliding sheaves which would isolate the deck pendant from tensions generated by purchase-cable acceleration; in this case the deck-pendant motion (prior to engagement of aircraft) is independent of the purchase cable, so that the analysis of the case actually treated would apply.

In the case treated, preacceleration of the purchase cable and energy absorber is considered to be independent of preacceleration of the deck pendant. The device which detects the incoming aircraft and senses its position and velocity can continue to sense even after the purchase cable and energy absorber are up to speed, so that the very latest data can be used to determine the proper instant for deck-pendant pop-up.

The entire timing problem consists of the determination of two instants:

- 1) The instant at which the purchase cable preacceleration is to be started.
- 2) The instant at which the deck pendant ejection is to be initiated.

Of the two, the former is much less of a problem in that the timing tolerance requirements are not anywhere as strict as for the latter.

The instant of the beginning of the purchase cable preacceleration does not have to be very closely controlled, because if preacceleration is completed before it is time for the deck pendant to be ejected, then the purchase cable with its associated equipment goes into coasting, and continues coasting until the pop-up time has arrived. While the purchase cable accelerating mechanism is coasting, extra length in the purchase cable is being consumed so that the maximum allowable duration of coasting (which is a measure of timing tolerance) can be given by the following expression:

$$t_c = \frac{L_c - L_{pa}}{V_c}$$

where

t_c = maximum allowable coasting time

L_c = extra length of purchase cable available for runout of the preaccelerating device

L_{pa} = length of cable consumed during the preacceleration period

V_c = cable coasting velocity

The tolerance of timing the preacceleration of purchase cable is equal to $t_c/2$, i.e. the preacceleration may be started as much as $t_c/2$ sec earlier or later than the theoretical aiming instant (an instant such that the time duration from it to the instant of popping-up is equal to $t_c/2$).

The problem of timing the exact instant of deck pendant ejection is very much more difficult and exacting, and it is this problem which is being discussed in the text to follow. It must be emphasized that from this point on no mention of the problem of purchase cable preacceleration will be made. In all the subsequent discussions it is to be understood that the purchase cable is in the coasting phase when the events associated with the deck pendant are taking place.

3.2 Problem Defined

Given any normal landing maneuver of an aircraft, the problem is to adjust the performance parameters of the arrestment device such that interception occurs when the aircraft is either coasting on the runway or still in flight just above the ground. Furthermore, it is desirable to adjust the performance parameters of the pop-up device in such a way that the "extrapolated" trajectory time t is as short as possible for any particular landing maneuver. The shorter the "extrapolated" trajectory time t , the less runway length is needed, and the less will be the effect of errors in detecting the aircraft velocity and deceleration.

3.3 Extent and Limitations

Any physically reasonable system of aircraft arrestment is subject to certain very obvious limitations.

1) The deck pendant is preaccelerated so that when ejected it has a vertical component of velocity as well as a horizontal one, and the horizontal component has the same direction as the motion of the aircraft. To the analysis of this section it is entirely immaterial how this horizontal velocity component is generated - whether by preaccelerating the whole pop-up device with the deck pendant, or by ejecting the deck pendant from a stationary pop-up device with the deck pendant, or by ejecting the deck pendant from a stationary pop-up device at an angle θ (see Figure 2), or any combination of previous two methods. The only assumption made was that at some time $t = T$ the cable is at height zero, position x_0 along the runway, and travelling with a horizontal velocity component $\dot{\xi}_0$ and vertical velocity component $\dot{\zeta}_0$ and is subject only to air drag and gravity.

2) The horizontal component of cable velocity at the instant of interception ($t = \tau$) is less than the aircraft velocity (but it may be higher at the instant of ejection, so that the aircraft always overtakes the cable going through its short trajectory and catches it from behind).

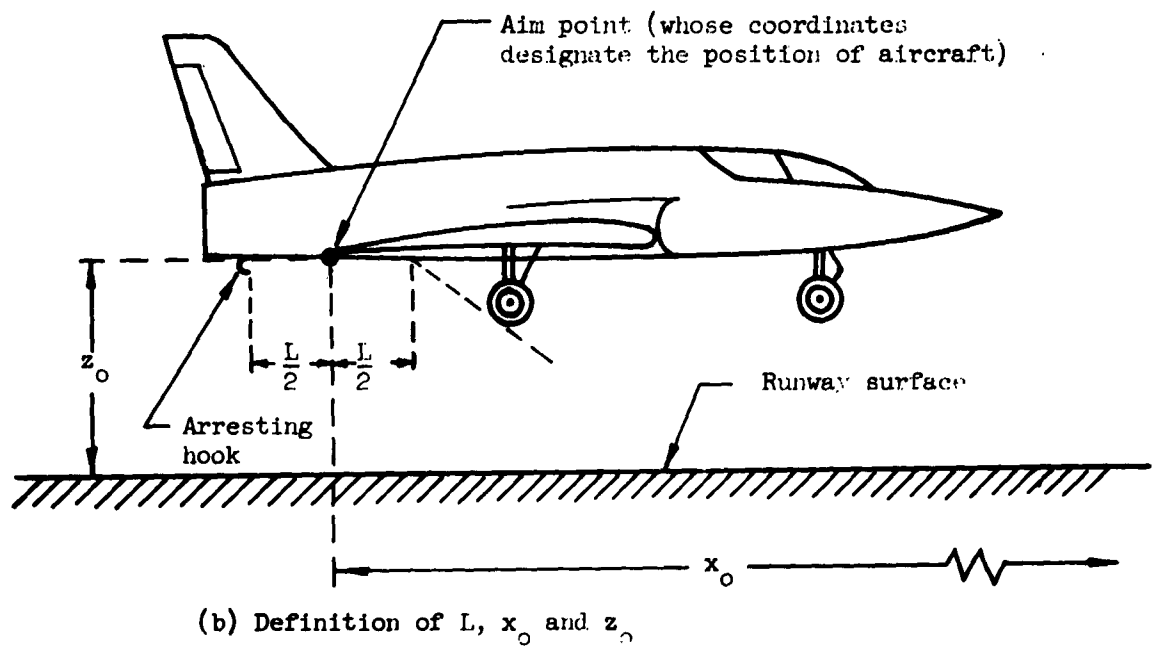
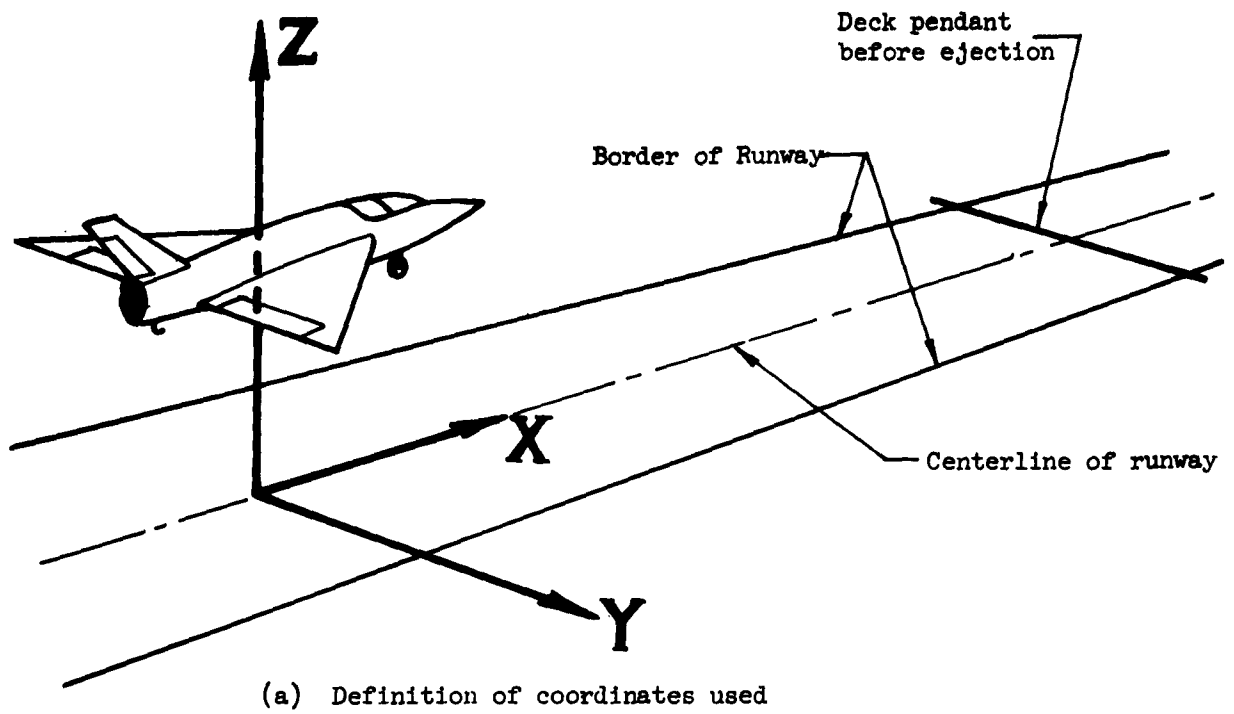


Figure 1

Coordinate System and Initial Position

3) Lack of parallelism of the flight path with the centerline of the runway, and side drift (due to cross wind) were neglected in this section - the trajectory of the aircraft was assumed to lie in the XZ - plane. It was also assumed that the aircraft strikes the deck pendant at its center or close to it (i. e. , in that region of the deck pendant which after ejection behaves like a straight rod*) as it translates - the X and Z coordinates of each point in that "straight rod" region being the same as those of the center of the deck pendant.

4) As the shape of the cable trajectory in general resembles a parabola, it was assumed that for the sake of a more accurate prediction of the interception time τ the aircraft must snag the cable while it is still rising (i. e. , before the cable has reached the peak of its trajectory).

5) The duration of the aircraft detection and ranging from its beginning to the instant of last detection does not enter into this analysis except in determining the numerical values of aircraft parameters to be used in predicting the future behavior of the aircraft. The upper bound for the region of interest of both t and T is at most 8 sec. In 8 sec. an airplane landing, for instance, at 400 knots will have travelled 5400 feet along the runway before being intercepted - and this already seems like wasting too much runway length.

3.4 System Analyzed

The aircraft-arresting system considered in this report and its operation may be briefly described as follows. As the aircraft is coming in for a landing and is gliding down the runway, the detection and timing apparatus (ground-located and "looking" in the direction of the approaching aircraft) is constantly in operation estimating the distance from the deck pendant, the ground speed, rate of descent, etc. , of the aircraft. As the aircraft passes a certain position

*) For discussion of the shape (i. e. , space curve) of a popped-up deck pendant, see Reference No. 3.

along the runway, known as the position of last detection, the detection and timing apparatus takes its last reading and feeds this final information into a computer, which then adjusts the performance of the pop-up device, determining at least one of the following: instant of firing (delay time), velocity components, distance x_0 , etc. Upon receiving the signal from the computer, the cable-popping mechanism immediately ejects (pops-up) the deck-pendant portion of the arresting cable. The ejection is timed so that when the deck pendant is going thru its short trajectory the aircraft is in the proper position for interception. i. e., the aircraft overtakes the slower-moving cable and with its arresting hook snags the cable (at approximately the center of the deck pendant). From that point on, the aircraft pulls on the cable, and the cable offers braking resistance until the aircraft has come to a full stop. The arresting cycle is then complete.

3.5 Mathematical Analysis of the Timing Problem

The analytical approach to the problem of detection and timing consists mainly of the simultaneous solution of equations of motion for the airplane and the deck pendant. The implicit solution thus obtained will indicate the relationship between the popping-up instant ($t = T$), the interception instant ($t = \tau$), the different trajectory parameters and the distances x_0 and z_0 . The equations of motion to be used when solving the timing problem have to be defined for the time interval of $0 \leq t \leq \tau$ only. To the solution of the timing problem, neither the motion before $t = 0$ (except, of course, as it determines the numerical values of the aircraft parameters) nor after $t = \tau$ is important. (The equations of motion for the interval $0 \leq t \leq \tau$ do not hold for $t > \tau$ because after interception the aircraft is being strongly decelerated by the arresting cable). In as gen-

eral a way as possible, the equations of motion may be graphically illustrated as shown in Figures 3, 4, and 5, and the trajectories (which are obtainable from these equations of motion by the elimination of t between them) in two dimensions (the XZ - plane) are shown in Figure 2. The trajectories as shown represent the general case of a landing maneuver with interception by an arresting cable, the only departure from perfect generality being three requirements (already mentioned in the Section 3.3 on Extent), as follows:

- a) The aircraft is either losing altitude or maintaining level flight (or already on the runway).
- b) Aircraft is moving faster than the deck pendant.
- c) Interception takes place before the cable has reached the peak of its trajectory.

3.5.1 Equations of Motion

3.5.1.1 General Discussion

In the region of interest (between the instant of last detection, $t = 0$, and the instant of interception, $t = \tau$) the positions of the landing aircraft and the popped-up deck pendant may always be determined from a set of parametric equations, where t is the independent variable, and x and z are the position coordinates (see Figure 1). For any $0 < t < \tau$, the position of the aircraft will be given by

$$x = f_a(t, k_1) \quad z = g_a(t, K_1) \quad (3.1)$$

and the position of the center of span of the deck pendant is given by

$$\xi = f_c(t-T, m_1) \quad \zeta = g_c(t-T, M_1) \quad (3.2)$$

for $\tau < T < t$; (for $0 < t < T$, $\xi = \zeta = 0$)

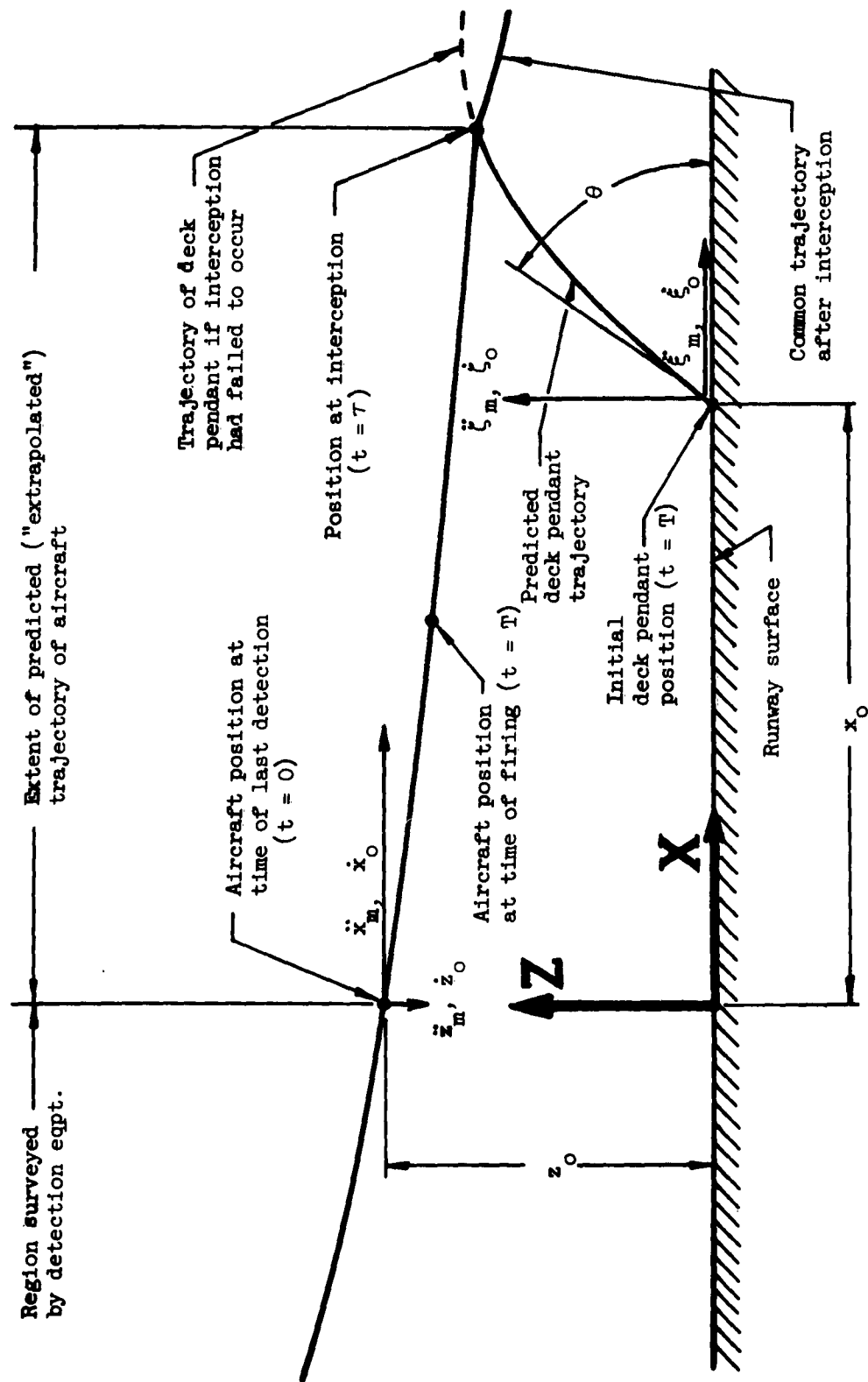


Figure 2
Aircraft and Deck Pendant Trajectories
Before Interception
(Vertical Scale Exaggerated)

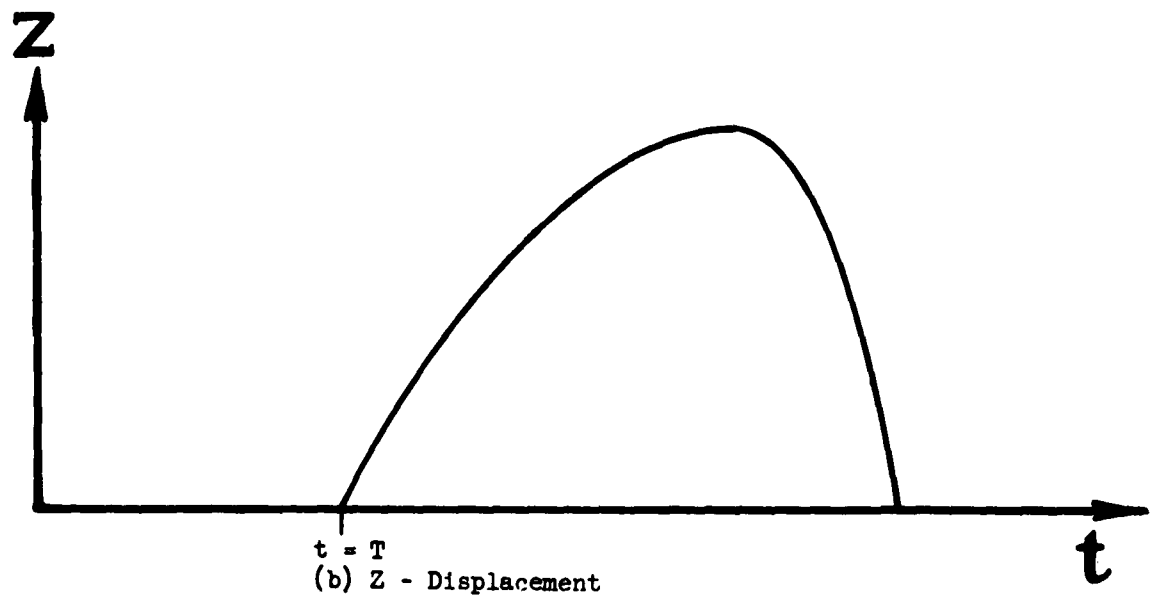
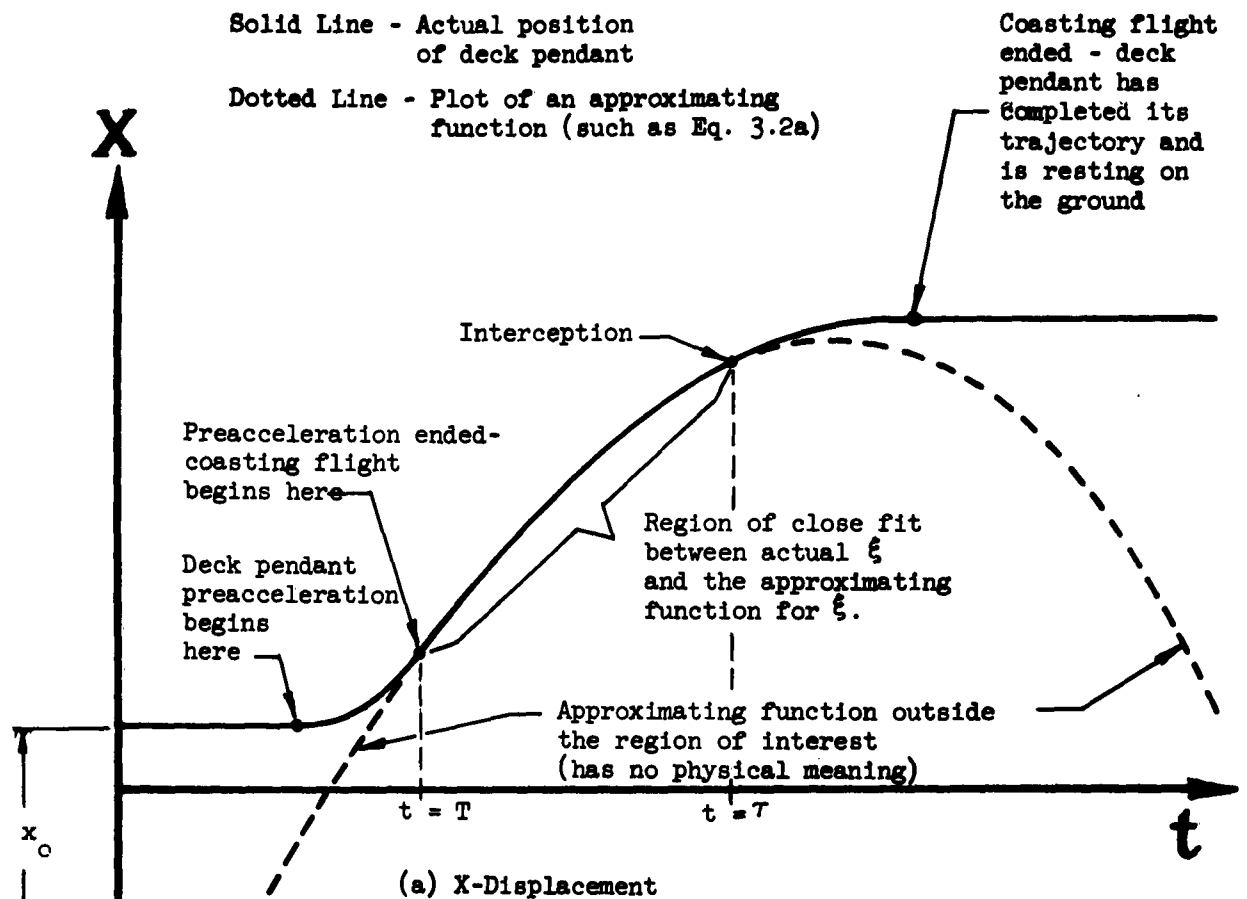


Figure 3
 Time Vs. Position Plots of the Deck Pendant Alone
 (Effect of Aircraft Not Shown)

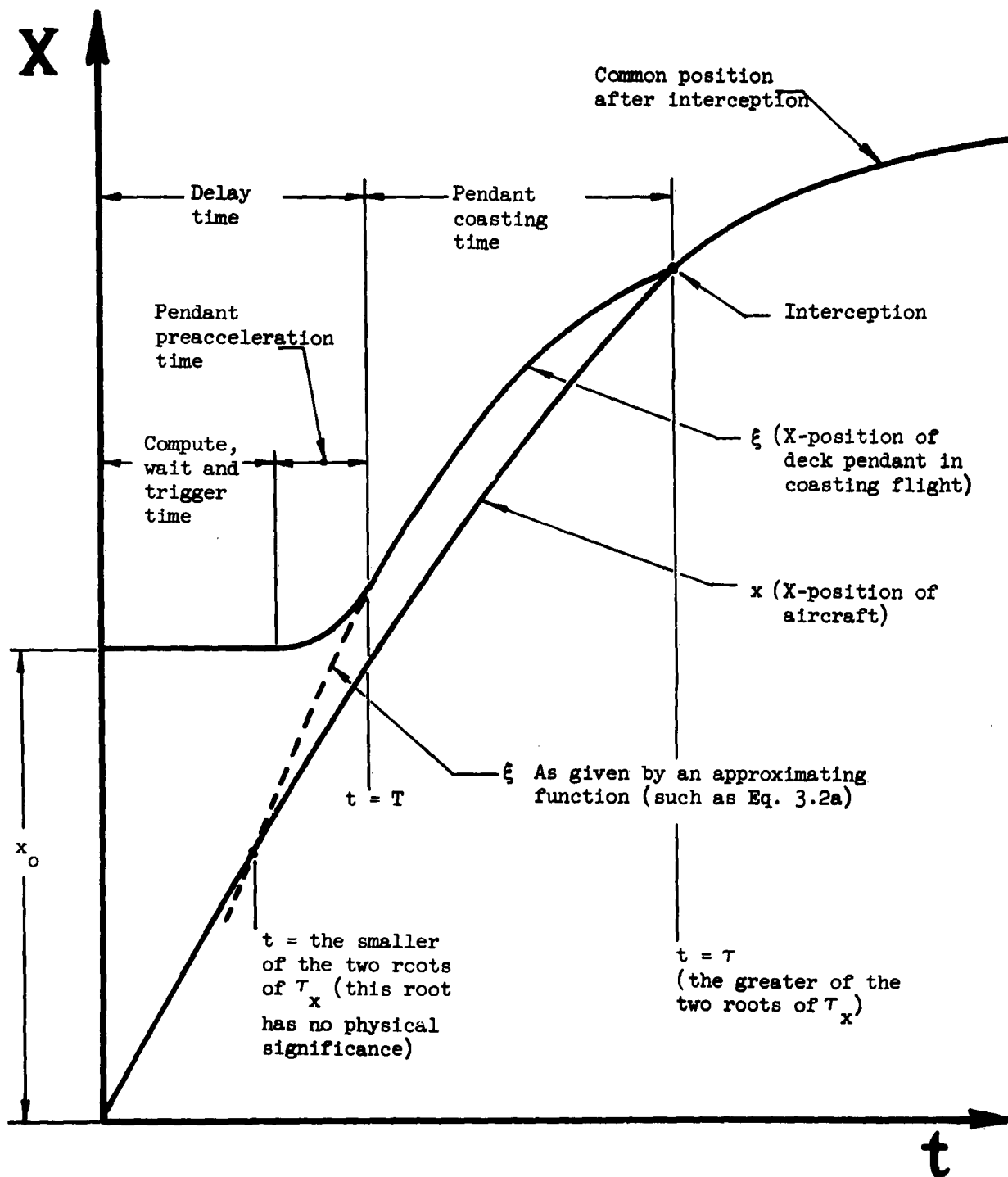


Figure 4
Time History of X - Displacements

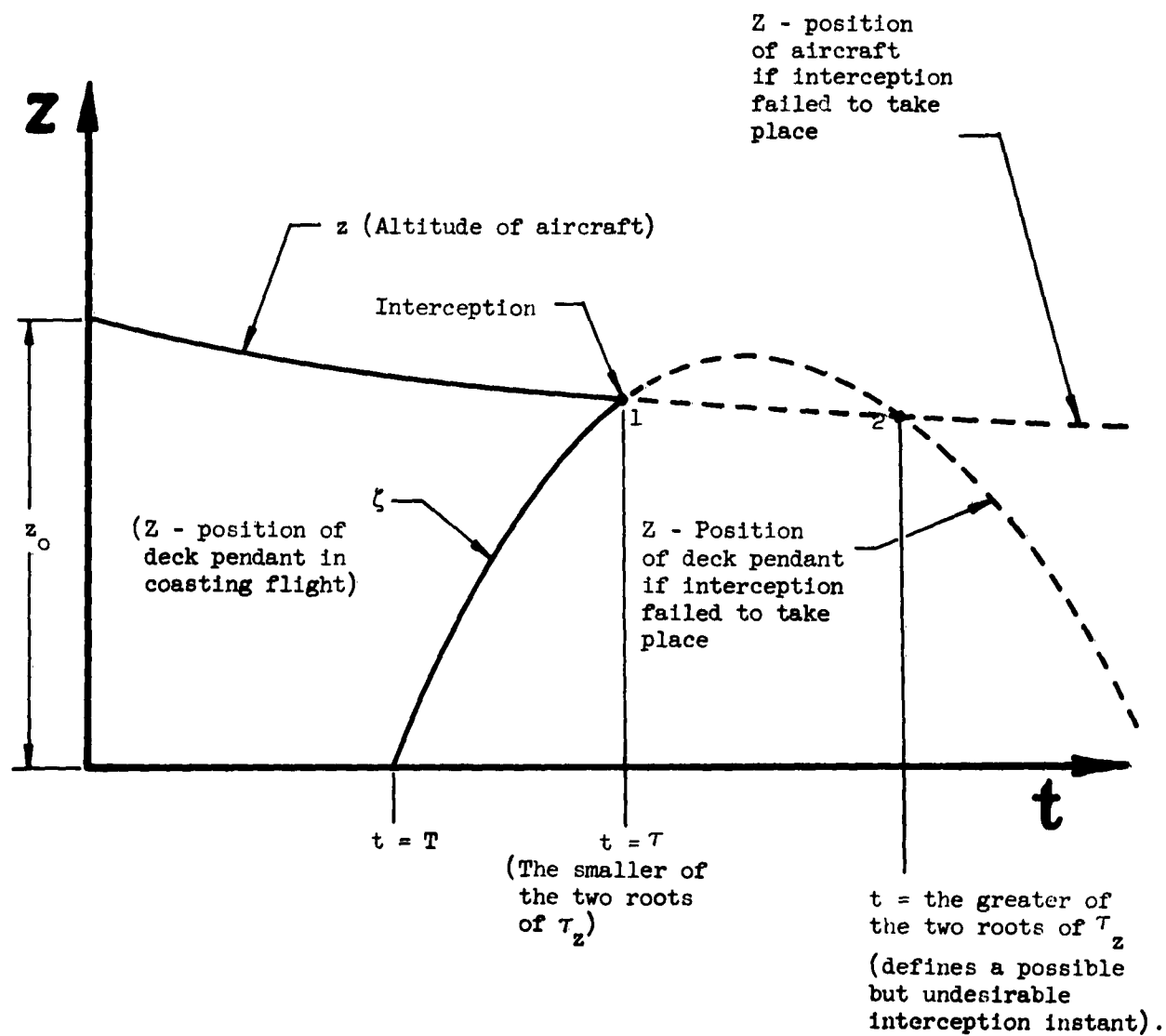


Figure 5
Time History of Z - Displacements

In the above expressions, t is the time variable, and k_i , K_i , m_i , M_i , are sets of trajectory parameters.

If the deck pendant were just simply preaccelerated and ejected into the air in the absence of a landing aircraft, it would fly thru a short trajectory and then end up lying on the runway. Such a trivial case is illustrated in Figure 3a and 3b in a general manner. The important thing to note there is this: the actual ξ and ζ curves will be established by design calculations and/or test results. These, however, may be quite complicated, so that for practical computational purposes (computing the delay time) it becomes necessary to approximate the actual ξ and ζ curves by some mathematically less complicated functional relationship, called here the approximating function. These approximating functions are chosen so that they fit the actual deck pendant displacements in the region of interest ($T < t < \tau$) rather closely, and may deviate from the actual curves considerably in the regions $t < T$ and $t > \tau$. The functions f_c and g_c used in Equations (3.2) will be some approximating functions, and not the exact actual functions (which may not even be known, especially if only a set of test results is available).

Perfectly general conditions for interception require that:

$$f_a(\tau, k_i) = f_c(\tau - T, m_i) \quad (3.3)$$

and

$$g_a(\tau, K_i) = g_c(\tau - T, M_i) \quad (3.4)$$

These implicitly define 2 relationships:

$$\text{From Eq. (3.3): } \tau_x = F(T, k_i, m_i) \quad (3.5)$$

$$\text{From Eq. (3.4): } \tau_z = G(T, K_i, M_i) \quad (3.6)$$

In general, for an arbitrary values of performance parameters and delay time T , τ_x will not equal τ_z . The physical interpretation of this statement is the following: if at a time τ_x the horizontal positions of aircraft and cable are equal, the vertical positions are not; and if at τ_z the vertical positions of aircraft and cable are equal, horizontal displacements do not coincide (See Figure 6 and 7 for visual explanation of the preceding statement). For optimum interception (in the complete absence of error), both the horizontal and the vertical positions of aircraft and cable must coincide at the same instant, i. e. , $\tau_x = \tau_z = \tau$. In terms of equations it means that $F(T, k_1, m_1) = G(T, K_1, M_1)$, which for any given set of trajectory parameters can be satisfied by a unique value of T . The computation of the delay time T such that $F = G$ be satisfied is accomplished by the on-site computer. Once the computer has determined T , the timing problem for that particular landing maneuver is solved: the interception instant is automatically fixed by the above value of T and the trajectory parameters.

3.5.1.2 Particular Example

In general, the accuracy with which τ and T can be determined depends upon how well the functions f_a , g_a , f_c and g_c approximate the actual motion of the aircraft and the popped-up cable in the region of interest ($0 < t < \tau$). Essentially, the exact physical relationships are unknowable exactly. They can only be predicted approximately. The motion of the aircraft must be predicted from its behavior prior to last detection ($t < 0$), and the trajectory of the center of an ejected deck pendant must also be known from previous test results or theoretical considerations. It must be emphasized here that the trajectory of the aircraft from $t = 0$ to $t = \tau$ is necessarily a result of

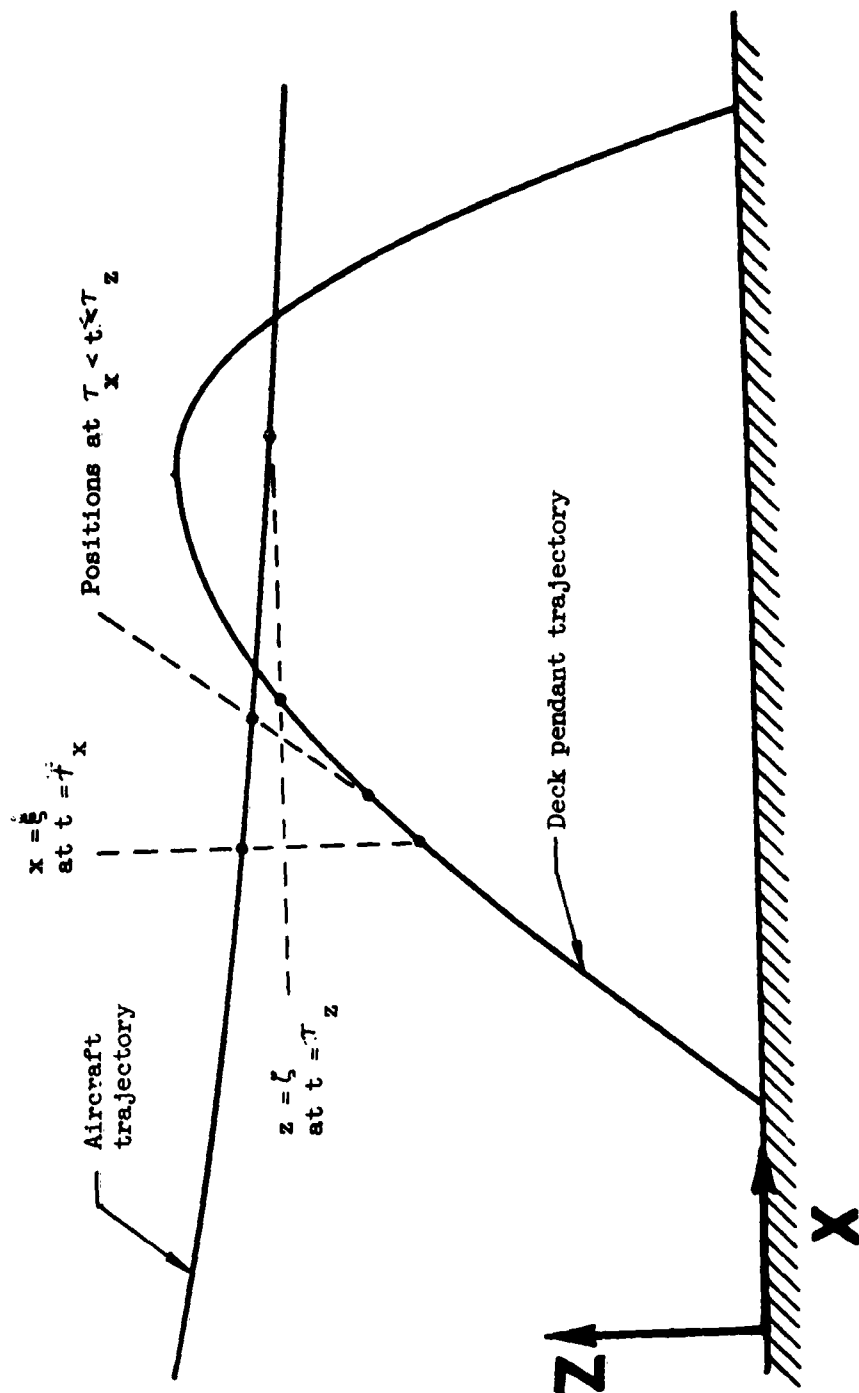


Figure 6
Positions of Aircraft and Deck Pendant
For $\tau_x < \tau_z$ (This Condition Exists When
the Cable is Fired too Late)

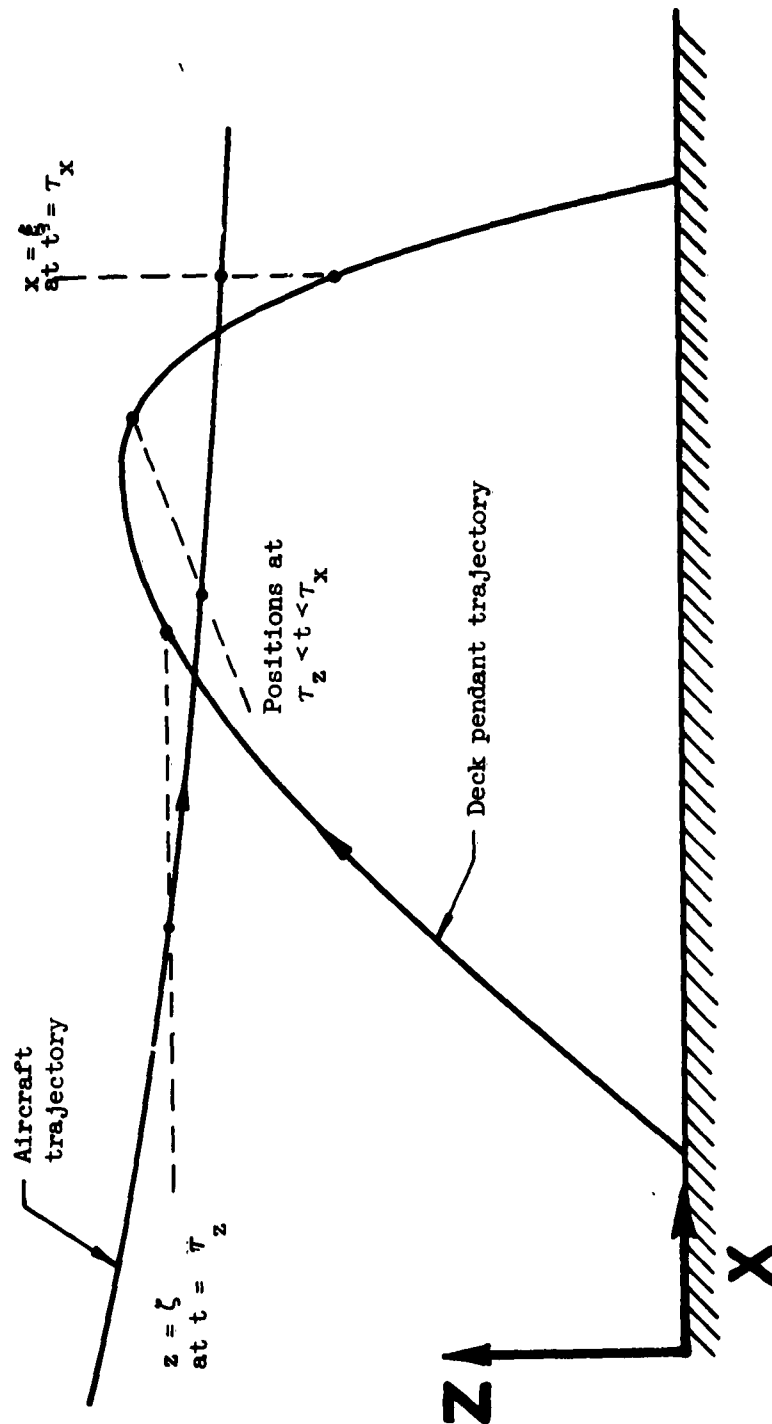


Figure 7
Positions of Aircraft and Deck Pendant
For $\tau_x > \tau_z$ (This Condition Exists
When the Cable is Fired too Early).

extrapolation of the flight path prior to $t = 0$.

Although equations (3. 1) and (3. 2) may assume a number of functional forms, each one of them approximating the extrapolated trajectory of aircraft and the predicted trajectory of cable to a greater or lesser degree of accuracy, in this section for illustration of the analytical procedure it was assumed that all four of the equations of motion can be cast in the quadratic form, $At^2 + Bt + C$. The justification for assuming such a simple functional form lies in the fact that for small values of t (up to 8 sec), by properly selecting the parameters A , B , & C , a parabola can be made to approximate a short segment of any actual trajectory reasonably well. Another reason for assuming a quadratic form is the relative ease of working with it in numerical computations (as compared to transcendental functions or a cubic function, for instance) - and a quadratic relationship is not as trivial as a linear one (there just aren't any straight line trajectories!). Furthermore, when the horizontal and vertical displacements are represented by such a quadratic form, then the independent parameters A , B , and C have definite physical interpretations: A equals one half of the acceleration (an average value over the "extrapolation" period $0 < t < \tau$), B equals the initial velocity and C stands for some initial displacement at $t = 0$. Then the equations of motion (3. 1) and (3. 2) in our illustrative example become the following (using the symbols given in the table of Notation for Section 3):

For the aircraft:

$$\begin{aligned} x &= \frac{1}{2} \ddot{x}_m t^2 + \dot{x}_0 t \\ z &= \frac{1}{2} \ddot{z}_m t^2 + \dot{z}_0 t + z_0 \end{aligned} \tag{3. 1a}$$

For the deck pendant:

$$\begin{aligned} \xi &= \frac{1}{2} \ddot{\xi}_m (t - T)^2 + \dot{\xi}_0 (t - T) + x_0 \\ \zeta &= \frac{1}{2} \ddot{\zeta}_m (t - T)^2 + \dot{\zeta}_0 (t - T) \end{aligned} \tag{3. 2a}$$

One of the conditions for interception is that at $t = \tau$ the horizontal positions of aircraft and cable must coincide:

$$x = \xi, \text{ or}$$

$$\frac{1}{2} \ddot{x}_m \tau^2 + \dot{x}_0 \tau = \frac{1}{2} \ddot{\xi}_m (\tau - T)^2 + \dot{\xi}_0 (\tau - T) + x_0 \quad (3.3a)$$

from which an explicit solution for τ can be obtained:

$$*) \tau_x = \frac{-(\dot{x}_0 - \dot{\xi}_0 + \ddot{\xi}_m T) + \sqrt{(\dot{x}_0 - \dot{\xi}_0 + \ddot{\xi}_m T)^2 + (\ddot{x}_m - \ddot{\xi}_m)(2x_0 - 2\dot{\xi}_0 T + \ddot{\xi}_m T^2)}}{(\ddot{x}_m - \ddot{\xi}_m)} \quad (3.5a)$$

For small values of \ddot{x}_m and $\ddot{\xi}_m$ Eq. (3.5a) approaches the indeterminate form $0/0$, so that numerical evaluation of τ_x becomes increasingly difficult. To avoid this difficulty, an alternate form (3.5b) (which is obtained from Eq (3.5a) by rationalizing the numerator) may be used, which for small values of \ddot{x}_m and $\ddot{\xi}_m$ approaches the form $\tau_x \approx \frac{\text{displacement}}{\text{velocity}}$

$$\tau_x = \frac{2x_0 - 2\dot{\xi}_0 T + \ddot{\xi}_m T^2}{(\dot{x}_0 - \dot{\xi}_0 + \ddot{\xi}_m T) + \sqrt{(\dot{x}_0 - \dot{\xi}_0 + \ddot{\xi}_m T)^2 + (\ddot{x}_m - \ddot{\xi}_m)(2x_0 - 2\dot{\xi}_0 T + \ddot{\xi}_m T^2)}} \quad (3.5b)$$

The second condition for interception is the coincidence of vertical positions at $t = \tau$:

$$z = \zeta, \text{ or}$$

$$\frac{1}{2} \ddot{z}_m \tau^2 + \dot{z}_0 \tau + c_2 = \frac{1}{2} \ddot{\zeta}_m (\tau - T)^2 + \dot{\zeta}_0 (\tau - T) \quad (3.4a)$$

from which another explicit solution for τ can be obtained:

$$**) \tau_z = \frac{-(\dot{z}_0 - \dot{\zeta}_0 + \ddot{\zeta}_m T) - \sqrt{(\dot{z}_0 - \dot{\zeta}_0 + \ddot{\zeta}_m T)^2 - (\ddot{z}_m - \ddot{\zeta}_m)(2z_0 - 2\dot{\zeta}_0 T + \ddot{\zeta}_m T^2)}}{(\ddot{z}_m - \ddot{\zeta}_m)} \quad (3.6a)$$

*) The reason for taking only the plus sign before the radical (i. e., the larger of the two roots of τ_x) is clearly seen in Figure 3.

**) Explanation of the negative sign before the radical can be found in Figure 5.

or its equivalent after rationalization of the numerator:

$$\tau_z = \frac{-2z_0 + 2\ddot{\zeta}_m T^2 - \dot{\zeta}_0 T}{(\dot{z}_0 - \dot{\zeta}_0 + \dot{\zeta}_m T) - \sqrt{(\dot{z}_0 - \dot{\zeta}_0 + \dot{\zeta}_m T)^2 - (\ddot{z}_m - \ddot{\zeta}_m)(2z_0 - 2\ddot{\zeta}_m T^2 + \dot{\zeta}_0 T)}} \quad (3.6b)$$

Now clearly, τ_x must equal τ_z if interception is to take place; this means that the expressions (3.4a) and (3.6a) or (3.4b) and (3.6b) must be equal. For any given set of trajectory parameters *) there may be more than one value of T that satisfies the equality $\tau_x = \tau_z$. From the practical standpoint, however, only the smallest root is important. This determination of the optimum delay time T will be accomplished by the on-site computer.

The function of the on-site computer may be divided into two main parts. Part one is the interpretation of the data of aircraft detection apparatus - at certain time intervals the computer receives sets of detection apparatus readings (which are six in any set of readings: position along the runway, vertical components of speed and acceleration) and from this data it determines parameters $\ddot{x}_m, \ddot{z}_m, \dot{x}_0, \dot{z}_0$ which describe the "extrapolated" part of the aircraft trajectory (i.e., the positions the aircraft assumes between $t = 0$ and $t = T$). Part two is the determination of the cable performance parameters such that the cable pops up at the right position along the runway (parameter x_0), at the right time $t = T$ and with the correct velocity components to effect a successful engagement of the cable by the arresting hook of the aircraft. The number of the parameters ($x_0, T, \dot{x}_0, \dot{z}_0$) to be determined depends on the physical configuration of a particular arresting system used, for instance: whether the pop-up device is stationary or movable with respect to runway, whether the pop-up device ejects

*) These parameters are constant with time (by definition) for a particular landing

the deck pendant at a fixed or a variable angle θ (measured from the horizontal), a fixed or a variable (i. e. adjustable) ejection velocity. If, as in the illustratory case analyzed in this section, the pop-up device is stationary at x_0 feet from the position of last detection, and the pop-up velocity and angle are fixed and of known magnitudes, then all the computer has to do is to calculate the optimum delay time T and feed that bit of information to the pop-up device.

3.6 Tolerance Requirements

The purpose of this subsection is the finding of the following two relationships:

- a) Equation for the estimation of the maximum permissible variation (tolerance) $\Delta\tau_p$ in the computed value of τ , in terms of aircraft dimensions and the velocities at impact (i. e. interception) of both the aircraft and the cable.
- b) Equation showing how variation of the actual τ - value from the theoretical (computed) depends upon small variations in the individual trajectory parameters, i. e., demonstrating the component parts of τ .

The following discussion is based entirely on the preceding investigation of the detection and timing problem, and therefore is subject to the same limitations; however, it is general enough not to be restricted to the illustrative case analyzed both in the preceding subsection and this one.

3.6.1 Motivation for the Tolerance Problem

It must be emphasized that what the on-site computer determines and adjusts (firing instant T , or cable trajectory parameters, or both) will yield a theoretically perfect interception instant (the x and z coordinates of the aim point on the aircraft, and the center of cable will simultaneously coincide) and two intersecting trajectories (mathematical lines). The theoretical time will

actually never be realized (unless by a rare coincidence) - the actual interception time τ_a will differ from τ a little due to slight errors in the evaluation of trajectory parameters and firing instant T and due to the inability of the control mechanism to time the instant of cable ejection exactly even if the true optimum time of ejection were known. Likewise, the actual trajectories will differ, however slightly, from the theoretical (i. e. the ones described by the equations of motion, Eq. 3.1 and Eq. 3.2) ones, so that the actual interception point (intersection of the two trajectories) will not coincide with the theoretical one. However, as it is not important where exactly and when exactly the interception occurs so long as it does occur, the problem of tolerance evaluation was approached by considering the deviation of the actual interception point from the theoretical one.

3.6.2 Problem Defined

The subproblem of setting-up of tolerance requirements in the overall problem of timing and detection may be defined as follows:

Consider a given landing maneuver and a given arresting system. This means a given set of data from which the on-site computer extracts (computes) the different trajectory parameters to be used in the solution for the optimum delay time T, and/or other cable trajectory parameters. The question is: How large a variation from expected values in each of the parameters involved is permissible, and how large can the summation of the effects of those individual parameters be such that a successful interception is effected (i. e. such that the cable impinges upon the aircraft somewhere within the permissible impact region, Figure 8a).

3.6.3 Effect of an Error in τ

Before discussing the effect of an error in τ it is necessary to take a closer look at what is happening at the instant of interception, and to define

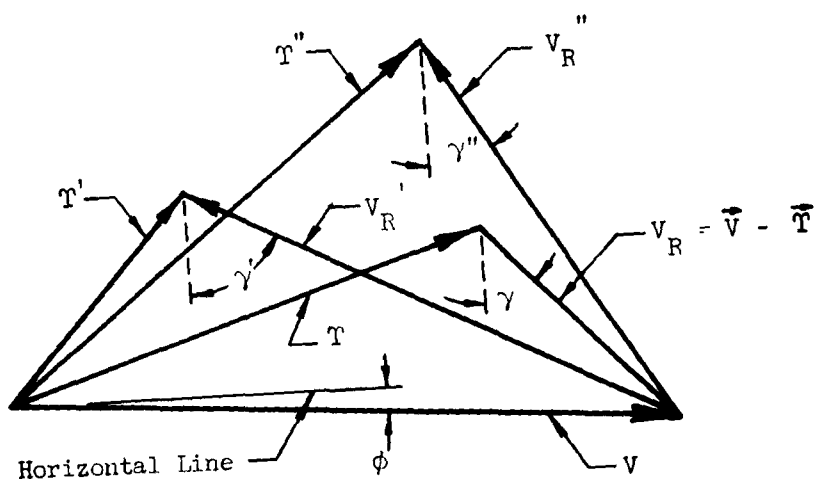
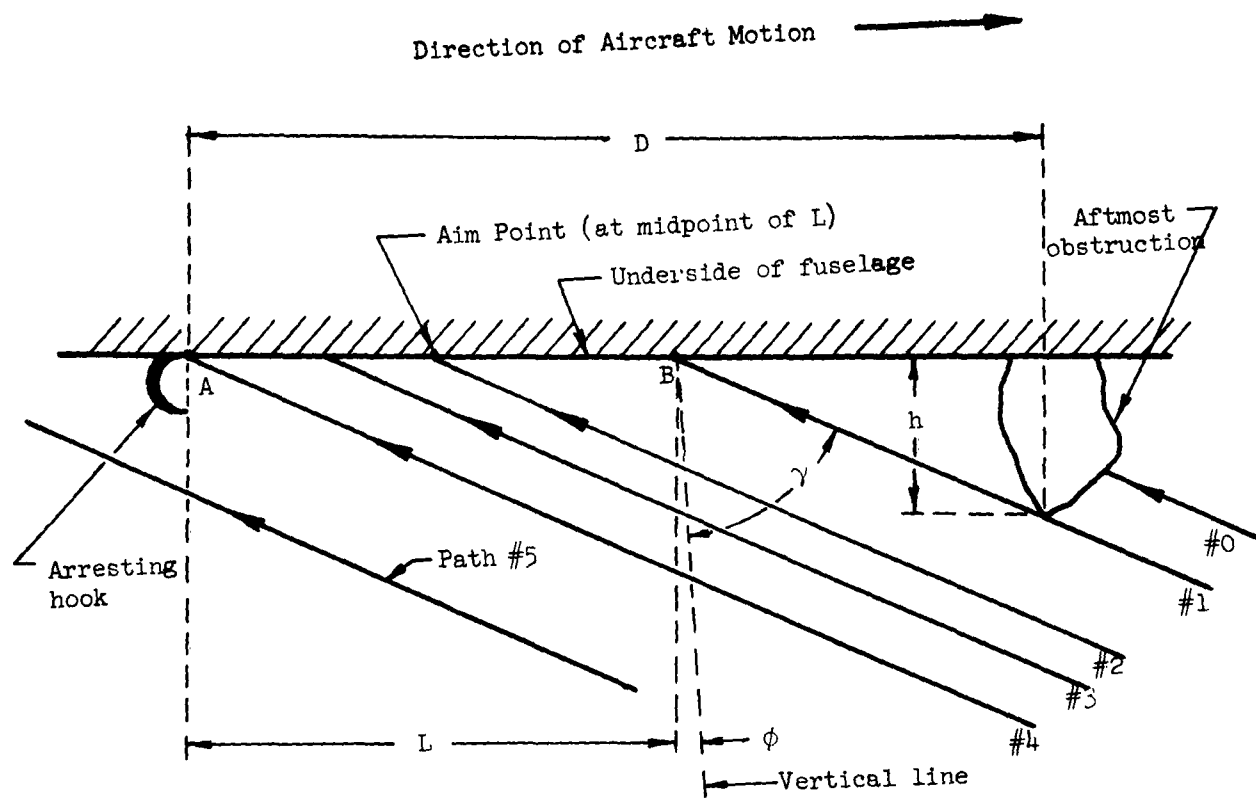


Figure 8
Space and Velocity Relations Between Aircraft and
The Deck Pendant Just Before Impact

a few more terms.

It was stipulated in Sec. (3.3) that "the aircraft must snag the cable while it is still rising". The justification for this requirement becomes evident after this consideration: from Fig. (8a, b) it is seen that when a rising cable impinges upon the aircraft, the impact takes place on the belly of the aircraft. If the interception were to take place when the cable has already passed its zenith and is descending (such as at point 2 in Figure 5), it is evident that the cable then would land on top of the aircraft. The desirability of such a case is highly questionable, so that the assumption that the cable must hit the aircraft from below seems quite reasonable. Hence, the requirement that the interception take place before the cable has reached its zenith.

Since the arresting hook and the associated cable impact area must be on the underside of the aircraft, such a general picture is shown in Figure (8a).

From the velocity diagram in Figure 8 it can be seen that so long as the aircraft velocity $V (= \sqrt{\dot{x}_T^2 + \dot{z}_T^2})$ at $t = \tau$ is greater than the cable velocity $T (= \sqrt{\dot{x}_T^2 + \dot{z}_T^2})$ at $t = \tau$, then the cable will approach the aircraft with a relative velocity V_r that is directed upward and rearward at an angle γ , called the angle of incidence (see Figure 8a and 8b). The cable impacts the aircraft fuselage at an angle $(\gamma + \phi)$, then after impact it slides along the belly of the fuselage till it hits the arresting hook and becomes lodged there. With this event the interception phase of the arrestment is completed. This event marks the end of the time interval for which the equations of motion were defined.

3.6.3.1 Conditions for Interception

For the interception to be successful the cable has to approach the aircraft in such a manner that it strikes the belly of the aircraft any-
where forward of the hook and aft of the aftmost obstruction *). Fig. (8a)

*) Aftmost obstruction - anything significantly protruding from the smooth underside of the fuselage and wings, such as the landing gear, for instance

illustrates the impact region AB with its associated cable approach paths (Paths #1 thru #4), as well as two typical approach paths exemplifying unsuccessful interception.

In Fig. (8a) the angle of incidence γ is determined from the velocity diagram Fig. (8b) - any cable approach path has the same direction as the relative velocity V_R at the time $t = \tau$. If the cable approaches along any path between the two extremes #1 and #4, then it is snagged by the hook and the interception is successful. If it approaches along a path such as #0, then it hits the aftmost obstruction, most probably with disastrous results. If the cable approaches along a path such as #5, it misses the hook completely so that the aircraft continues on its course unhindered.

Since the aircraft trajectory at $t = \tau$ will in general be almost horizontal (ϕ very small in Fig. 8b) and the cable velocity T will always be lower than the aircraft velocity V , then it is seen from Fig. (8b) that the relative velocity V_R (cable velocity at impact) will always be directed upward and rearward, thus making the angle of incidence γ always less than 90° in the direction shown in Figure 8a. This angle γ together with the height of aftmost obstruction h and the horizontal distance D (between the hook and obstruction) determines the length of impact region L for any particular aircraft, as follows:

$$L = D - h \tan (\gamma + \phi) \quad (3.7)$$

where

$$\tan (\gamma + \phi) = \left(\frac{\dot{x} - \dot{\xi}}{\dot{z} - \dot{\zeta}} \right)_{t = \tau}$$

so that finally

$$L = D - h \left(\frac{\dot{x} - \dot{\xi}}{\dot{z} - \dot{\zeta}} \right)_{t = \tau} \quad (3.8)$$

From the above it can be observed that L is not a unique quantity for a given aircraft because it also depends upon the velocities of the aircraft and the cable. This means that the aim point (defined as the midpoint of the impact region AB) is not a fixed point on the aircraft.

3. 6. 3. 2 Range of L and Location of Aim Point

As can be seen in Fig. 8a, the L can range from zero (when γ is approximately equal to $\arctan D/h < 90^\circ$, which in terms of velocities means that T is small in comparison to V) to almost $L = D$ (when γ is almost zero, which in terms of velocities means that $\dot{x}_T = \dot{\xi}_T$). Thus the aim point can lie anywhere between the hook and the midpoint of distance D .

3. 6. 3. 3 Meaning of L and Aim Point

The quantity L as given by Eq. (3. 7) defines a region on the fuselage belly such that if the cable impacts the fuselage inside this region, interception is insured; if outside this region - no interception takes place. The midpoint of L defines the position of an imaginary point on the aircraft - the aim point - whose x and z -coordinates were employed in Sec. (3. 5. 1. 1) to specify the aircraft position by means of the equations of motion, Eq. (3. 1).

Large values of L mean that the "aiming" problem is not as difficult, because a large "target area" (impact region) permits greater deviations from the "bull's eye" (the aim point in our case). And a large L means that the angle of incidence must be small, and this in turn means that the cable velocity must be high relative to the aircraft velocity (see Fig. 6b)

3. 6. 4 Method of Approach to Solution

In the previous discussion the conditions for interception were defined as being the requirement that when $z_T = \zeta_T$, then also x_T must be equal to ξ_T at some time $t = \tau$. This, however, is a very stringent physical requirement

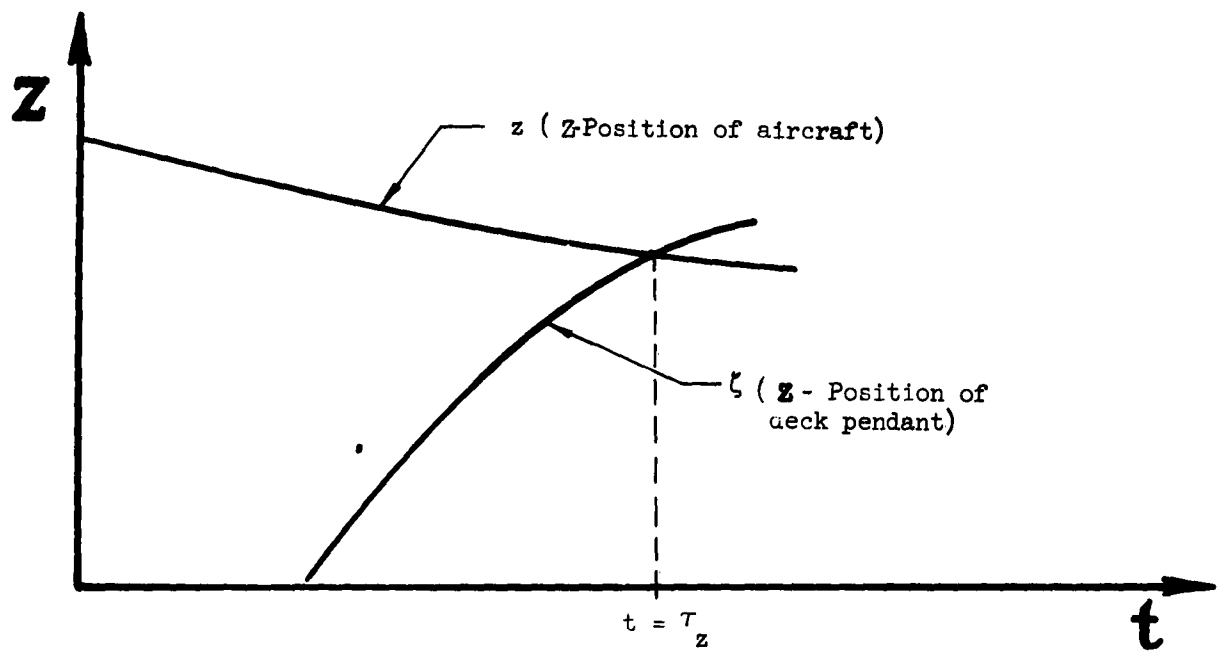
(but more easily solved analytically), and it implies a "perfect", or theoretical interception (it is sort of a "bull's eye" hit, in this case the "bull's-eye" being a point). A less stringent physical (but more difficult analytically) condition would be as follows: when $z_{\tau} = \xi_{\tau}$, then $x_{\tau} = \xi_{\tau} \pm \Delta x$ where Δx is any specified, small quantity. It is this latter condition that the tolerance requirements problem is based upon, and a graphic representation of it is found in Figure 9.

In Figure 9a is shown a general case of the functions $z = g_a(t, K_i)$ and $\xi = g_c(t-T, P_i)$ plotted against t . At $t = \tau_z$ the Z coordinates are equal, which means that the cable is at the same height as the underside of the fuselage. A look at Figure 9b reveals the fact that at $t = \tau_z$, $x_{\tau} \neq \xi_{\tau}$, but differ by a small quantity Δx . The physical interpretation is this: at $t = \tau_z$, although the cable is touching the aircraft belly ($z = \xi$), the impact has not taken place at the aim point, but either forward of it ($\Delta x'$) or aft of it ($\Delta x''$), as the case may be. So long as either $\Delta x'$ or $\Delta x''$ does not exceed $L/2$, interception is successful. So here is one statement of maximum tolerance:

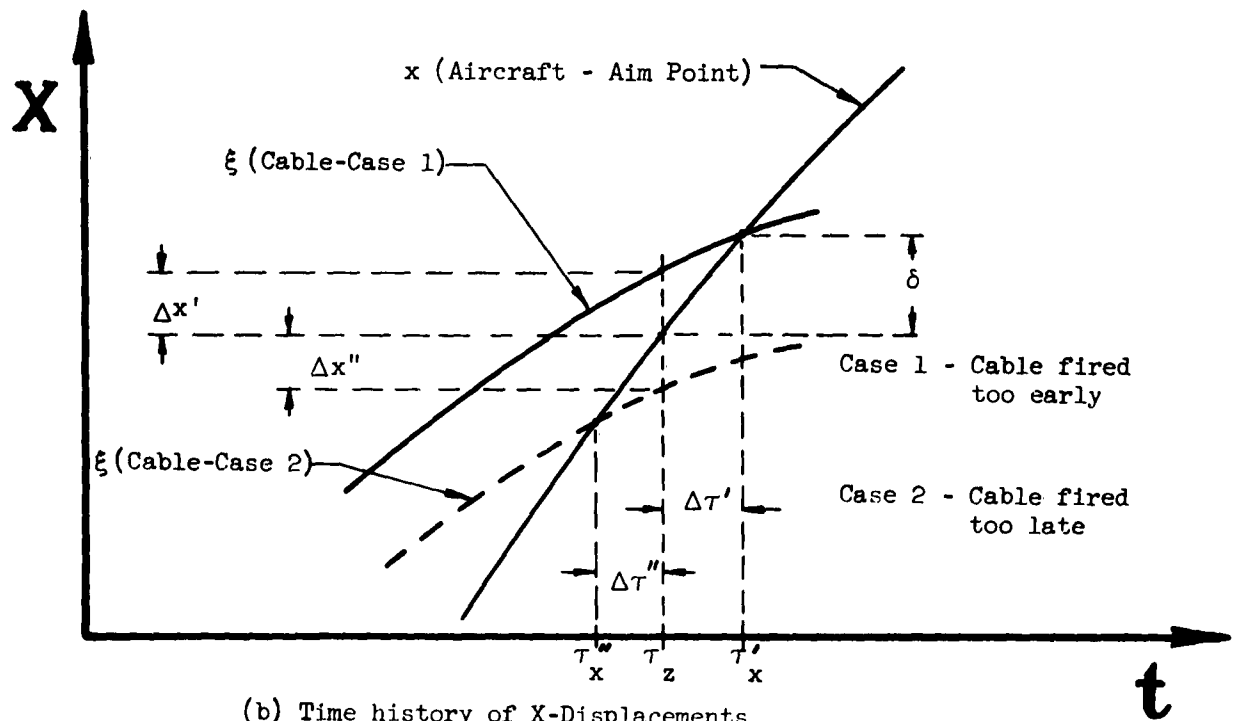
$$\Delta x < \frac{L}{2}, \text{ where } \Delta x = x_{\tau} - \xi_{\tau} \quad (3.9)$$

Investigating Figure 9b further, it can be seen that if there had been no aircraft to interfere with the motion of the cable, the cable would have been overtaken by the aim point at some later (or earlier) instant τ_x (or τ_x''). (Note that at $t = \tau_z$ the X coordinates no longer coincide). The difference between the instant when the Z -coordinates coincide ($t = \tau_z$) and the instant when the X -coordinates coincide ($t = \tau_x$) is denoted $\Delta \tau$, and called the actual timing error:

$$\Delta \tau = \tau_x - \tau_z \quad (3.10)$$



(a) Time history of Z - Displacements



(b) Time history of X-Displacements

Figure 9
Definition of Terms (Δx , $\Delta \tau$) Used In
The Timing Tolerance Problem

If this $\Delta \tau$ could be somehow related to Δx , then a way would have been found in defining the tolerance requirements. Such a relationship actually exists. Referring to Fig. 9b, and assuming that the quantities Δx and $\Delta \tau$ are small enough so that in the interval $\tau_z < t < \tau_x$ the x and ξ - curves are practically straight lines, it can be observed that the following is approximately true:

$$\delta = \frac{dx}{dt} \Delta \tau = \dot{x} \Delta \tau$$

and

$$\delta - \Delta x = \frac{d\xi}{dt} \Delta \tau = \dot{\xi} \Delta \tau$$

After elimination of δ between the two equations:

$$\Delta \tau = \frac{\Delta x}{\dot{x} - \dot{\xi}} \quad (3.11)$$

Then the maximum permissible timing tolerance will be defined as

$$\Delta \tau_p = \frac{L/2}{\dot{x} - \dot{\xi}} \quad (3.12)$$

If in Eq. (3.12) L is replaced by the expression given by Eq. (3.8) then the following is obtained:

$$\Delta \tau_p = \frac{D}{2(\dot{x}_T - \dot{\xi}_T)} - \frac{h}{2(\dot{z}_T - \dot{\xi}_T)} \quad (3.12a)$$

It is evident that for successful interception $\Delta \tau$ must always be less than $\Delta \tau_p$, or

$$\Delta \tau < \frac{L/2}{\dot{x}_T - \dot{\xi}_T} \quad (3.13)$$

3.6.5 Evaluation of the Actual Timing Error $\Delta \tau$

Assuming that the functions $\tau_x = F(p_1)$ and $\tau_z = G(p_j)$ (Eq. 3.5 and Eq. 3.6, respectively) are analytical in the region of interest, then they can be expanded in Taylor's Series about a given point, called the theoretical

point *) in this discussion. Furthermore, since for a successful interception the numerical values of τ_x and τ_z must be nearly equal, then of interest are only small variations in τ_x and τ_z . Then τ_x and τ_z may be approximated by a Taylor's series, expanded about the theoretical point. Using only first order terms, i.e. $\tau_x = \tau + \Delta\tau_x$, $\tau_z = \tau + \Delta\tau_z$ where $\Delta\tau_x$ is the total

$$\text{differential} = \sum_{i=1}^n \frac{\partial \tau}{\partial p_i} \Delta p_i$$

$$\tau_x = \tau + \frac{\partial \tau_x}{\partial T} \Delta T + \sum_{i=1}^n \frac{\partial \tau}{\partial p_i} \Delta p_i \quad (3.5c)$$

and

$$\tau_z = \tau + \frac{\partial \tau_z}{\partial T} \Delta T + \sum_{j=1}^m \frac{\partial \tau_z}{\partial p_j} \Delta p_j \quad (3.6c)$$

Here p_i, p_j = various parameters, excluding T

$$\Delta p = \begin{vmatrix} p_{\text{actual}} - p_{\text{theoretical}} \end{vmatrix}$$

and

$$\Delta T = \begin{vmatrix} T_{\text{actual}} - T \end{vmatrix}, \text{ where}$$

T - as previously defined

T_{actual} - actual delay time that occurs on a particular landing.

(So that ΔT is the result of the inability of the apparatus to exactly control the instant of pop-up).

But by definition the theoretical interception instant τ is:

$$\tau = F(p_i)_{\text{theo.}} - G(p_j)_{\text{theo.}}$$

Now, Eq (3.5c) and (3.6c) may be written in a more compact form:

$$\tau_x = \tau + \Delta\tau_x \quad (3.5d)$$

$$\tau_z = \tau + \Delta\tau_z \quad (3.6d)$$

In Sec. (3.6.4) the actual timing error $\Delta\tau$ was defined as

$$\Delta\tau = \tau_x - \tau_z \quad (3.10)$$

*) The theoretical point is that which is given by those values of the parameters p_i and p_j that are evaluated by the on-site computer.

When Eqs. (3.5d) and (3.6d) are substituted into (3.10), the τ cancels out and the following is obtained:

$$\begin{aligned}
 \Delta\tau &= \tau_x - \tau_z \leq |\Delta\tau_x - \Delta\tau_z| \leq \\
 &\leq |\Delta\tau_x| + |-\Delta\tau_z| = |\Delta\tau_x| + |\Delta\tau_z| = \\
 &= \left| \left(\frac{\partial\tau_x}{\partial T} - \frac{\partial\tau_z}{\partial T} \right) \Delta T \right| + \left| \sum \left(\frac{\partial F}{\partial p_j} \right)_{\text{Theo.}} \Delta p_j \right| \\
 &+ \left| \sum \left(\frac{\partial G}{\partial p_j} \right)_{\text{Theo.}} \Delta p_j \right| \leq \left| \left(\frac{\partial\tau_x}{\partial T} - \frac{\partial\tau_z}{\partial T} \right) \Delta T \right| + \\
 &+ \sum \left| \left(\frac{\partial F}{\partial p_j} \right) \Delta p_j \right| + \sum \left| \left(\frac{\partial G}{\partial p_j} \right) \Delta p_j \right| = \\
 &= \left| \frac{\partial\tau_x - \partial\tau_z}{\partial T} \right| |\Delta T| + \sum \left| \frac{\partial F}{\partial p_j} \right| |\Delta p_j| + \sum \left| \frac{\partial G}{\partial p_j} \right| |\Delta p_j|
 \end{aligned}$$

3.6.6 Formula for Evaluation of Tolerances

Interception in the worst possible case is certain, provided that

$$\left| \left(\frac{\partial\tau_x - \partial\tau_z}{\partial T} \right) \Delta T \right| + \sum \left| \frac{\partial F}{\partial p_j} \Delta p_j \right| + \sum \left| \frac{\partial G}{\partial p_j} \Delta p_j \right| \leq \left| \frac{L/2}{\dot{x}_\tau - \dot{\xi}_\tau} \right| \quad (3.13)$$

In the above formula the right-hand side of the inequality, namely

$$\Delta\tau_p = \frac{L/2}{\dot{x}_\tau - \dot{\xi}_\tau}, \text{ may be evaluated from the alternate form of Eq. (3.12):}$$

$$\Delta\tau_p = \frac{D}{2(\dot{x}_\tau - \dot{\xi}_\tau)} - \frac{h}{2(\dot{z}_\tau - \dot{\xi}_\tau)} \quad (3.12a)$$

An alternate, more readily usable and visualizable form of (3.13) from which the effect of small changes in the parameters can be estimated, is given below:

$$1 \geq \left| \frac{\frac{\Delta T}{L/2}}{\left(\frac{\partial\tau_x}{\partial T} - \frac{\partial\tau_z}{\partial T} \right) (\dot{x}_\tau - \dot{\xi}_\tau)} \right| + \sum_{i=1}^n \left| \frac{\frac{\Delta p_i}{L/2}}{\frac{\partial F}{\partial p_i} (\dot{x}_\tau - \dot{\xi}_\tau)} \right| + \sum_{j=1}^m \left| \frac{\frac{\Delta p_j}{L/2}}{\frac{\partial G}{\partial p_j} (\dot{x}_\tau - \dot{\xi}_\tau)} \right|$$

(3.13a)

3.6.7 Particular Example

To illustrate more specifically what is meant by the foregoing statements, the specific example of Sec (3.5.1.2) will be continued.

To repeat, in the illustrative problem the equations of motion were of the form

$$\begin{aligned}x &= \frac{1}{2} \ddot{x}_m t^2 + \dot{x}_o t \\z &= \frac{1}{2} \ddot{z}_m t^2 + \dot{z}_o t + z_o\end{aligned}\quad (3.1a)$$

and

$$\begin{aligned}\xi &= \frac{1}{2} \ddot{\xi}_m (t - T)^2 + \dot{\xi}_o (t - T) + x_o \\ \zeta &= \frac{1}{2} \ddot{\zeta}_m (t - T)^2 + \dot{\zeta}_o (t - T)\end{aligned}\quad (3.2a)$$

from which the implicit expressions for τ_x and τ_z were obtained:

$$\frac{1}{2} \ddot{x}_m \tau_x^2 + \dot{x}_o \tau_x = \frac{1}{2} \ddot{\xi}_m (\tau_x - T)^2 + \dot{\xi}_o (\tau_x - T) + x_o \quad (3.3a)$$

and

$$\frac{1}{2} \ddot{z}_m \tau_z^2 + \dot{z}_o \tau_z + z_o = \frac{1}{2} \ddot{\zeta}_m (\tau_z - T)^2 + \dot{\zeta}_o (\tau_z - T) \quad (3.4a)$$

Partial differentiation of (3.3a) leads to the expressions for $\left(\frac{\partial \tau_x}{\partial T}\right)$ and

$\left(\frac{\partial \tau_x}{\partial p_1}\right)$'s as follows:

$$\begin{aligned}\frac{\partial \tau_x}{\partial \ddot{x}_m} &= \frac{-1/2 \tau_x^2}{\nabla_1} ; & \frac{\partial \tau_x}{\partial \ddot{\xi}_m} &= \frac{-1/2 (\tau_x - T)^2}{\nabla_1} \\ \frac{\partial \tau_x}{\partial \dot{x}_o} &= \frac{-\tau_x}{\nabla_1} ; & \frac{\partial \tau_x}{\partial \dot{\xi}_o} &= \frac{(\tau_x - T)}{\nabla_1} \\ \frac{\partial \tau_x}{\partial T} &= \frac{\ddot{\xi}_m (T - \tau_x) - \dot{\xi}_o}{\nabla_1} ; & \frac{\partial \tau_x}{\partial x_o} &= \frac{1}{\nabla_1}\end{aligned}$$

where $\nabla_1 = (\ddot{x}_m - \ddot{\xi}_m) \tau_x + \dot{x}_o - \dot{\xi}_o + \ddot{\xi}_m T$

Similarly, partial differentiation of (3.4a) yields a series of analogous expressions for $\left(\frac{\partial \tau_z}{\partial T}\right)$ and the $\left(\frac{\partial \tau_x}{\partial p_j}\right)$'s:

$$\begin{aligned} \frac{\partial \tau_z}{\partial \ddot{z}_m} &= \frac{-1/2\tau_z^2}{\nabla_z} & \frac{\partial \tau_z}{\partial \ddot{\xi}_m} &= \frac{1/2(\tau_z - T)^2}{\nabla_z} \\ \frac{\partial \tau_z}{\partial \dot{z}_o} &= \frac{-\tau_z}{\nabla_z} & \frac{\partial \tau_z}{\partial \dot{\xi}_o} &= \frac{(\tau_z - T)}{\nabla_z} \\ \frac{\partial \tau_z}{\partial T} &= \frac{\xi_m (T - \tau_z) - \xi_o}{\nabla_z} & \frac{\partial \tau_z}{\partial z_o} &= \frac{-1}{\nabla_z} \end{aligned}$$

where $\nabla_z = (\ddot{z}_m - \ddot{\xi}_m)\tau_z + \dot{z}_o - \dot{\xi}_o + \xi_m T$

Substitution of the above expressions into Eq. (3.10) yields an expression for the actual timing error, where the partial derivatives were evaluated at p_i 's and p_j 's equal to their theoretical values, T = the approximate root obtained

$$\begin{aligned} \Delta \tau &= \left| \left(\frac{\partial \tau_x}{\partial T} - \frac{\partial \tau_z}{\partial T} \right) \Delta T \right| + \left| \left(\frac{\partial \tau_x}{\partial \ddot{x}_m} \right) \Delta \ddot{x}_m \right| + \left| \left(\frac{\partial \tau_x}{\partial \dot{x}_o} \right) \Delta \dot{x}_o \right| \\ &+ \left| \left(\frac{\partial \tau_x}{\partial \ddot{\xi}_m} \right) \Delta \ddot{\xi}_m \right| + \left| \left(\frac{\partial \tau_x}{\partial \dot{\xi}_o} \right) \Delta \dot{\xi}_o \right| + \left| \left(\frac{\partial \tau_z}{\partial \ddot{z}_m} \right) \Delta \ddot{z}_m \right| \\ &+ \left| \left(\frac{\partial \tau_z}{\partial \dot{z}_o} \right) \Delta \dot{z}_o \right| + \left| \left(\frac{\partial \tau_z}{\partial \ddot{\xi}_m} \right) \Delta \ddot{\xi}_m \right| + \left| \left(\frac{\partial \tau_z}{\partial \dot{\xi}_o} \right) \Delta \dot{\xi}_o \right| + \left| \left(\frac{\partial \tau_z}{\partial z_o} \right) \Delta z_o \right| \\ &\cong \left| \frac{1/2}{x_{\tau} - \xi_{\tau}} \right| \end{aligned}$$

The above expression may now be rearranged so as to assume the form of

Eq. (3.13a):

$$\begin{aligned}
 & \frac{|\Delta T|}{L_T} + \frac{|\Delta \ddot{x}_m|}{L_{\ddot{x}}} + \frac{|\Delta \dot{x}_o|}{L_{\dot{x}}} + \frac{|\Delta x_o|}{L_x} + \frac{|\Delta \ddot{\xi}_m|}{L_{\ddot{\xi}}} + \\
 & \frac{|\Delta \dot{\xi}_o|}{L_{\dot{\xi}}} + \frac{|\Delta \ddot{z}_m|}{L_{\ddot{z}}} + \frac{|\Delta \dot{z}_o|}{L_{\dot{z}}} + \frac{|\Delta z_o|}{L_z} + \frac{|\Delta \ddot{\zeta}_m|}{L_{\ddot{\zeta}}} \\
 & + \frac{|\Delta \dot{\zeta}_o|}{L_{\dot{\zeta}}} \leq 1
 \end{aligned} \tag{3.13b}$$

where the subscripted L's - called the parameter error limits - are given by the following expressions (these L's have nothing common with the L given by Eq. 3.7):

$$\begin{aligned}
 L_T &= \left| \frac{L/2}{(\dot{x}_T - \dot{\xi}_T) \left(\frac{\partial \tau_x}{\partial T} - \frac{\partial \tau_z}{\partial T} \right)} \right| \\
 L_{\ddot{x}} &= \left| \frac{L/2}{(\dot{x}_T - \dot{\xi}_T) \left(\frac{\partial \tau_x}{\partial \ddot{x}_m} \right)} \right| & L_{\dot{x}} &= \left| \frac{L/2}{(\dot{x}_T - \dot{\xi}_T) \left(\frac{\partial \tau_x}{\partial \dot{x}_o} \right)} \right| \\
 L_x &= \left| \frac{L/2}{(\dot{x}_T - \dot{\xi}_T) \left(\frac{\partial \tau_x}{\partial x_o} \right)} \right| & L_{\ddot{\xi}} &= \left| \frac{L/2}{(\dot{x}_T - \dot{\xi}_T) \left(\frac{\partial \tau_x}{\partial \ddot{\xi}_m} \right)} \right| \\
 L_{\dot{\xi}} &= \left| \frac{L/2}{(\dot{x}_T - \dot{\xi}_T) \left(\frac{\partial \tau_x}{\partial \dot{\xi}_o} \right)} \right| & L_{\ddot{z}} &= \left| \frac{L/2}{(\dot{x}_T - \dot{\xi}_T) \left(\frac{\partial \tau_z}{\partial \ddot{z}_m} \right)} \right| \\
 L_{\dot{z}} &= \left| \frac{L/2}{(\dot{x}_T - \dot{\xi}_T) \left(\frac{\partial \tau_z}{\partial \dot{z}_o} \right)} \right| & L_z &= \left| \frac{L/2}{(\dot{x}_T - \dot{\xi}_T) \left(\frac{\partial \tau_z}{\partial z_o} \right)} \right| \\
 L_{\ddot{\zeta}} &= \left| \frac{L/2}{(\dot{x}_T - \dot{\xi}_T) \left(\frac{\partial \tau_z}{\partial \ddot{\zeta}_m} \right)} \right| & L_{\dot{\zeta}} &= \left| \frac{L/2}{(\dot{x}_T - \dot{\xi}_T) \left(\frac{\partial \tau_z}{\partial \dot{\zeta}_o} \right)} \right|
 \end{aligned}$$

3.7 Discussion of the Side Drift Tolerance

The allowable tolerance in the lateral (Y) direction (the allowable side drift of the aircraft, measured from the centerline of runway) is the minimum of the following: the width of the runway, the distance between kinks in the cable (the straight portion of the deck pendant) at $t = \tau$, or the distance (at $t = \tau$) from one kink to the opposite edge of runway - if the other kink is outside, not above the runway. The actual lateral deviation (or side drift) of the aircraft - which must be less than the allowable tolerance - is equal to the following:

(The error in the final detected position of aircraft) + (the Y - component of aircraft velocity) $\times t + \frac{1}{2} t^2 \times$ (the acceleration or deceleration in the Y - direction).

3.8 Summary of Procedure Followed in Obtaining the Computed Results

The computed results plotted in the graphs of this report were obtained by following the procedure outlined below (which is identical with the procedure of the illustrative example):

1. For the equations of motion a functional form was chosen - a quadratic, in particular.
2. Particular values were assigned to the parameters (of those quadratic equations of motion) - values which were thought to be of interest.
3. The proper delay time T was found which would be required to cause impact (interception).
4. On the basis of this value of T the expected time of engagement (interception) was computed.
5. On the basis of the particular values of parameters and the resulting values of T and τ the partial derivatives with respect to parameters and to T were evaluated. The expressions that were partially differ-

entiated were the implicit equations for τ_x and τ_z .

6. Using these values of partial derivatives and the maximum permissible timing tolerance, the effects of errors in any one of the parameters as compared to the overall tolerance were calculated.
7. Specific tolerance values for different parts of the hardware can now be estimated by assigning a certain variation to the parameter(s) controlled by that particular part. The formula to be used for the evaluation of those allowable tolerance values is Eq. (3.13b) which indicates how much error in the estimated values of individual parameters can be tolerated if the aircraft is to be successfully intercepted. For instance: suppose that all of the parameters evaluated by the on-site computer are exact (i. e. if used in the equations of motion, they would exactly represent the actual motions) except for one, namely the velocity \dot{x}_0 , then for a successful interception the difference \dot{x}_0 between the exact theoretical and the actually estimated value of \dot{x}_0 must be less than the quantity L_x (from Eq. 3.13b: $\left(\frac{\Delta \dot{x}_0}{L_x}\right) \leq 1$, all the other terms vanishing

because by assumption $\Delta \ddot{x}_m = \Delta \ddot{\xi}_m = \dots, \text{etc.} \dots = 0$)

3.9 Modification of the Computational Procedure

If it is decided that the simple quadratic form for the equations of motion is a much too coarse approximation of the actual motions of aircraft and deck pendant, then a set of different, more accurate approximating functions *) may be employed. The computational procedure as given by Sec. (3.8) is not changed as a result of a different choice of functions for the equations of motion - Steps 2 thru 7 remain the same, only Step 1 should read:

*) For the definition of approximating functions, see Sec. (3.5.1).

"The functional form of the equations of motion was chosen as a power series (or Fourier series, etc., as the case may be)."

3.10 Explanation of the Curves

The data for the curves of this section was obtained by the process already outlined in Sec. (3.8) and partially illustrated in Sec. (3.5.1.2) and Sec. (3.6.7).

The optimum delay time T , time of impact τ , velocity difference at impact $V_R = \vec{V} - \vec{T} = \sqrt{(\dot{x} - \dot{\xi}_\tau)^2 + (\dot{z} - \dot{\zeta}_\tau)^2}$, and the parameter error limits L_N 's (where $N = \ddot{x}, \dot{x}, \ddot{\xi}, \dot{\xi}, \ddot{z}, \dot{z}, \ddot{\zeta}, \dot{\zeta}, x, z$) were plotted as functions of the difference in initial vertical velocities (i.e., the algebraic difference $\dot{\xi}_0 - \dot{z}_0$). The five curves on each sheet correspond (as labeled) to five different combinations of values for \dot{x}_0 , $(\dot{x}_0 - \dot{\xi}_0)$, and \dot{z}_0 . For all curves the values of the following parameters were held fixed:

$$\begin{array}{l|l} \ddot{z}_m = 5 \text{ ft/sec}^2 \text{ (rate of descent decreasing)} & \\ \dot{z}_0 = -15 \text{ ft/sec (descending)} & \dot{\xi}_m = -100 \text{ ft/sec}^2 \text{ (slowing down)} \\ \ddot{x}_m = -30 \text{ ft/sec}^2 \text{ (slowing down)} & \ddot{\zeta}_m = -80 \text{ ft/sec}^2 \text{ (slowing down)} \\ x_0 = 100 \text{ ft} & L = 5 \text{ ft } \frac{1}{\text{ft}} \end{array}$$

A note on the values of parameter z : the descent of aircraft stops as soon as its height reaches 5 ft, and from that instant on the height stays constant at 5 ft. It was assumed that by the time the belly of the aircraft has reached that height the wheels would already be on the ground. Therefore for the curves labeled $z_0 = 5 \text{ ft}$ the following is to be understood:

$$\ddot{z}_m = 0, \dot{z}_0 = 0 \text{ and } z = z_0 = 5 \text{ ft.}$$

1/ The length of successful impact region was chosen as 5 ft merely as an example. The curves of this section are still readily usable for other values of L , since the dependent variable in each case is directly proportional to L . For instance, if the actual value of L is 6.52 ft, then the corrected value for L_x will be $(6.52/5.00) \times$ (the value of L_x as read off the curves).

3.11 Conclusion

In an arresting system which is preaccelerated to engage the aircraft, there must be a rational basis on which to establish a set of tolerances on error in measurement and variation in execution. Permissible combinations of tolerances on the engaging-system parameters can be found readily from the parameter-error limits calculated according to the preceding analysis.

These error limits are essentially a set of scale factors for converting the parameter tolerances to such a dimensionless form that their sum need only be less than unity to assure engagement of the aircraft. If any one tolerance is made equal to its error limit, then its dimensionless value is unity and there remains no margin for error in any other parameter. If equal shares of the permissible total system error are allotted to the eleven parameters, each dimensionless tolerance would be one-eleventh. If any require less than an equal share, then greater tolerances are available for the others.

Parameter-error limits for five families of numerical examples are plotted in Figures 13 through 23. Examination of the curves shows that the error limits on \ddot{x} , $\ddot{\xi}$, and \ddot{z} are so generous that routine measurement or achievement of these parameters would require far less than an equal share of the permissible total system error. Error limits on $\ddot{\zeta}$ and \ddot{z} show variation by factors of 10 to 100 or more; with judicious design, the larger error limits would become applicable and these parameters also would then require less than an equal share of the permissible total system error. The most stringent tolerance requirements are on T , $\dot{\xi}$, x , $\dot{\zeta}$, z , and especially \dot{x} . However, these parameters, in comparison with the accelerations, are more easily measurable in the case of the aircraft and reproducible in the case of the cable.

Design of a system within permitted tolerances appears feasible but will require some precision equipment to assure the required accuracy of measurement and degree of reproducibility.

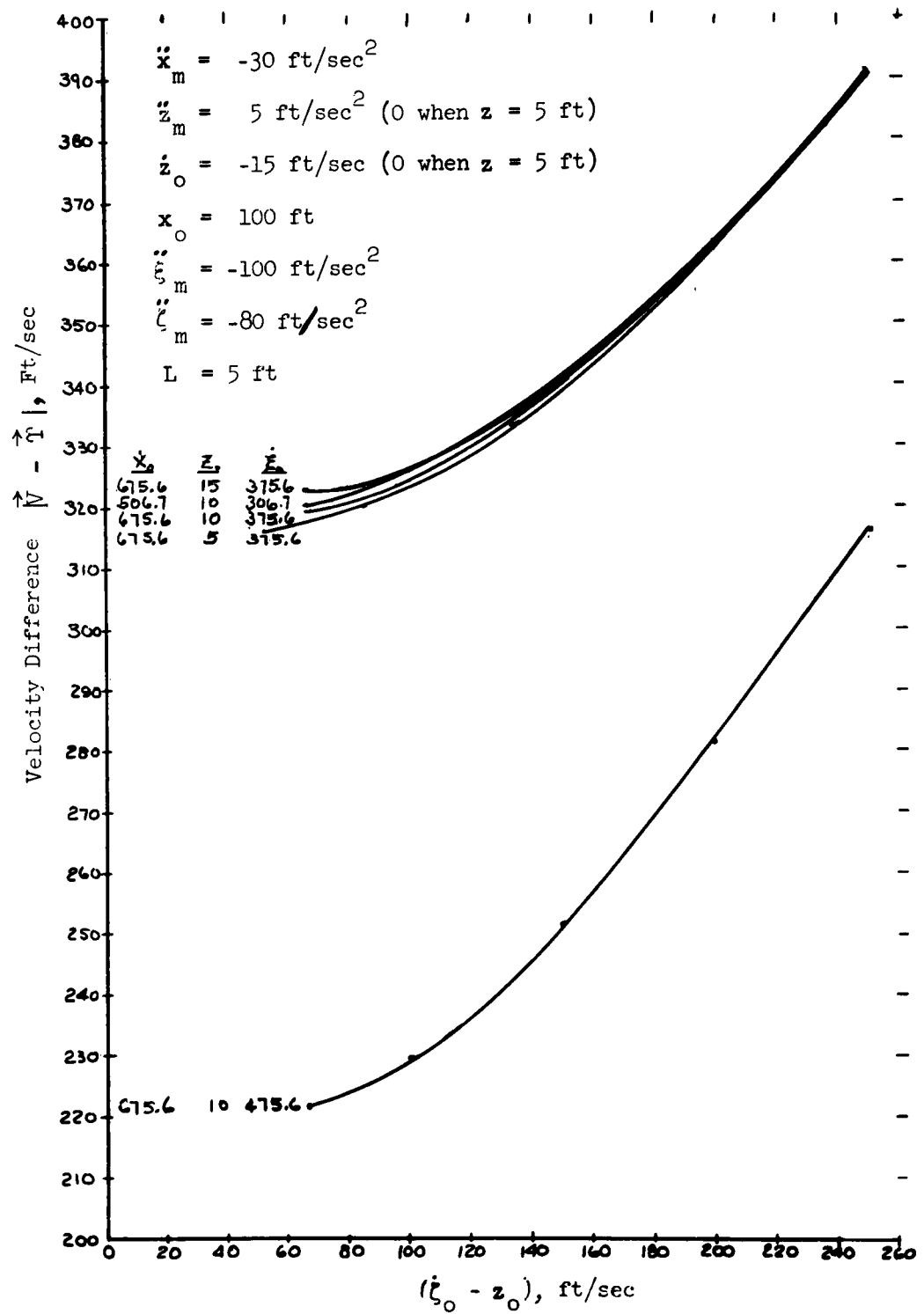


Fig. 10 Velocity Difference at Time of Impact

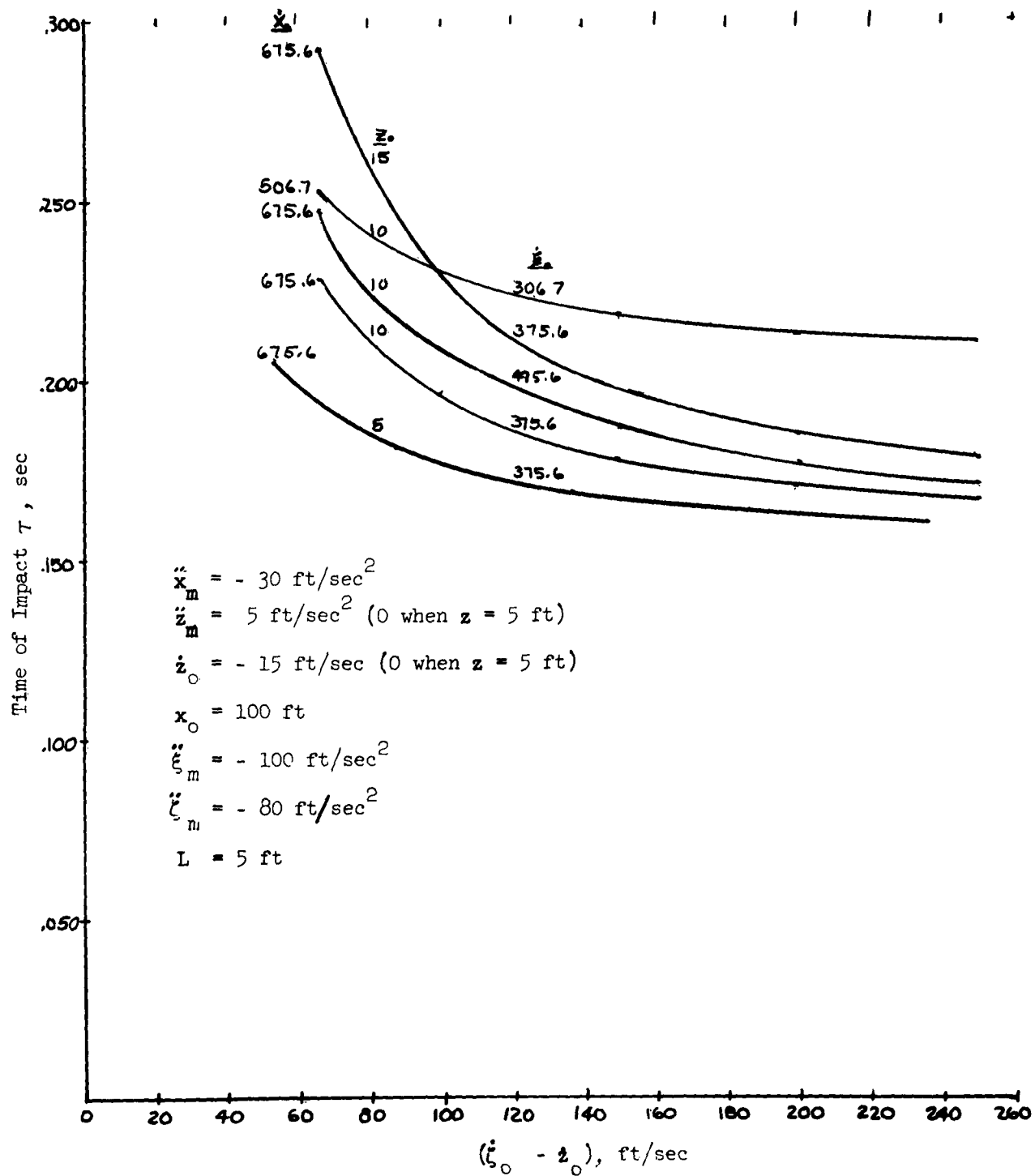


Fig. 11 Time of Impact

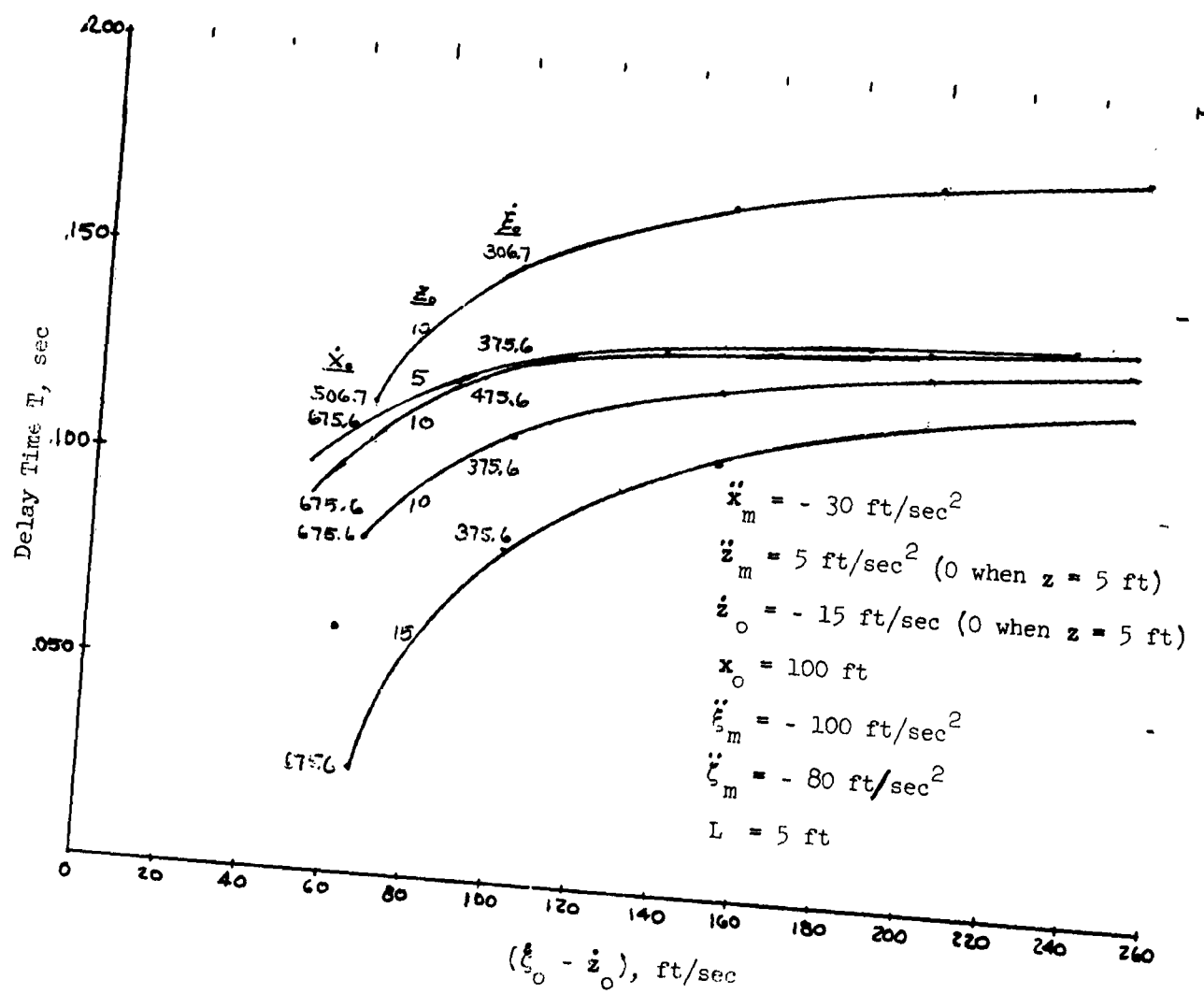


Fig. 12 Target Delay Time

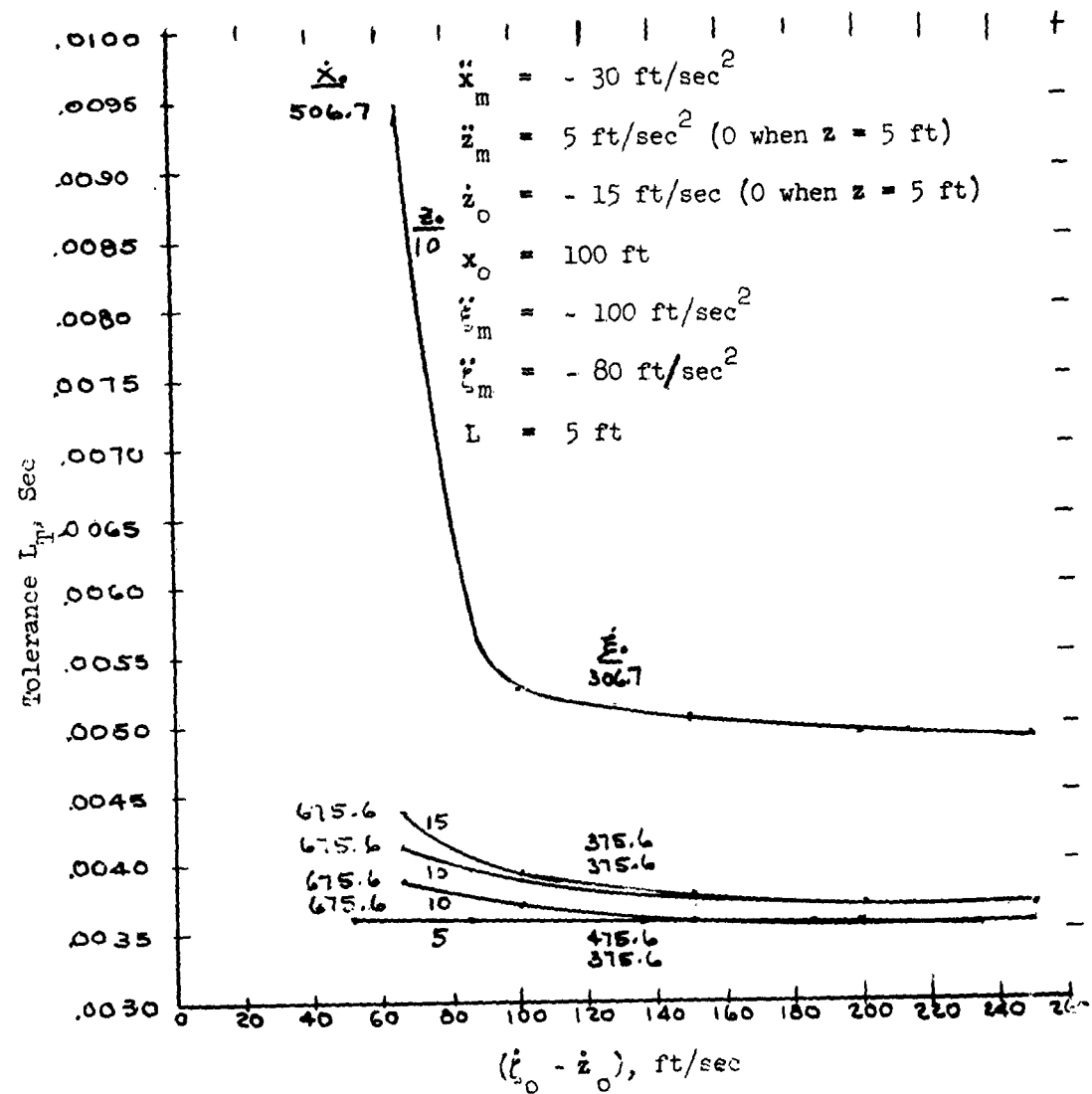


Fig. 13 Maximum Tolerance on Delay Time

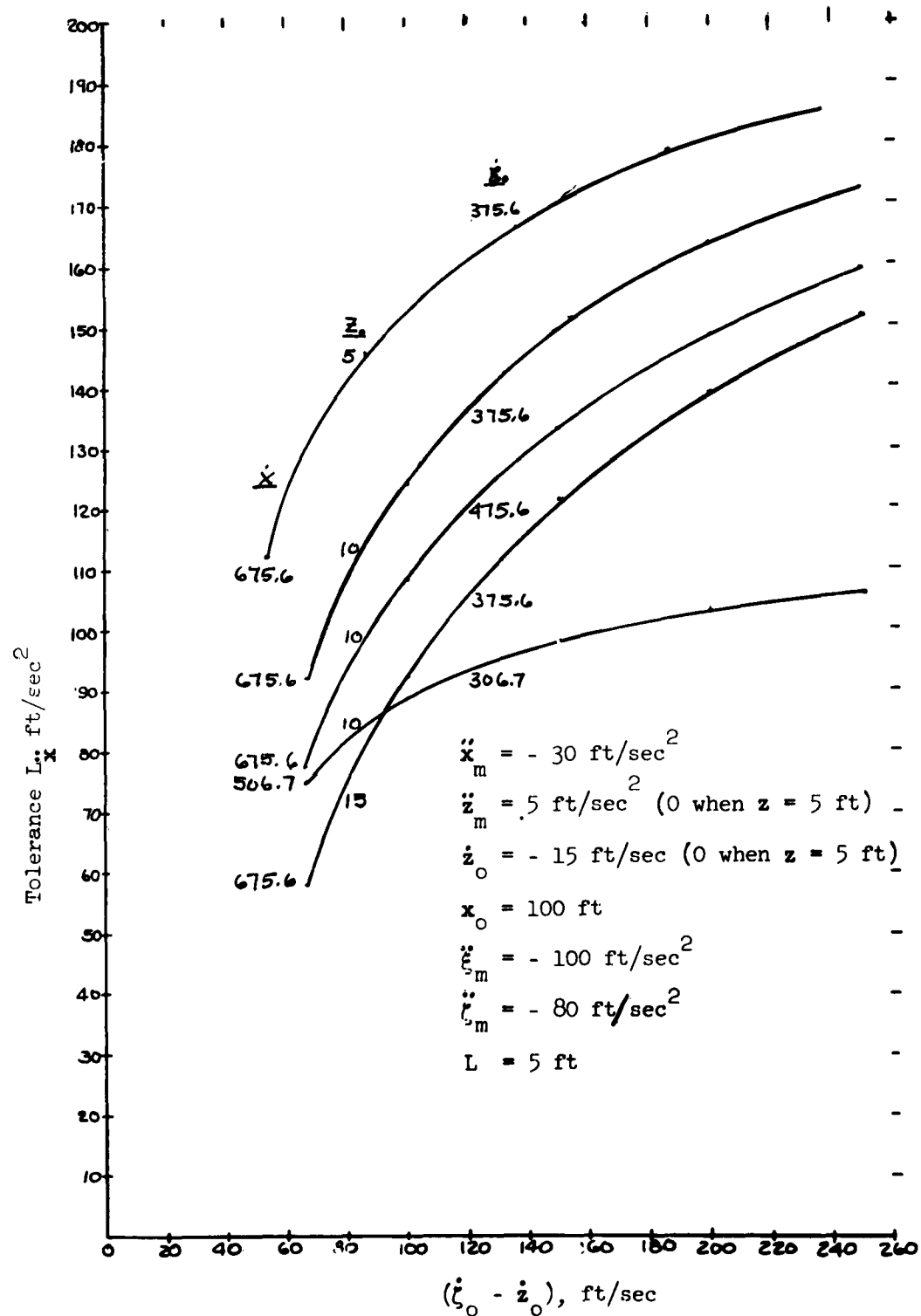


Fig. 14 Maximum Tolerance on Horizontal Component of Average Aircraft Deceleration

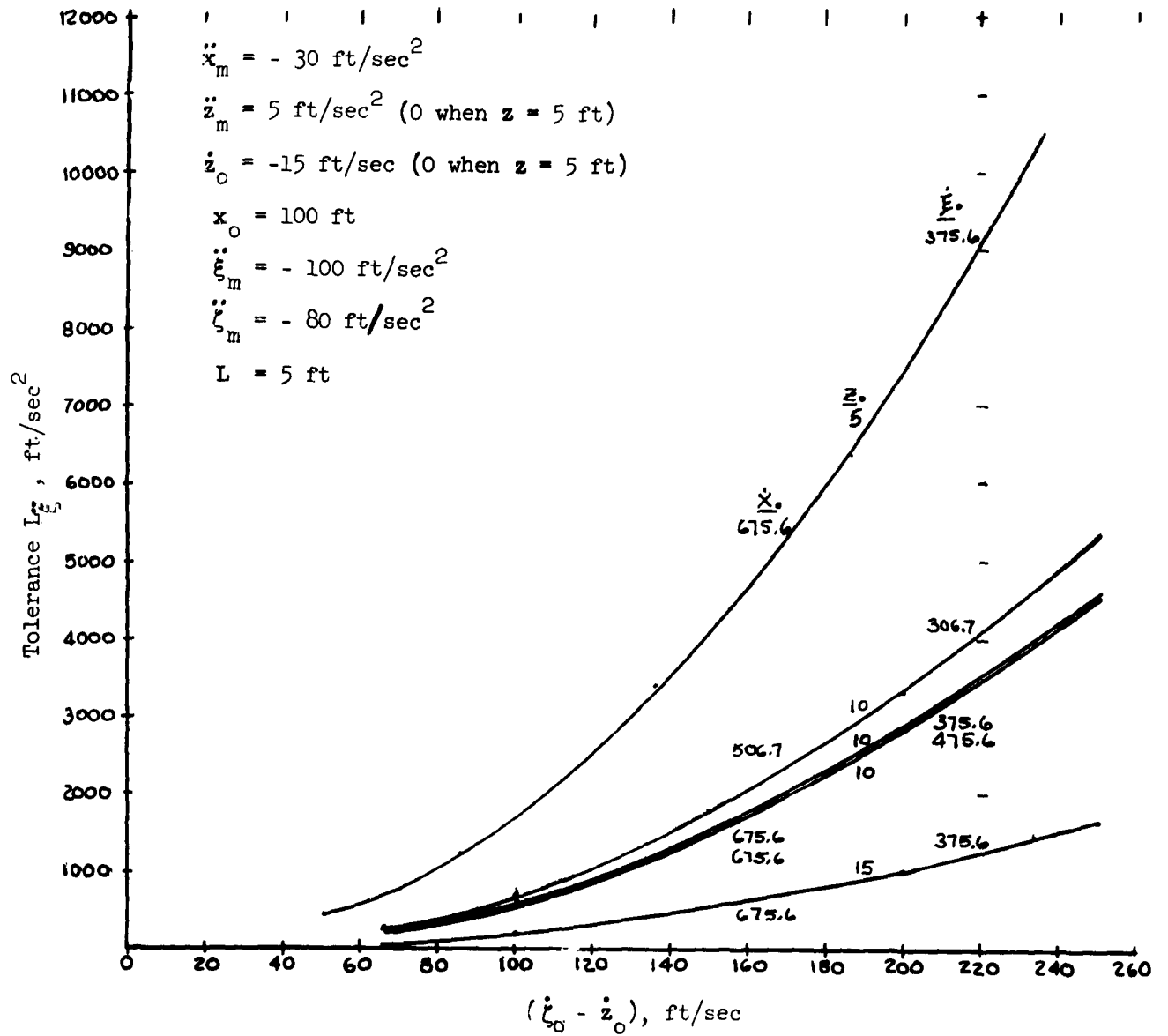


Fig. 15 Maximum Tolerance on Horizontal Component of Average Cable Deceleration

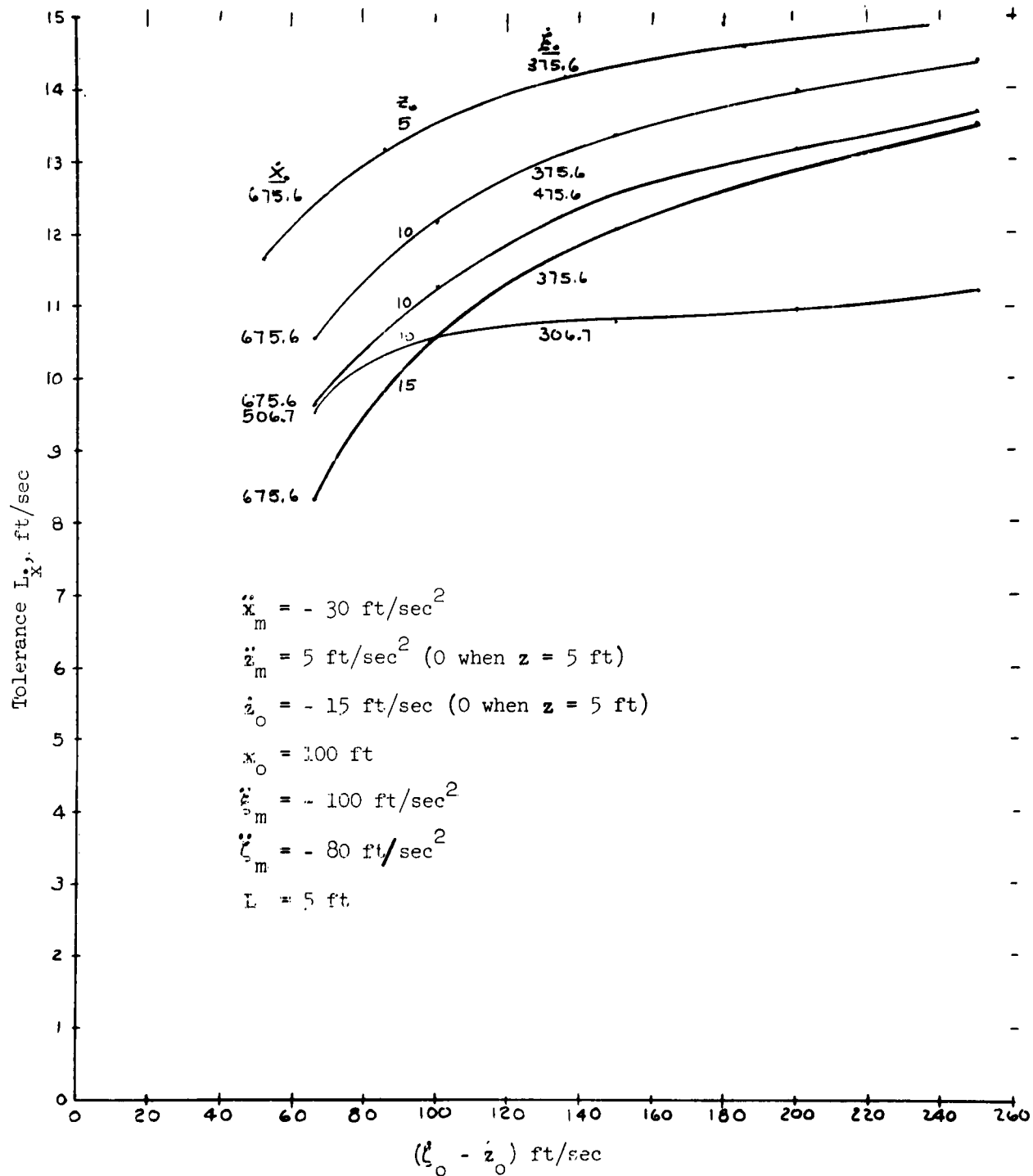


Fig. 16 Maximum Tolerance on Horizontal Component of Aircraft Velocity

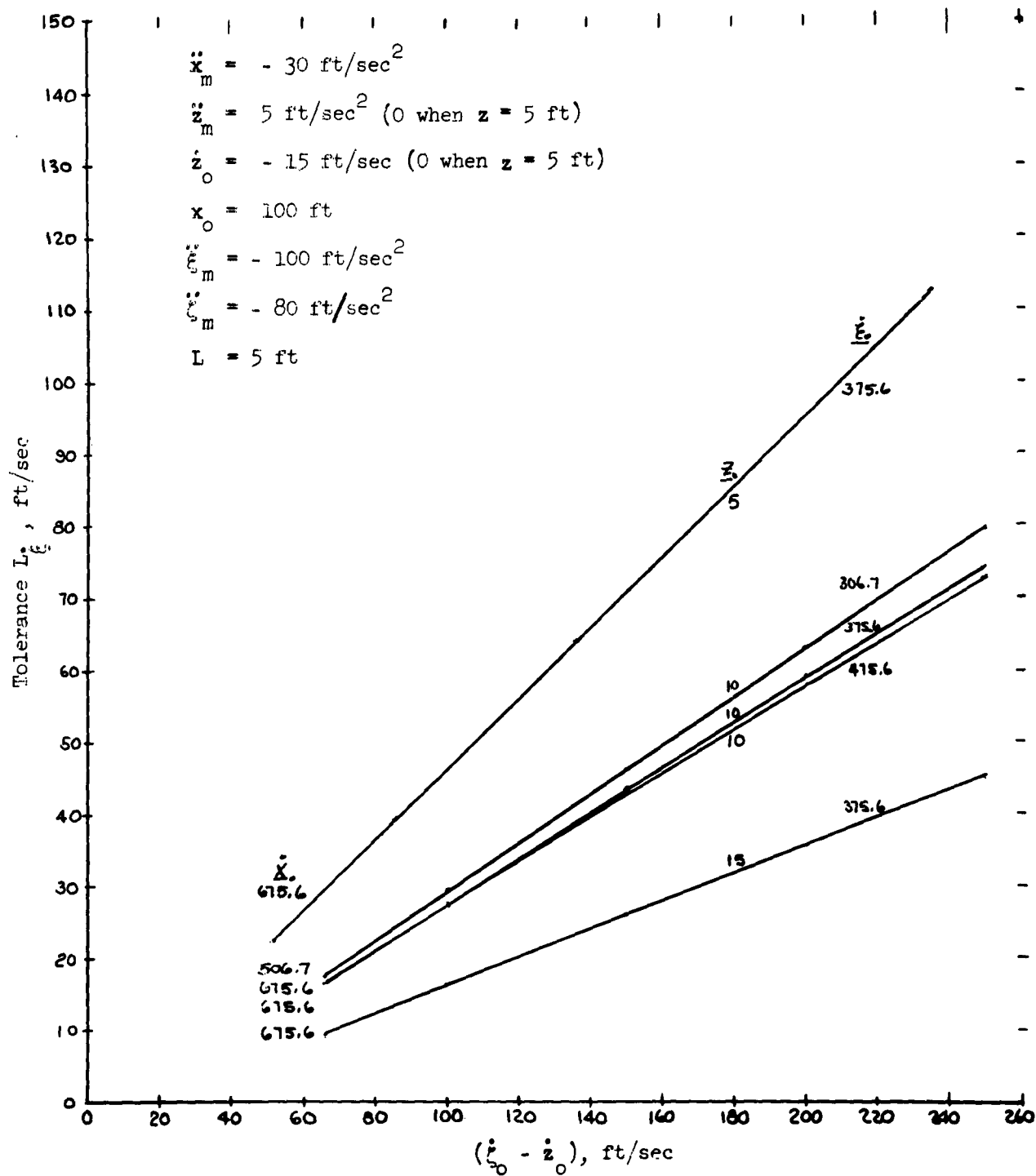


Fig. 17 Maximum Tolerance on Horizontal Component of Cable Velocity

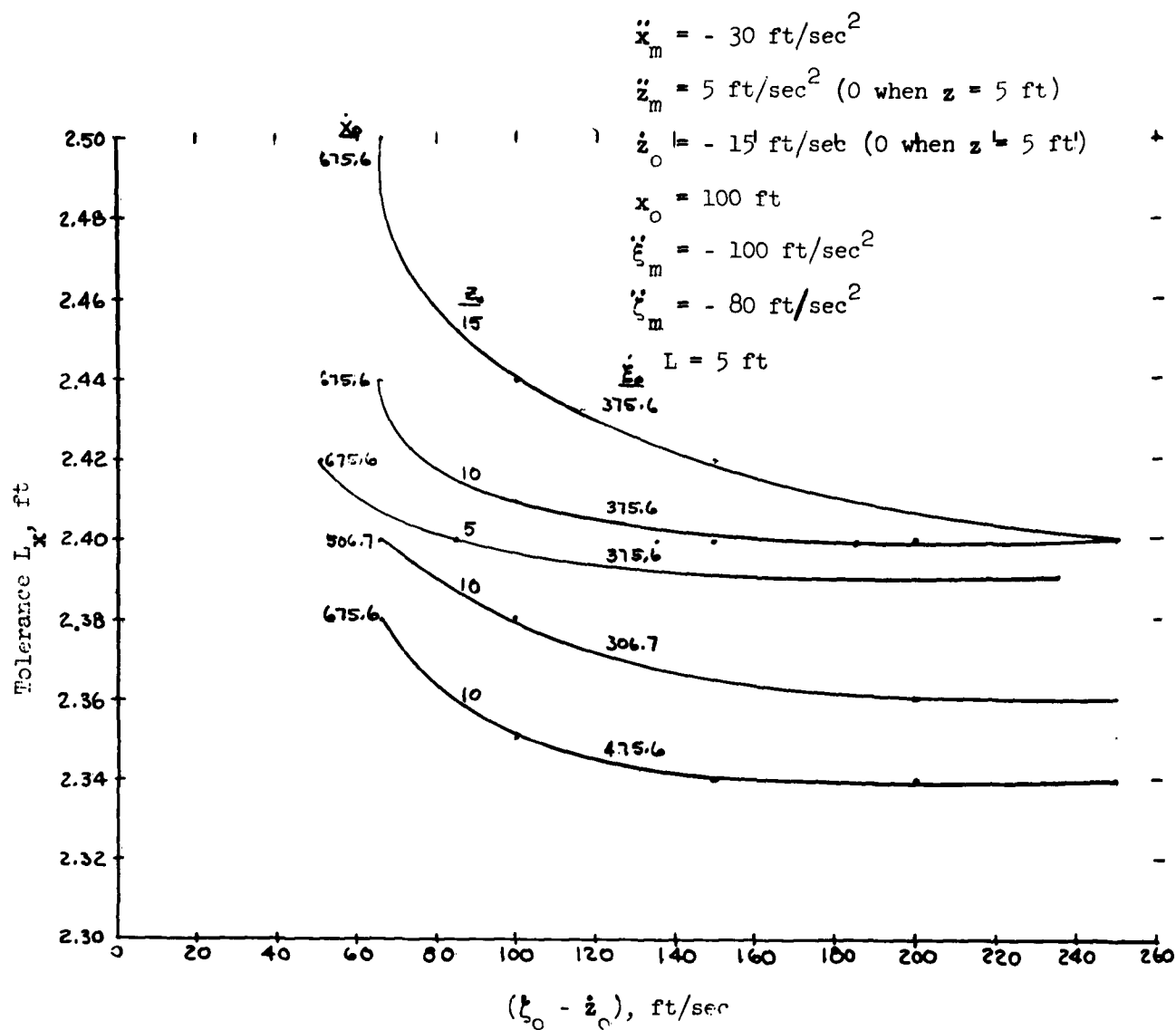


Fig. 18 Maximum Tolerance on Horizontal Position of Aircraft

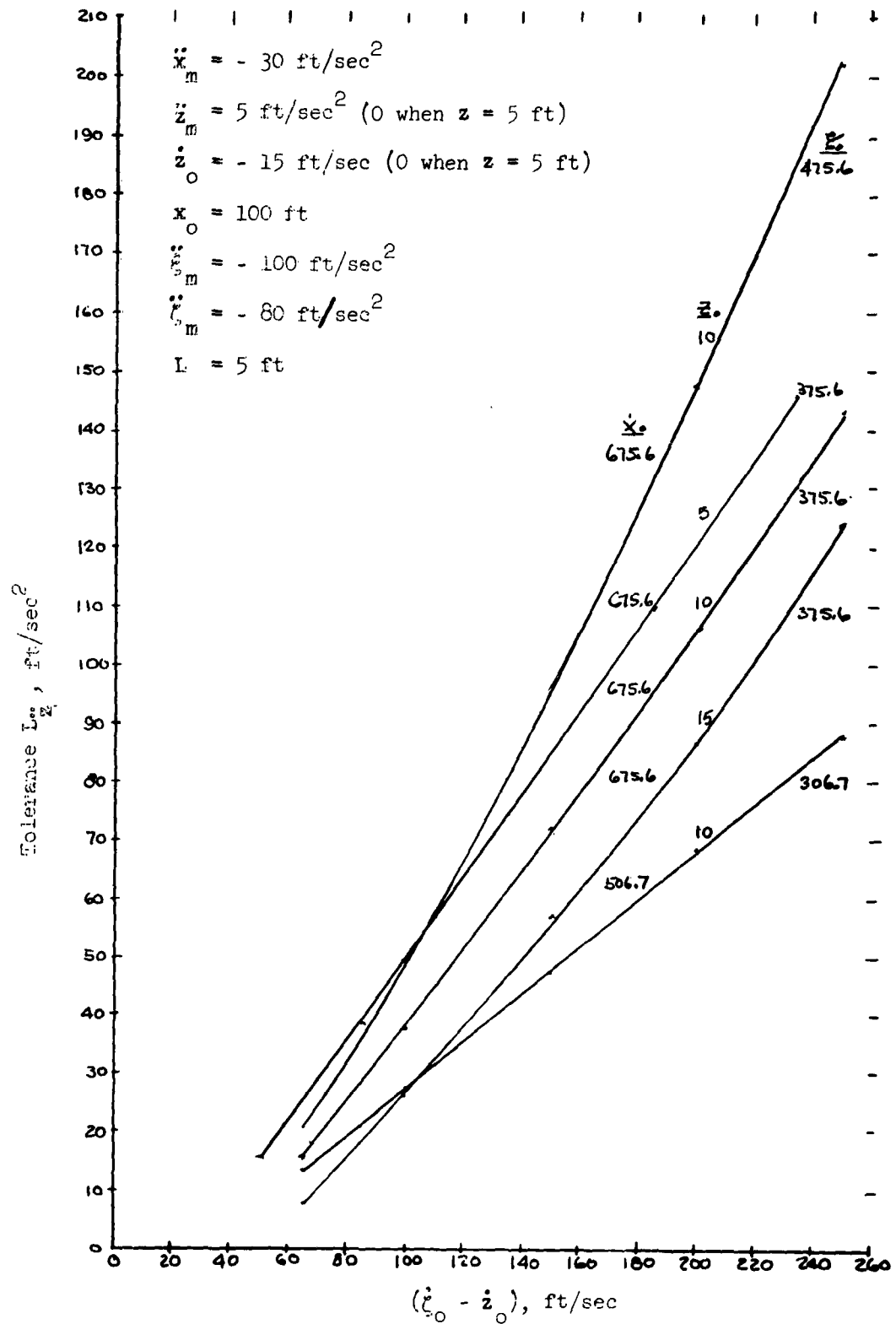


Fig. 19 Maximum Tolerance on Vertical Component of Average Aircraft Deceleration

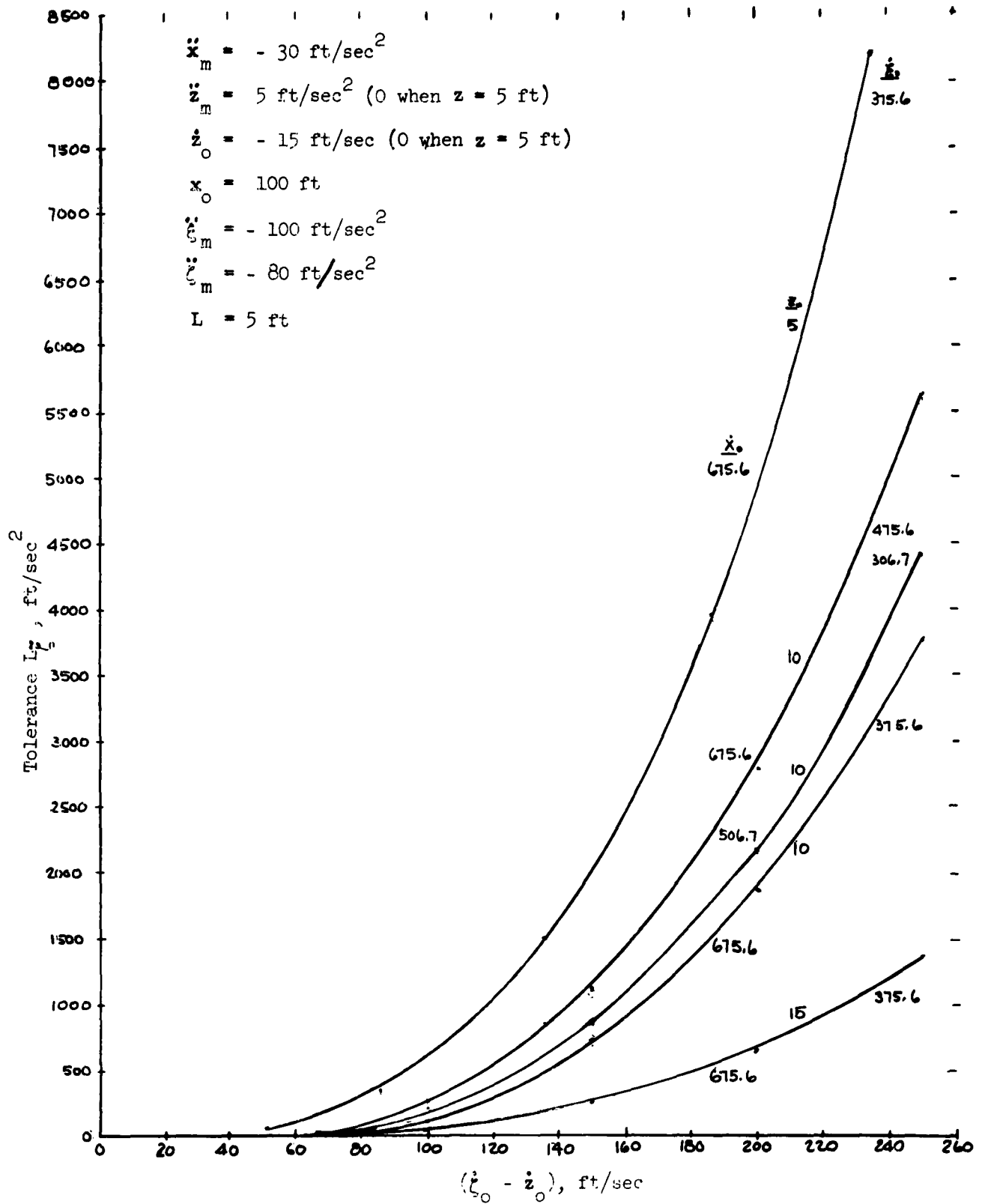


Fig. 20 Maximum Tolerance on Vertical Component of Average Cable Deceleration

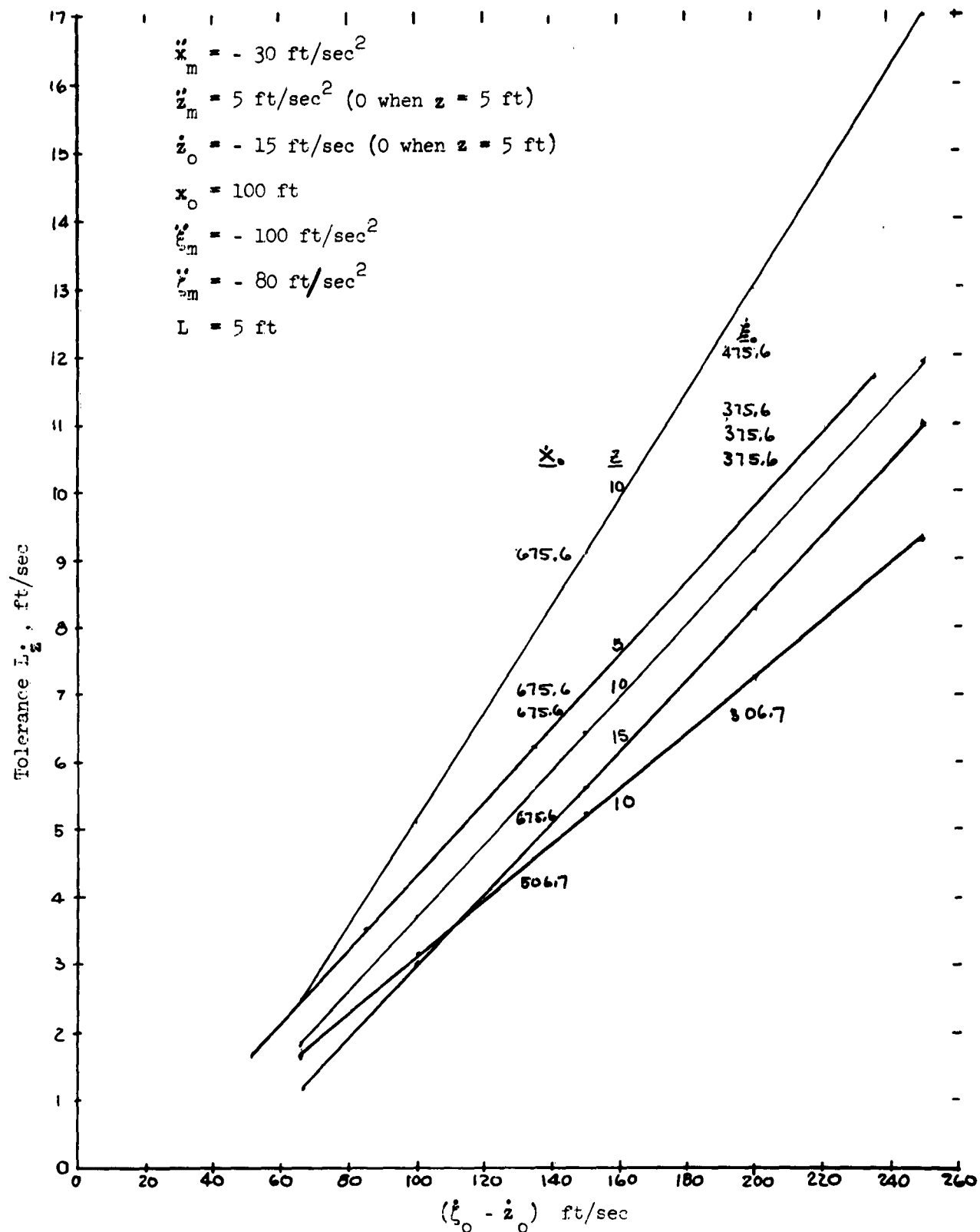


Fig. 21 Maximum Tolerance on Vertical Component of Aircraft Velocity

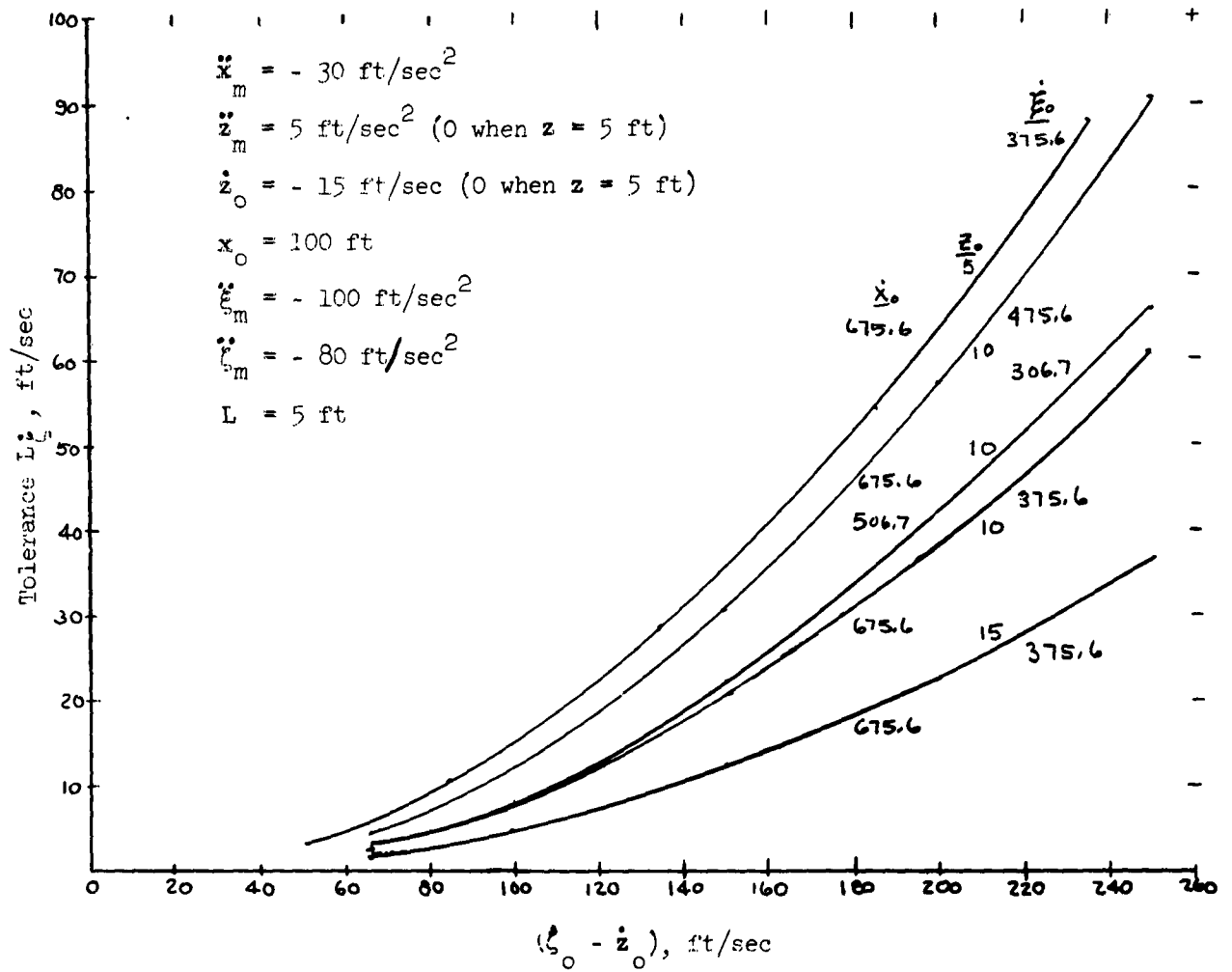


Fig. 22 Maximum Tolerance on Vertical Component of Cable Velocity

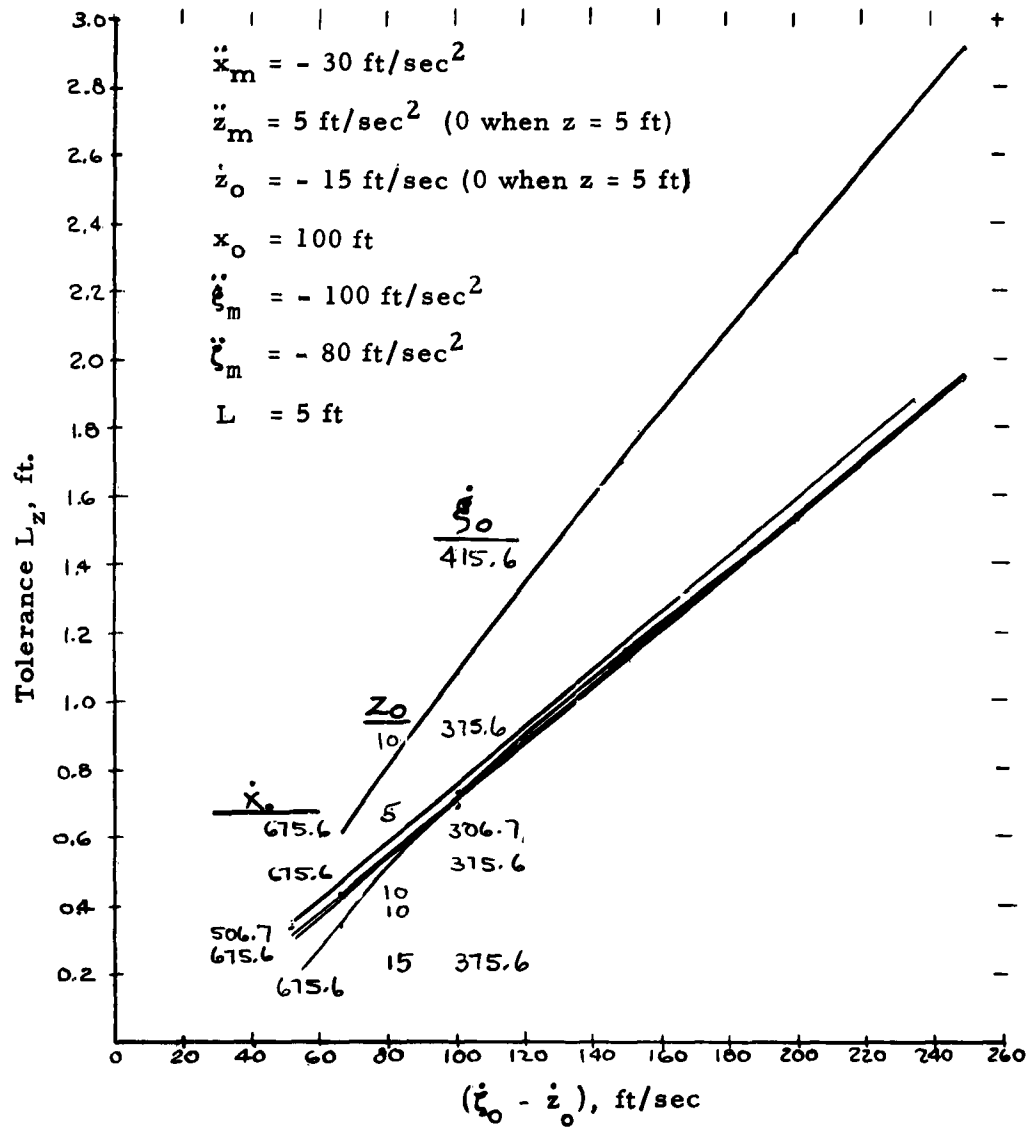


Fig. 23 Maximum Tolerance on Vertical Position of Aircraft

Notation for Section 4

AE_e	Tension member elastic modulus, pounds
AE_p	Tension member plastic modulus, pounds
c	Strain wave velocity, feet/second
\underline{c}	Strain wave velocity (unloading portion of curve), feet/second
c^*	Kink velocity relative to cable, feet/second
c_{\bullet}	Kink velocity when $c = c^*$, feet/second
C_D	Coefficient of drag per unit of wetted area of cable, dimensionless
d	Diameter of cable, inches
E	Initial stress-strain modulus (elastic) pounds/inch ²
l	Length of wetted cable, feet or inches
m	Mass of aircraft, slugs
t	Time, seconds
$U \equiv \int_0^{\epsilon} c(\epsilon) d\epsilon$, feet/second
u	Cable particle velocity, feet/second
V	Aircraft velocity, feet/second
x	Position coordinate along cable relative to hook, feet
α	Acute angle subtended by path of aircraft and cable at hook subsequent to impact, angular degrees
β	Acute angle subtended by path of aircraft and cable at hook, angular degrees
γ	Angle subtended by cable wrapped around sheave, angular degrees
$\delta u, \delta \epsilon$	Increments of cable particle velocity and cable strain, feet/second and dimensionless
ϵ	Cable strain, dimensionless
ϵ_{\bullet}	Cable strain when $c = c^*$, dimensionless
θ	Acute angle subtended by normal to aircraft path and cable, angular degrees

μ	Lineal mass density of cable, slugs/foot
ρ	Mass density of material, slugs/foot ³
σ	Stress normal to cross-section of cable, pounds/inch ²
ϕ	Kink angle, angular degrees

SECTION 4

USE OF ENERGY ABSORBING MATERIALS

In the presently employed arresting gear systems the tension member absorbs only a portion of the kinetic energy which must be dissipated after impacts, and auxiliary equipment must be used to dispose of the remaining energy. Tension members capable of absorbing the entire energy input through plastic deformation would eliminate these auxiliary devices and greatly simplify the arresting gear system. However, such members have an undesirable characteristic in that their plastic deformation process exhibits an irreversible cycle and restricts their use to a single aircraft recovery.

In addition to the energy absorption property a tension member must possess an impact tolerance associated with a free ended condition (Reference 1) such that this tolerance exceeds the required impact properties by an amount sufficient to withstand the effects of reflected wave interactions under conditions other than free ended. An energy absorbing system will involve end conditions other than free. Therefore, the strain produced by the initial impact will be augmented by the additional strains imposed through the reflections of the initial strain wave and the resulting wave interactions. The problem, then, becomes one of selecting end conditions such that the sum total of the initial and subsequent strains at any point in the tension member shall not exceed the allowable strain of the tension member.

The strain wave phenomena following impact in plastic materials are complex and not amenable to elementary solution nor reducible to the techniques presented in Reference 2 for linear materials, i. e., materials having a constant modulus of elasticity (E).

As developed in Reference 2, when the modulus of elasticity (E) in a linear material is a constant, then $c^2 = \frac{1}{\mu} \cdot \frac{dT}{d\epsilon}$ reduces to $c^2 = \frac{1}{\mu} \frac{T}{\epsilon}$ which can be written as $c^2 = \frac{1}{\rho \frac{A}{A_0}} \frac{\sigma A}{\epsilon} = \frac{1}{\rho} \frac{\sigma}{\epsilon} = \frac{E}{\rho}$ and $c = \sqrt{\frac{E}{\rho}}$ which is a constant. The cable particle longitudinal velocity u is then given as $u = c(\epsilon - \epsilon_0)$ which is essentially the linearized form of the integral $u = \int_{\epsilon_0}^{\epsilon} c d\epsilon$ with c as a constant. However, for a non-linear material, which includes the plastic materials, E is not a constant and c therefore is not a constant but depends on ϵ . The cable particle velocity is now designated as $u = \int_{\epsilon_0}^{\epsilon} c(\epsilon) d\epsilon$ and the integral must be evaluated to obtain u.

Because of the above limitations, the problem of selecting suitable end conditions was approached by first conducting a theoretical investigation of strain-wave interactions in the plastic region under conditions applicable to the present study; these solutions were then applied to specific arresting techniques to determine their practicability.

In the arresting systems studied, the performance of a specific cable for a particular aircraft weight and landing velocity is found. The methods of analysis do not lend themselves to generalized solutions and the performance of a particular technique must be found on a trial and error basis. However, an extensive computer solution in which all ranges of variables are considered,

would establish a performance envelope so that the practical limitations of any technique could be determined. It is intended in this Technical Note, to show only a specific case for a particular end condition and to indicate whether cable failure occurs before the aircraft is brought to rest.

4.1 Wave Interactions in the Plastic Region.

Wave interactions which occur in the dynamic treatment of a plastic arresting cable are formulated in this section. Although the nature of wave propagation in nonlinear media is a field which is still under current investigation, the strain levels which arise in a cable after aircraft engagement are predicted in this report by using approximate methods of solution. For example, the only type of transverse wave considered in the development of basic formulas is an isolated singularity or a kink. Actually, due to the occurrence of continuously distributed strain fields along the cable, transverse waves will eventually emerge as continuous changes in the orientation of the cable. Thus, in application of the basic formulas the principle of coincidization (formulated in Ref. 2) will often be relied upon to coalesce the total change in cable orientation to a single finite kink.

The analysis is limited to materials which exhibit a stress-strain relationship in which the curve is concave downward in the direction of increasing strain (see Fig. 24 for an example of a concave downward curve) and hence dispersion, rather than shock conditions, are present in the sections of the cable which are subjected to increasing loads.

It is further assumed that the engagement of the aircraft is symmetric with respect to the arresting cable pay-out and that deck sheaves can be adequately represented by mathematical points.

4.1.1 Propagation of Singularities

There are, in effect, two disturbances present under a transverse impact condition: a strain-wave singularity and a transverse disturbance or kink. These phenomena are analytically investigated in what follows. However, prior to the study of the various applicable cases two parameters essential to the analysis must be evaluated. These two parameters are the longitudinal particle velocity (u) and the kink velocity (c^*).

In the following formulations the positive direction for the particle velocity (u) is taken towards the right as seen by the reader. Thus the strain-velocity (ϵ, u) relationships for a leftward-running longitudinal wave is governed by the equation (see Reference 2, Appendix A)

$$\delta u = + c (\epsilon) \delta \epsilon \quad (4.1)$$

while the corresponding relation between strain (ϵ) and particle velocity (u) when the longitudinal wave is propagating in the same direction as positive cable velocity is

$$\delta u = - c (\epsilon) \delta \epsilon \quad (4.2)$$

Thus the notation is purposely chosen to be consistent with that presented in Reference 2. In the above equations, the velocity at which the disturbance

is propagated depends, of course, on the local strain differential. Integration of equations (4.1) and (4.2) over a wave front yields the relationships,

$$u_2 - u_1 = + \int_{\epsilon_1}^{\epsilon_2} c(\epsilon) d\epsilon \quad (4.3)$$

and,

$$u_2 - u_1 = - \int_{\epsilon_1}^{\epsilon_2} c(\epsilon) d\epsilon \quad (4.4)$$

To evaluate the integral $\int_{\epsilon_1}^{\epsilon_2} c(\epsilon) d\epsilon$ it is expedient to introduce a new function $U(\epsilon)$ defined by

$$U(\epsilon) = \int_0^{\epsilon} c(\epsilon) d\epsilon$$

$$\text{Thus } \int_{\epsilon_1}^{\epsilon_2} c(\epsilon) d\epsilon = \int_{\epsilon_0}^{\epsilon_2} c(\epsilon) d\epsilon - \int_{\epsilon_0}^{\epsilon_1} c(\epsilon) d\epsilon = U_2 - U_1.$$

The functions c versus ϵ and U versus ϵ can be represented graphically as shown in Figures 25 and 26 respectively.

The velocity of a transverse disturbance (kink) relative to the cable at strain ϵ and tension $T(\epsilon)$ is given in Reference 2 as

$$(c^*)^2 = \frac{T(1+\epsilon)}{\mu} = \frac{\sigma(1+\epsilon)}{\rho} \quad (4.5)$$

where μ is the mass of a unit length of the cable and ρ is the density.

Curves of $T(\epsilon)$, $c(\epsilon)$, and $c^*(\epsilon)$ for a stainless steel cable are included for illustrative purposes. These curves were previously presented as a part of Reference 1 and are reproduced here as Figures 24 and 25.

7 x 19 Stainless Steel Wire Rope

Metal Area = 1.55 in²

$\mu = 0.164$ slugs/ft

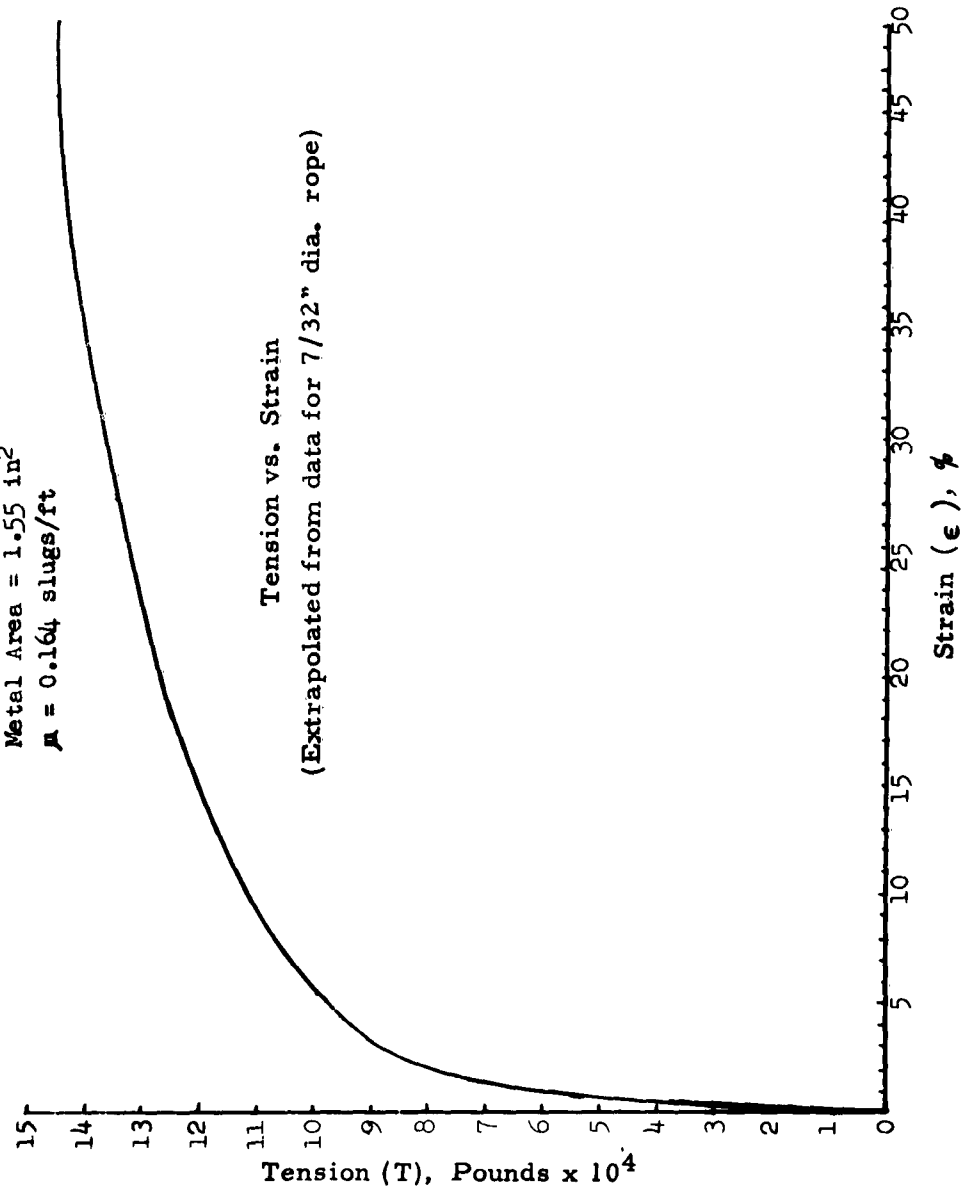


Figure 24

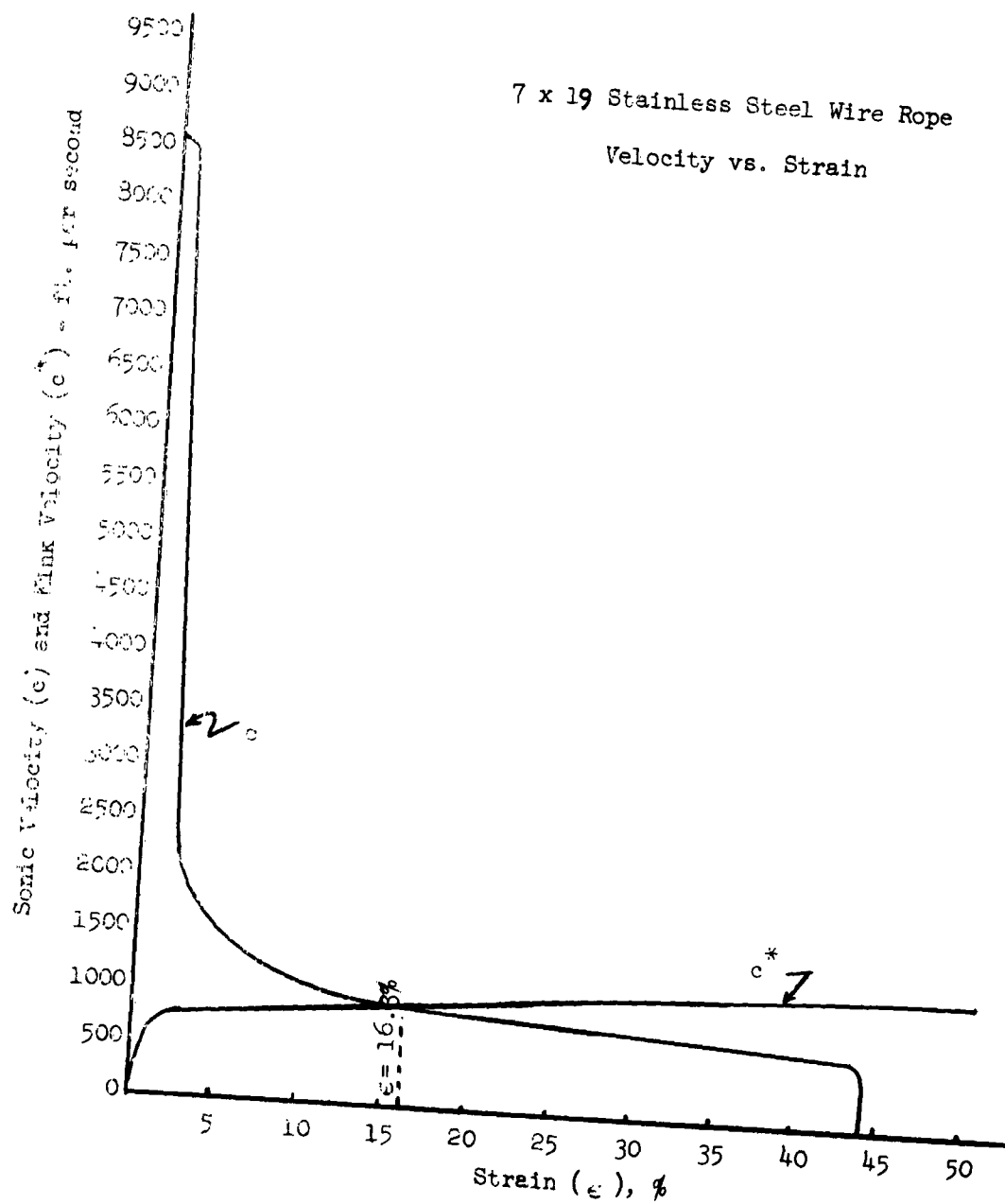


Figure 25

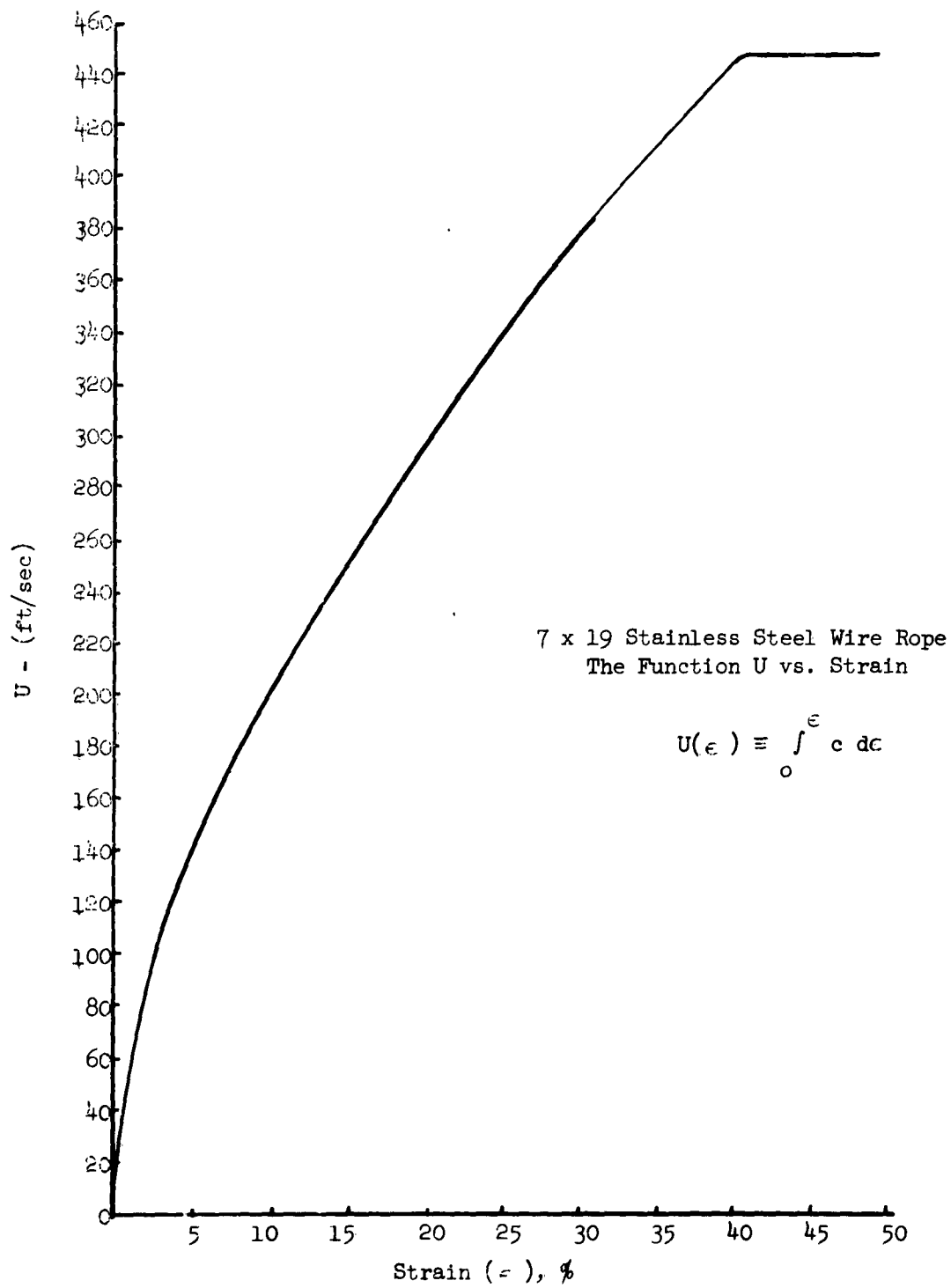


Figure 26

For the purposes of this investigation a series of cases applicable to the present study are theoretically analyzed. They are presented below as a series of individual kink and strain-wave interactions under different environmental situations. It is intended that they represent a range of conditions pertinent to the applicability studies which follow them.

4.1.2.1 Transverse Impact (Kink Lags Wave Front)

Figure 27 page 75 represents the strain levels which are present in the cable immediately after aircraft engagement. The cable is supposedly at rest ($U_0 = 0$) and at strain ϵ_0 prior to aircraft impact at a given velocity v_t . The aircraft landing path is at an angle β with the initial direction of the deck pendant. Since the distances which are depicted in the figure are given in terms of a product of velocity and a prescribed time, the figure can be considered as a velocity diagram. The wave front, W, represents a loading wave. Ahead of the front, such as point A, the cable is still undisturbed and hence is at the strain ϵ_0 and motionless ($U_0 = 0$). Behind the wave front, the uniform strain level is represented by ϵ .

Corresponding to this strain, the cable moves to the right with a velocity, u , given by equation (4.3), since $U_0 = 0$, as

$$\bar{U} - U_0 = u = \int_{\epsilon_0}^{\epsilon} c \, d\epsilon \quad (\text{see page 33 of Reference 1})$$

Because the hook is tacitly assumed to have no slippage with respect to the cable, point Q is moving away from point R with the velocity c^* . Thus the point

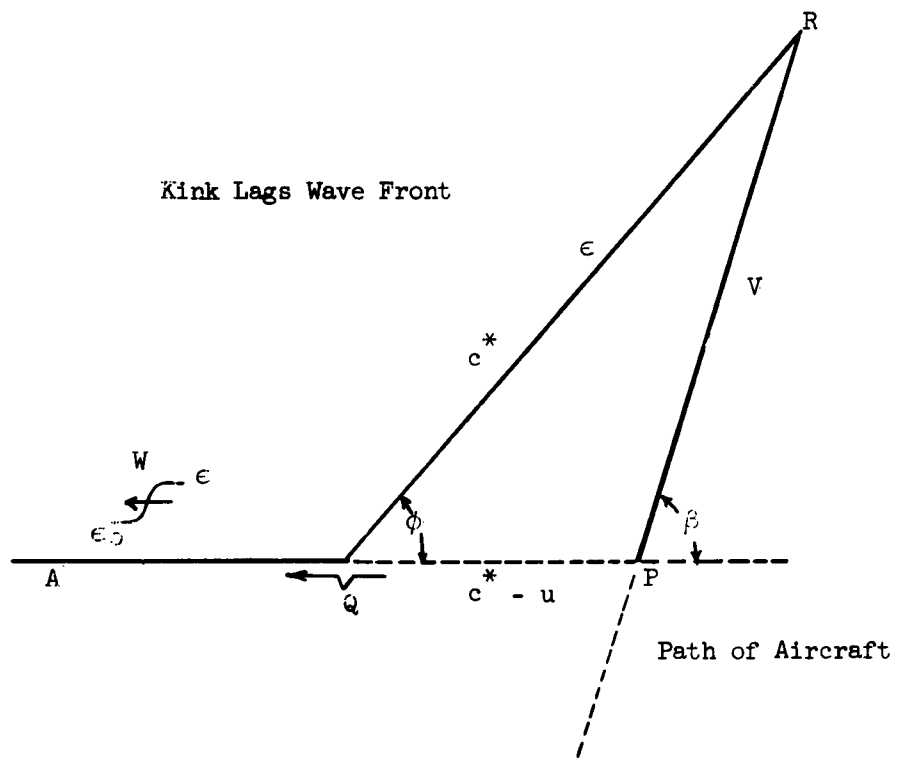


Figure 27
Velocity Diagram for Transverse Impact

Q moves away from the point of impact P with the velocity $c^* - U$ and the hook R moves away from P with the velocity V .

The sides of the velocity triangle and the angle β are related by the law of cosines,

$$(c^*)^2 = (q^* - u)^2 + V^2 + 2V (c^* - u) \cos \beta, \quad (4.6)$$

where, in view of the above velocity-strain relationship, and since c^* is given in equation (4.5) as a function of the strain ϵ , only ϵ is unknown. The c^* vs. ϵ relationship given in Equation (4.5) can be graphically represented as shown in Figure 25.

Consequently the triangle relationship can be written,

$$(c^*)^2 = (q^* - U + U_0)^2 + V^2 + 2V (c^* - U + U_0) \cos \beta. \quad (4.7)$$

In the above equation, U_0 is meant to be $U(\epsilon_0) = \int_0^{\epsilon} c \, d\epsilon$ and U denotes $U(\epsilon)$ as previously defined. The function U is not the particle velocity ahead of Q. The particle velocity is given by

$$u = \int_{\epsilon_0}^{\epsilon} c \, d\epsilon = U - U_0$$

The kink angle ϕ can be found by the law of sines,

$$\frac{\sin \phi}{V} = \frac{\sin \beta}{c^*}$$

Here we must restrict our strain such that $c(\epsilon) > c^*(\epsilon)$ so that all parts of the wave front are travelling faster than the kink (as indicated in the figure). If the resultant strain is high enough, then the kink will be travelling

faster than some part of the wave front for, in accordance with the assumed stress-strain relationship, c^* is a monotonically increasing function of strain while c is a monotonically decreasing function of strain. Thus at some strain, say ϵ^0 , $c^*(\epsilon^0) = c(\epsilon^0)$. In view of this last relationship, the case considered restricts ϵ to $\epsilon < \epsilon^0$. The case where $\epsilon > \epsilon^0$ is treated in the following section.

It is noted that if c_0 is assumed to be zero, then $U_0 = 0$ and the particle velocity u is equal to U . Consequently equation (4.7) reduces to

$$(c^*)^2 = (c^* - U)^2 + V^2 + 2 V^2 (c^* - U) \cos \beta ,$$

which is equivalent to equation (3.5) of Reference 1.

4.1.1.2 Transverse Impact (Kink Travels With Wave Front)

If the impact velocity is high enough, the maximum strain will be greater than ϵ^0 so that some portions of the wave front will lag behind the kink. Except for this modification, the formulation is the same as in the previous section.

The velocity diagram of Figure 28 indicates the strain field and velocities associated with particular points of the cable immediately after impact. A continuous wave front (W) of strain is formed. The lower strains propagate to the left ahead of the kink Q. Behind Q the strains continuously increase to the uniform strain ϵ . At some point of the increasing wave front, the longitudinal disturbance velocity and the kink velocity are the same, i.e., $c(\epsilon) = c^*(\epsilon)$. The strain level at this point is denoted by ϵ^0 and both $c(\epsilon^0)$ and $c^*(\epsilon^0)$ are denoted as c^0 . At every point behind the leading edge of the wave front, the cable is in motion according to equation (4.3).

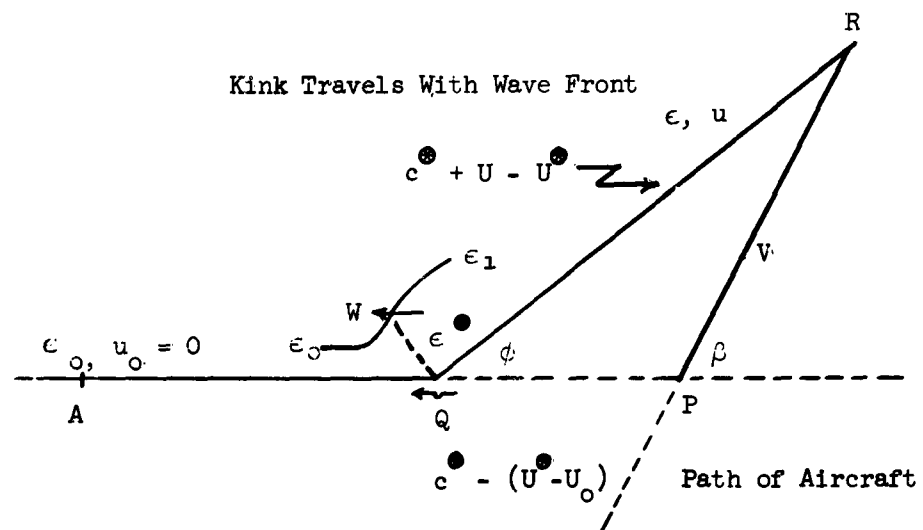


Figure 28

The component of the cable velocity along the ϕ direction and with respect to the ground is denoted by u and corresponds to the segment of the cable under a strain ϵ . Analogously, $u^\bullet = u(\epsilon^\bullet)$ denotes the cable velocity with respect to the ground at the point Q where $\epsilon = \epsilon^\bullet$. Thus the kink Q moves away from P with the velocity $c^*(\epsilon^\bullet) - u^\bullet$ or $c^\bullet - u^\bullet$. This result can also be found by realizing that the point Q is moving towards the undisturbed point A of the cable at the same rate at which it is moving away from the fixed point P . Thus, according to equation (4.3)

$$u^\bullet - u_p = + \int_{\epsilon_0}^{\epsilon^\bullet} c d\epsilon \quad \text{or} \quad u^\bullet = U^\bullet - U_0$$

in view of the initial condition that $u_0 = 0$. Since the kink is moving relative to the cable (at strain ϵ^\bullet) by the amount c^\bullet , and since the cable at Q is moving to the right relative to A by the amount of u^\bullet , the kink is approaching A with the velocity $c^\bullet - u^\bullet$ which is the same velocity by which Q separates from P .

Writing a velocity-strain relationship between points of the cable under the strains ϵ^\bullet and ϵ yields,

$$u^\bullet - u = + \int_{\epsilon}^{\epsilon^\bullet} c d\epsilon$$

according to equation (4.3). As a consequence of the postulate that $\epsilon > \epsilon^\bullet$, it is immediately deduced from the above equation that $u^\bullet < u$, that is, the cable near Q is moving away and to the left with respect to points of the cable under the strain ϵ . Thus the velocity at which Q separates from point R is given by

$$c^\bullet + (u - u^\bullet)$$

Again, to exhibit the dependence of u and therefore $u - u^\bullet$ upon the strain, the velocity can be written as

$$c^\bullet - \int_{\epsilon}^{\epsilon^\bullet} c \, d\epsilon = c^\bullet + U - U^\bullet$$

These velocities are shown in the diagram of Figure 28. Using the law of cosines yields an equation in the unknown strain ϵ ,

$$(c^\bullet + U - U^\bullet)^2 = v^2 + [c^\bullet - (U^\bullet - U_0)]^2 + 2v [c^\bullet - (U^\bullet - U_0)] \cos \beta \quad (4.8)$$

For the case where $\epsilon_0 = 0$, the function U_0 vanishes, and as a consequence $u^\bullet = U^\bullet$ and $u = U$. Thus the above equation becomes

$$(c^\bullet + u - u^\bullet)^2 = v^2 + (c^\bullet - u^\bullet)^2 + 2v (c^\bullet - u^\bullet) \cos \beta$$

which is equivalent to Equation (3.6) of Reference 1.

The kink angle ϕ can be found from the law of sines for triangle QRP:

$$\frac{\sin \phi}{v_t} = \frac{\sin \beta}{c^\bullet + U - U^\bullet}$$

4.1.3.1 Kink Impact Against Sheave (Reflected Kink Lags Wave Front)

When a kink encounters a sheave (which is assumed frictionless) a new strain ϵ is propagated from the point of impact. The corresponding strain-wave front is propagated without hindrance around the sheave as are all longitudinal type disturbances. Figure 29 illustrates the conditions at the sheave just before, and just after impact.

Initially, the cable is moving clockwise around the sheave with a velocity u_1 and a strain ϵ_1 as illustrated in the small diagram of Figure 29. A kink K,

•

with angle θ_1 approaches the sheave. Since the kink is travelling under a strain of ϵ_1 , the kink approaches the fixed point P with velocity $c_1^* - u_1$.

The large diagram represents the situation just after impact. Two new strain waves are created and travel away from the sheave and a new kink Q moves away from the sheave. Behind the waves W and W' the strain is denoted by ϵ . The cable in front of each wave is as yet unaffected and hence the strain is still ϵ_1 .

The projection R of the unaffected cable is a continuation of the motion K. Thus R separates from P with velocity $c_1^* - u_1$.

Since Q is travelling under a strain ϵ_1 , the velocity of the kink with respect to a point of the cable along \overrightarrow{PQ} is given by c^* . If the new cable velocity around the sheave is denoted by u , then $c^* + u$ is the velocity by which Q moves away from the sheave. But according to equation (4.3) and by considering strain-velocities across W',

$$u = u_1 + \int_{\epsilon_1}^{\epsilon} c \, d\epsilon$$

$$u = u_1 + U - U_1$$

Hence \overrightarrow{PQ} represents the velocity

$$c^* + u_1 + U - U_1$$

With respect to the unaffected cable in front of W, the projection R has the velocity c_1^* . Between points of the cable just behind and just before the front W there exists a relative velocity. If u' and u'_1 denote the components of cable velocity just behind and just ahead of the front W,

$$u' - u'_1 = - \int_{\epsilon_1}^{\epsilon} c \, d\epsilon$$

which is in accordance with equation (4.4). Since $\epsilon > \epsilon_1$, it is noted that $u' < u'_1$. Physically, points behind W move down and to the left relative to points just ahead of W. Therefore Q approaches unaffected points ahead of W with velocity $c^* - (u'_1 - u')$. Hence R and Q separate with velocity

$$c_1^* + q^* - \int_{\epsilon_1}^{\epsilon} c \, d\epsilon$$

or

$$c_1^* + q^* - U + U_1,$$

as shown in the velocity diagram.

By the use of the cosine law for triangle RPQ, an equation is obtained in terms of the single unknown strain ϵ which can be solved numerically:

$$\begin{aligned} \left[c^* + u_1 + (U - U_1) \right]^2 &= (c_1^* - u_1)^2 + (c_1^* + c^* - U + U_1)^2 \\ &- 2 (c_1^* - u_1) (c_1^* + c^* - U + U_1) \cos \phi_1 \end{aligned}$$

The new kink angle, ϕ , can be found from the law of sines:

$$\frac{\sin \phi}{c_1^* - u_1} = \frac{\sin \phi_1}{c^* + u_1 + (U - U_1)}$$

As a consequence of representing the wave front W in front of the kink Q, it can be tacitly assumed that in the above formulation the new strain ϵ is restricted to values less than ϵ^* . The case where $\epsilon > \epsilon^*$ is treated in the following section.

4.1.3.2 Kink Impact Against Sheave (Reflected Kink With Wave Front)

The conditions which prevail along the cable prior to kink impact at the sheave are the same as those given in Section 4.1.3.1. However, if the strain ϵ_1 is large enough, the resulting strain ϵ will be so large that the kink will be travelling with the same speed as some portion of the wave front. The large diagram in Figure 30 shows the kink Q travelling with the same velocity as some portion of the wave W. Since the initial conditions are the same as those given in the previous section, R separates from the sheave P with velocity $c_1^* - u_1$.

With respect to the portion of the velocity diagram designated by PQ, kink Q is travelling with velocity c^\bullet with respect to the point of the cable under strain ϵ^\bullet . Using equation (4.4), however, a velocity-strain relationship can be written along the wave front W for conditions at ϵ^\bullet and ϵ , namely,

$$u^\bullet - u = - \int_{\epsilon}^{\epsilon^\bullet} c \, d\epsilon$$

Since ϵ was assumed to be greater than ϵ^\bullet , it may be deduced from this relationship that the portion of the cable under the strain ϵ^\bullet is moving away and to the right with respect to the portion of the cable under the strain ϵ . With respect to portions of the cable under strain ϵ^\bullet , the kink velocity of Q is given by c^\bullet ; thus kink Q separates from point P with the velocity,

$c^\bullet + (u^\bullet - u) + u = c^\bullet - U^\bullet + 2U + u_1 - U_1$. This last relationship is obtained with the aid of equation (4.3) across W'. This relationship is shown in the diagram (Figure 30).

[illegible]

85

By referring the velocities of points R and Q to an unaffected point of the cable ahead of the wave W and with the aid of equation (4.4), the separation velocity of R and Q is obtained as:

$$c_1^* + c^\bullet + U^\bullet + U_1.$$

Using the law of cosines on triangle RPQ, an equation is obtained for the unknown function U:

$$\begin{aligned} (c^\bullet - U^\bullet + u_1 + 2U - U_1)^2 &= (c_1^* - u_1)^2 + (c_1^* + c^\bullet - U^\bullet + U_1)^2 \\ &\quad - 2(c_1^* - u_1)(c_1^* + c^\bullet - U^\bullet + U_1) \cos \phi_1 \end{aligned}$$

which is quadratic in the function U. Determining U is equivalent to determining ϵ , since it has been assumed U is known as a function of ϵ .

The new kink angle ϕ can be obtained from the law of sines,

$$\frac{\sin \phi}{c_1^* - u_1} = \frac{\sin \phi_1}{c^\bullet - U^\bullet + u_1 + 2U - U_1}$$

4.1.3.3 Kink Impact Against Sheave. (Original Kink With Wave Front)

With reference to Figure 31, consider the case where a kink, K, with kink angle ϕ_1 approaches a sheave, P. The kink K is assumed to be travelling in the midst of a wave front W_0 , i.e., $c^\bullet = c(\epsilon^\bullet)$ is assumed to hold. Behind the wave front W_0 the strain is assumed to be at uniform ϵ_1 with velocity u_1 .

The large velocity diagram in the figure represents conditions along the cable immediately after kink impact against the sheave. Since impact against the sheave tends to increase the maximum strain level the new wave W will lag behind the new kink Q. The strains near the kink Q will not necessarily be at

Kink Impact Against Sheave

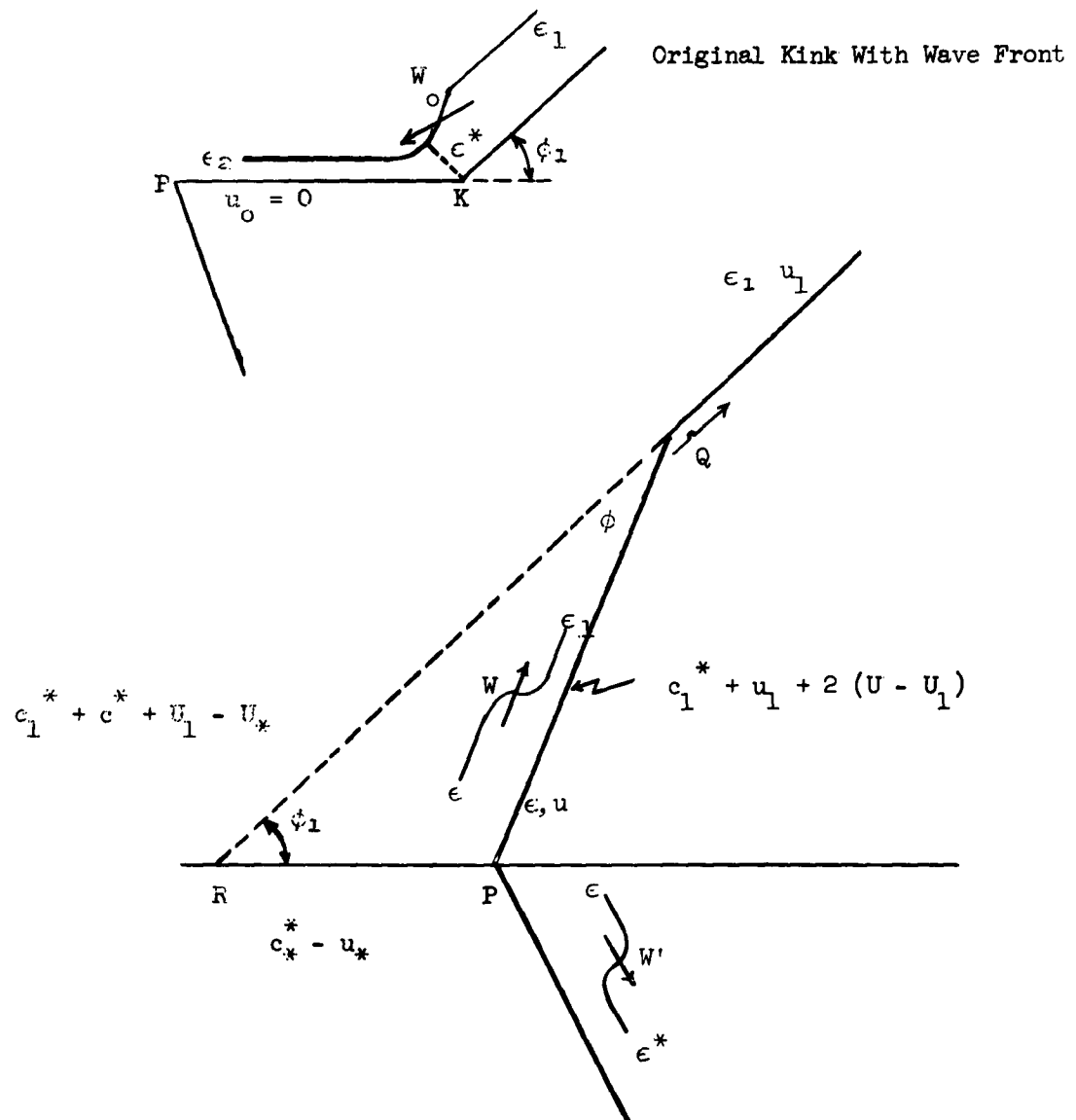


Figure 31

the uniform strain ϵ_1 ; rather, the rise of the front W may be interacting with the still oncoming rise of W_0 . However, this interaction is negligible for an instant. Below the point P another loading wave W' is represented and tends to travel upstream to the cable.

The velocity with which the projection R separates from the sheave P is the same as that by which kink K approaches point P. Thus RP of the velocity diagram is denoted by $c^* - u^*$. If desired, the value of u^* may be expressed in terms of the strain ahead of the wave W_0 by the use of equation (4.3).

With reference to PQ of the velocity diagram, the kink Q has a velocity c_1^* with respect to points of the cable along PQ which have the strain ϵ_1 . Between points just ahead of and just behind the wave front W, a relative velocity exists. If u represents the cable velocity behind W and u_1' denotes the cable velocity just ahead of W, then in accordance with equation (4.4)

$$u - u_1' = - \int_{\epsilon_1}^{\epsilon} c \, d\epsilon$$

Since c is greater than ϵ_1 , it may be deduced from the above relationship that points ahead of the wave move up and to the right with respect to points behind the wave W. Thus since the velocity of Q with respect to the cable is c_1^* , and since by u is meant the velocity at which the cable passes around the sheave P, the velocity at which the kink Q separates from P is given by

$$c_1^* + (u_1' - u) + u = c_1^* + u + \int_{\epsilon_1}^{\epsilon} c \, d\epsilon$$

or, by $c_1^* + u + U - U_1$. The velocity, u , of the cable is as yet unknown. However, by considering the continuous wave front W' and by the use of equation (4.3)

$$u - u^{\bullet} = + \int_{\epsilon^{\bullet}}^{\epsilon} c \, d\epsilon$$

Using this expression for u the velocity at which the kink Q separates from point P can be given completely in terms of the unknown strain ϵ :

$$c_1^* + u^{\bullet} - U_1 + 2U - U^{\bullet}$$

Again, the expression u^{\bullet} can be given in terms of the cable velocity corresponding to ϵ_1 by the velocity-strain relationship across W_0 . Therefore, the side PQ of the velocity triangle can be represented by,

$$c_1^* + u_1 + 2(U - U_1),$$

which is indicated in the figure.

The velocity by which R separates from an unaffected point of the cable ahead of the kink Q is the same as that by which K separates from the unaffected cable. Between portions of the wave front W_0 there exists a relative velocity. Using equation (4.3) between points of the wave front under strain ϵ^{\bullet} and ϵ_1 results in

$$u^{\bullet} - u_1 = + \int_{\epsilon_1}^{\epsilon^{\bullet}} c \, d\epsilon$$

Since ϵ_1 is greater than ϵ^{\bullet} , it can be deduced from the above equation that points of the cable under strain ϵ^{\bullet} move to the left and down with respect to points of the cable under strain ϵ_1 . Therefore the velocity by which kink K moves away from the unaffected portions of the cable is given by $c^{\bullet} + u_1 - u^{\bullet}$ or, in terms of the U function, by $c^{\bullet} + U_1 - U^{\bullet}$. The velocity of Q relative to a point of the cable under strain ϵ_1 is simply given by c_1^* . Hence points R and Q separate with velocity,

$$c_1^* + c^{\bullet} + U_1 - U^{\bullet}$$

and is indicated in the figure.

Using the law of cosines there results an equation in the single unknown ϵ :

$$[c_1^* + u_1 + 2(U - U_1)]^2 = (c^{\bullet} - u^{\bullet})^2 + (c_1^* + c^{\bullet} + U_1 - U^{\bullet})^2 - 2(c^{\bullet} - u^{\bullet})(c_1^* + c^{\bullet} + U_1 - U^{\bullet})\cos \phi_1.$$

The new kink angle ϕ can be found from the law of sines:

$$\frac{\sin \phi}{c^{\bullet} - u^{\bullet}} = \frac{\sin \phi_1}{c_1^* + u_1 + 2(U - U_1)}$$

4.1.4 Kink Impact Against Sheave With Disengagement

With reference to Figure 32, suppose that a cable under strain ϵ_1 is moving clockwise about a sheave, P, and further suppose that a kink K with kink angle ϕ_1 approaches the sheave from the right. Below the point P the cable continues to extend at an angle γ as indicated. The large diagram of Figure 32 represents the situation just after impact of the kink and the sheave has occurred. Two new waves are formed and propagated away from the point of impact. In addition, two kinks Q and J are formed and are also propagated away from the impact point. Since the new strain ϵ is larger than ϵ_1 , both waves W and W' are loading waves. Across each wave front there exists a difference in particle velocities. These are given by equations (4.3) and (4.4) for W' and W respectively. With these relationships, and by referring the velocity of the projection R and the velocity of Q to an unaffected point of the cable

Kink Impact At Sheave With Disengagement

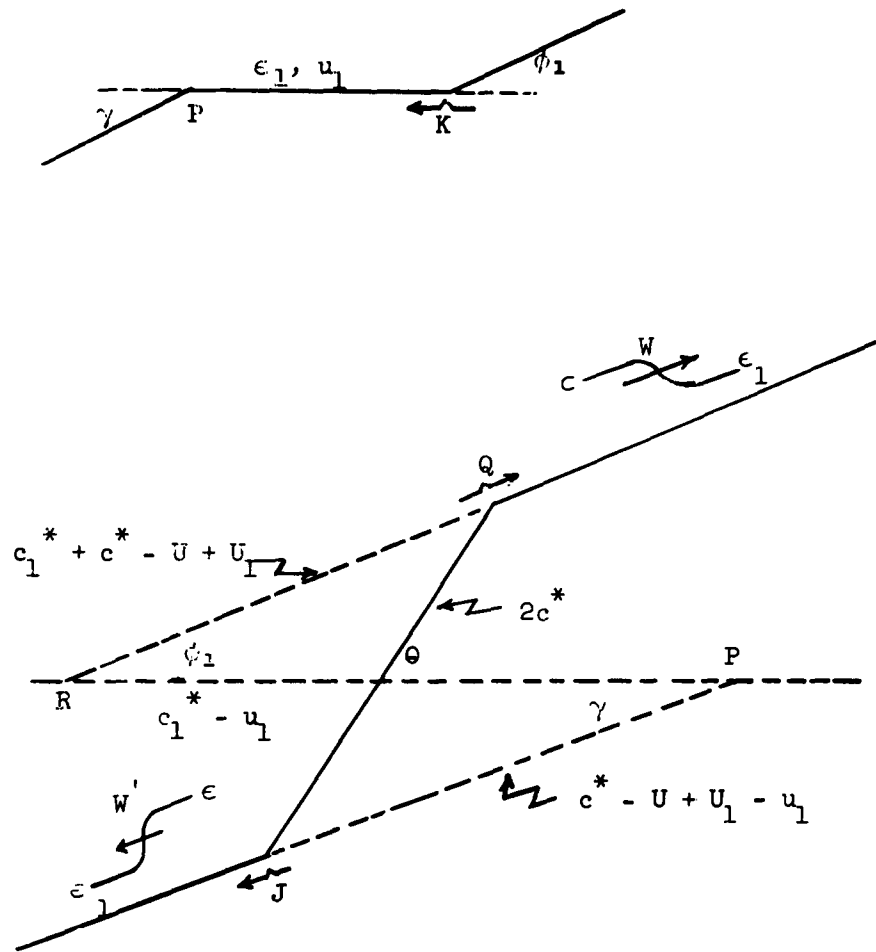


Figure 32

in front of W, the separation velocity between R and Q can be found. Likewise, by referring the velocities of the projection P and the kink J to an unaffected point of the cable in front of the wave W', the separation velocity existing between the points J and P can be found. Since J and Q are points of the cable under the same strain, their separation velocity is given by $2c^*$. The velocity by which the projection R separates from P is the same as that by which the original kink K approaches P and is given by $c_1^* - u_1$.

These velocities are shown in the diagram of Figure 32. From the diagram an equation is obtained in terms of the functions c^* and U which are known as functions of the unknown strain ϵ :

$$(2c^*)^2 = [(c_1^* + c^* - U + U_1) \sin \phi_1 + (c^* - U + U_1 - u_1) \sin \gamma]^2 \\ + [(c_1^* + c^* - U + U_1) \cos \phi_1 - (c_1^* - u_1) + (c^* - U + U_1 - u_1) \cos \gamma]^2$$

The new orientation angle θ can be found from

$$\tan \theta = \frac{(c_1^* + c^* - U + U_1) \sin \phi_1 + (c^* - U + U_1 - u_1) \sin \gamma}{(c_1^* + c^* - U + U_1) \cos \phi_1 - (c_1^* - u_1) + (c^* - U + U_1 - u_1) \cos \gamma}$$

If $\theta < \gamma$, then no disengagement occurs and one of the preceding formulations for the kink impact at the sheave applies.

4.1.5. Meeting of Kink and Tension Loading Wave

With reference to Figure 33, suppose that a kink K_0 with kink angle ϕ_1 is moving to the left under strain ϵ_1 . Further suppose that a continuous loading wave W_0 approaches the kink from the left. Behind the wave front the strain is designated by ϵ_2 .

Kink Encountering a Tension Loading Wave

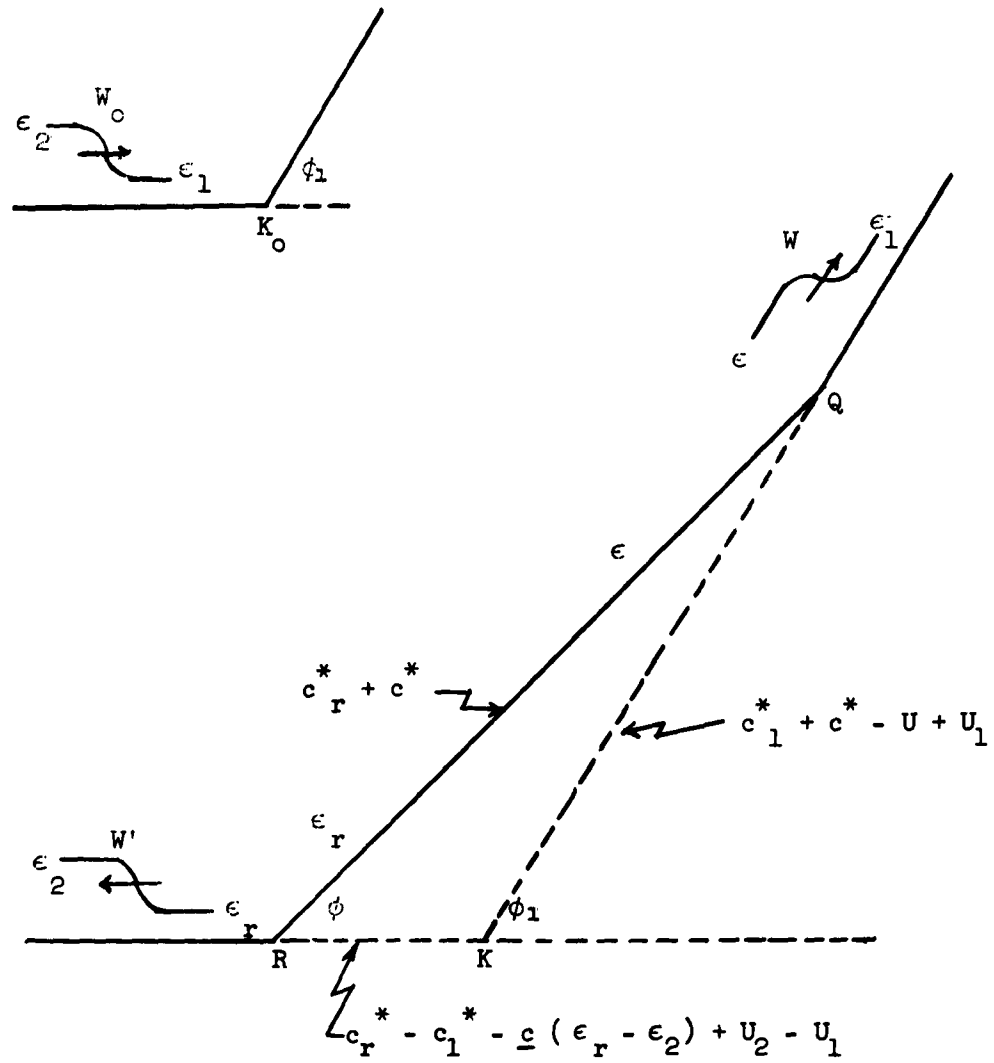


Figure 33

Since the wave front is continuous, a continuous interaction will take place between W_0 and K_0 . However, since the resulting transverse disturbances will be nondispersive, the principle of coincidization is applicable and they can be treated as kinks.

The large diagram of Figure 33 represents the situation after wave interaction with the kink has occurred. Two new longitudinal waves and two kinks are created from the point of impact as shown in the figure. The wave moving to the right, W , is a loading wave and behind it the strain is ϵ . The wave running to the left, W' , is an unloading wave and behind it the strain is designated by ϵ_r . The strain, ϵ_r , corresponds to the strain on the unloading segment of the stress-strain curve as shown in Figure 34. It is to be noted that if the stress-strain curve were to be nonlinear but perfectly elastic, then only the strain ϵ would be present. Thus a strain discontinuity occurs in segment RQ; however the stress contained therein is not discontinuous but rather force equilibrium must be observed. With reference to Figure 34 it is noted that the relationship,

$$\epsilon_r = \epsilon_2 - \frac{\sigma(\epsilon_2) - \sigma(\epsilon)}{E_1}$$

must hold in order for force equilibrium to be maintained. In the above relationship E_1 denotes the modulus which corresponds to the initial portion of the stress-strain curve.

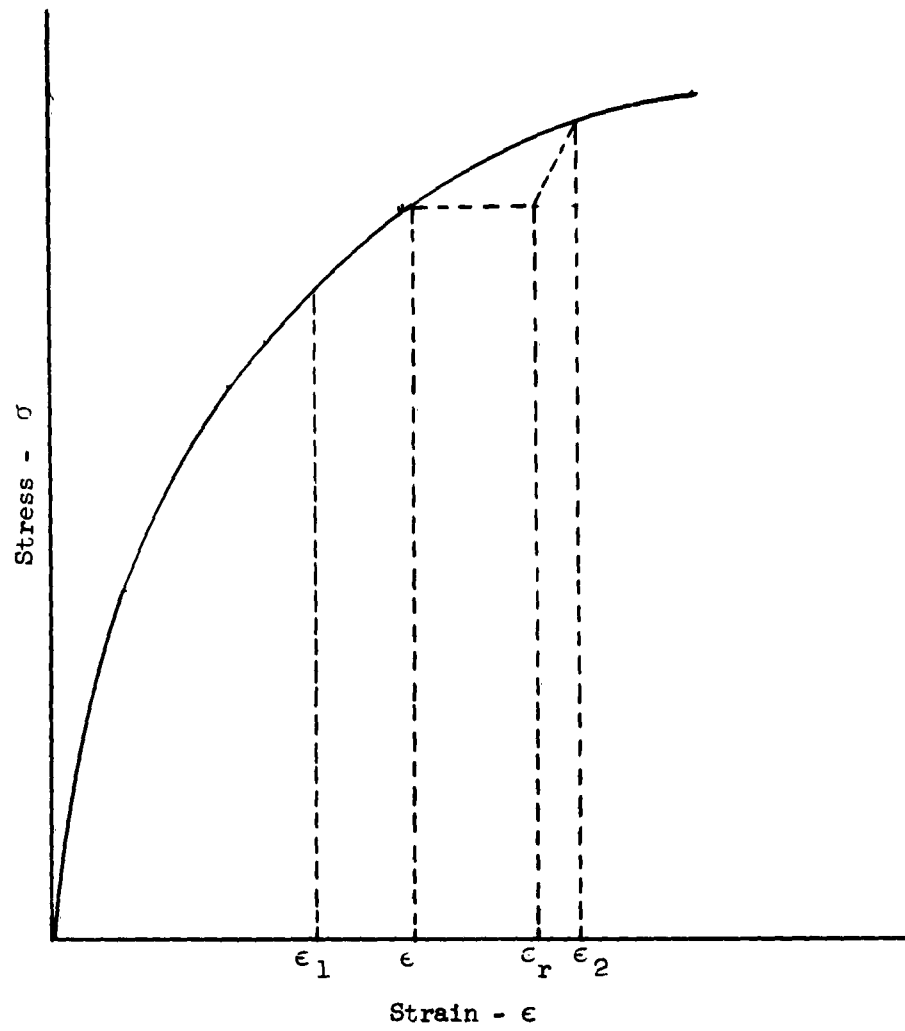


Figure 34
Schematic Stress-Strain Diagram Illustrating
An Unloading Strain Condition

Further, it is noted that across the wave W' and according to equation (4.3), the velocity strain relationship can be written,

$$u_r - u_2 = + \int_{\epsilon_2}^{\epsilon_r} c d\epsilon = \underline{c} (\epsilon_r - \epsilon_2)$$

where u_r and u_2 denote the particle velocity behind and in front of W' respectively. Since \underline{c} is a constant, the integration can be performed as indicated.

With the exception of the above modification the method of analysis proceeds in a similar manner to those previously presented. With the aid of the above relationship and by use of equation (4.4) on W_0 , the separation velocity of R with respect to the projection K can be found as:

$$c_r^* - c_1^* = \underline{c} (\epsilon_r - \epsilon_2) + U_2 - U_1$$

By the use of equation (4.4) on W and by referring the velocities of the projection K and the kink Q to unaffected points of the cable just in front of W under strain ϵ_1 , the separation velocity of points Q and K can be found as:

$$c_1^* + c^* = U + U_1$$

The velocity at which the two kinks separate is given by $c_r^* + c^*$. These velocities are indicated in the velocity diagram of Figure 33. From the velocity diagram an equation can be obtained as

$$\begin{aligned} (c_r^* + c^*)^2 &= (c_1^* + c^* - U + U_1)^2 + [c_r^* - c_1^* + \underline{c} (\epsilon_r - \epsilon_2) + U_2 - U_1]^2 \\ &+ 2 (c_1^* + c^* - U + U_1) [c_r^* - c_1^* - \underline{c} (\epsilon_r - \epsilon_2) + U_2 - U_1] \cos \phi_1 \end{aligned}$$

The above equation contains the two unknown strains ϵ_r and ϵ ; however ϵ_r can be expressed in terms of ϵ as previously shown. Therefore the unknown strain ϵ can be determined and hence ϵ_r .

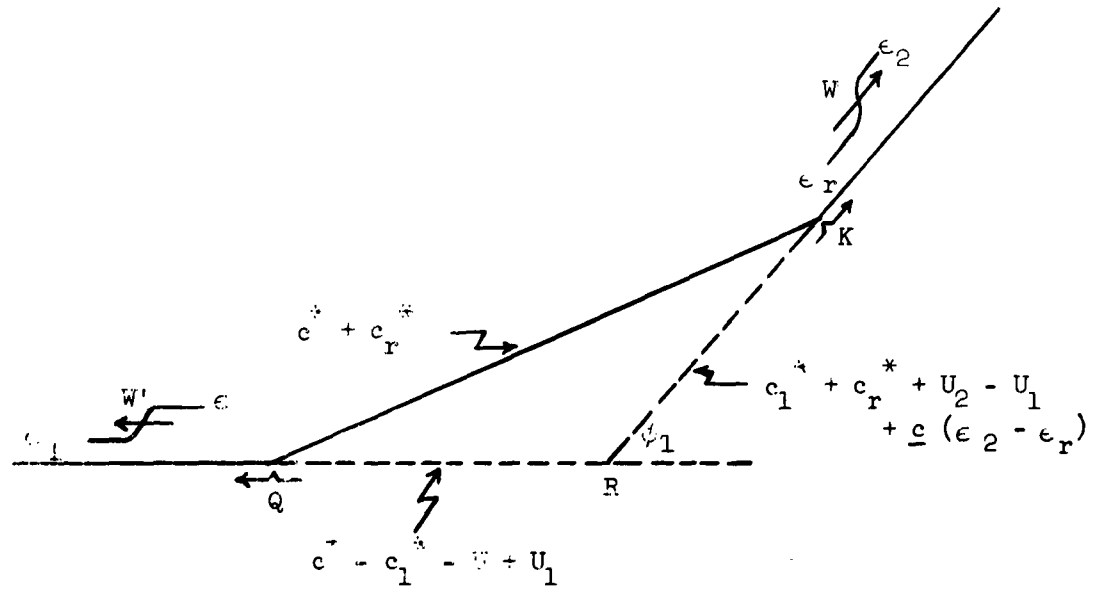
The new kink angle ϕ can be found from the diagram:

$$\frac{\sin \phi_1}{c_r^* + c^*} = \frac{\sin \phi}{c_1^* + c^* - U + U_1}$$

4.2.6 Kink Overtaken by Tension Jump

With reference to Figure 35, suppose that a kink Q' with kink angle ϕ_1 is moving to the left under strain ϵ_1 . Now suppose that a continuous longitudinal wave front, W_0 , interacts with the kink. Physically, since the wave front is dispersed, the interaction will occur over a finite time interval and along some length of the cable. However, in order to ascertain the final effects a similar procedure may be used such as was presented in the preceding sections.

The large diagram of Figure 35 represents the situation after the interaction has occurred. Due to the assumed form of the stress-strain curve (i.e., the unloading segment is distinct from the loading segment) there will exist a strain discontinuity in segment KQ. Again, the strain ϵ and the strain ϵ_r are related by the expression given in Section 4.1.5. Since the strain is uniform behind the wave front W and W' , (except for the discontinuity at one point) the velocity by which Q separates from K is given by $c^* + c_r^*$.



The velocity by which Q separates from R can be obtained by using equation (4.3) across W' and by relating the individual velocities to the unaffected portion of the cable in front of W' and is given by

$$c^* - c_1^* = U + U_1.$$

Similarly, the velocity by which K separates from R may be determined with the aid of equation (4.4) and by observing that W is an unloading wave and is given by

$$c_1^* + c_r^* + U_2 - U_1 + \underline{c} (\epsilon_2 - \epsilon_r)$$

These velocities are represented in the velocity diagram of Figure 35.

From the triangle QRK can be obtained an equation in terms of the unknown strains ϵ and ϵ_r ,

$$\begin{aligned} (c^* + c_r^*)^2 &= (c^* - c_1^* - U + U_1)^2 + [c_1^* + c_r^* + U_2 - U_1 + \underline{c} (\epsilon_2 - \epsilon_r)]^2 \\ &+ 2 (c^* - c_1^* - U + U_1) [c_1^* + c_r^* + U_2 - U_1 + \underline{c} (\epsilon_2 - \epsilon_r)] \cos \phi_1 \end{aligned}$$

The new kink angle ϕ can be found by the law of sines for the triangle:

$$\frac{\sin \phi}{c_1^* + c_r^* + U_2 - U_1 + \underline{c} (\epsilon_2 - \epsilon_r)} = \frac{\sin \phi_1}{c^* + c_r^*}.$$

4.1.7.1 Cable End Catapulted With Simultaneous Arrival of Kink And Tension Wave (Reflected Kink Travels With Wave Front)

With reference to Figure 36 suppose that a kink K with kink angle ϕ_1 is moving to the right towards the fixed cable end P under strain ϵ_1 . Further,

suppose that behind K there approaches a tension jump W_0 such that the maximum strain ϵ_2 strikes the kink K at the time the kink reaches the cable end. Moreover, suppose that the cable end is catapulted at a velocity V at the time of impact.

The diagram of Figure 36 represents the situation immediately after the kink and wave interaction has occurred. If the velocity V is low enough and if the strain ϵ_2 is high enough, then the new kink Q will move at the same velocity as some portion of the continuous wave front W. The strain at which this occurs is given by ϵ^* . In front of the wave front the strain is still ϵ_2 ; behind W the strain is given by ϵ .

The velocity by which projection R separates from the point P is the same as that which the kink K approaches point P and is simply c_1^* . By the use of equation (4.4) across W_0 and by equation (4.3) across W (from ϵ^* to ϵ_2), and further by comparing the velocities of the projection R and of the new kink Q with respect to unaffected points of the cable in front of W, the separation velocity between Q and R can be found. This is given as:

$$c_1^* + c^* + 2U_2 - U_1 - U^*$$

With the aid of equation (4.3) across the wave front W (between points of the cable under strain ϵ^* and ϵ), the velocity by which the new kink Q separates from the cable end under strain ϵ can be found and is

$$c^* - u^* + U$$

These velocities are indicated in the velocity diagram of Figure 36.

From the quadrilateral QMPR the following relationship can be obtained:

$$(c^{\bullet} - U^{\bullet} + U)^2 = [(c_1^* + c^{\bullet} + 2U_2 - U_1 - U^{\bullet}) \sin \phi_1 - V \sin \alpha]^2 + [(c_1^* + c^{\bullet} + 2U_2 - U_1 - U^{\bullet}) \cos \phi_1 - c_1^* - V \cos \alpha]^2,$$

which is an equation in U and c^* which are known functions of the unknown strain ϵ .

The new kink angle ϕ can be found from the relationship:

$$\tan (\phi + \phi_1) = \frac{(c_1^* + c^{\bullet} + 2U_2 - U_1 - U^{\bullet}) \sin \phi_1 - V \sin \alpha}{(c_1^* + c^{\bullet} + 2U_2 - U_1 - U^{\bullet}) \cos \phi_1 - V \cos \alpha - c_1^*}$$

From the case where $V = 0$ and ϵ_2 is equal to ϵ_1 , the above formulation applies to the case where a kink impacts against a fixed wall.

4.1.7.2 Cable End Catapulted With Simultaneous Arrival of Kink And Tension Wave (Resultant Unloading Wave)

As indicated in Figure 37, the initial conditions in this case are exactly the same as those presented in the previous section. However, now let us suppose that the cable end is catapulted with a velocity V large enough such that the resultant strain is lower than ϵ_2 . In this case the new wave front W will be of an unloading type and will precede the new kink Q . The strain ϵ is that strain which lies on the unloading segment of the stress-strain curve which passes through the point of the curve with coördinate ϵ_2 .

Since the strain along the segment QM is uniform, the velocity by which the kink separates from point M is given simply by c^* . The velocity by which

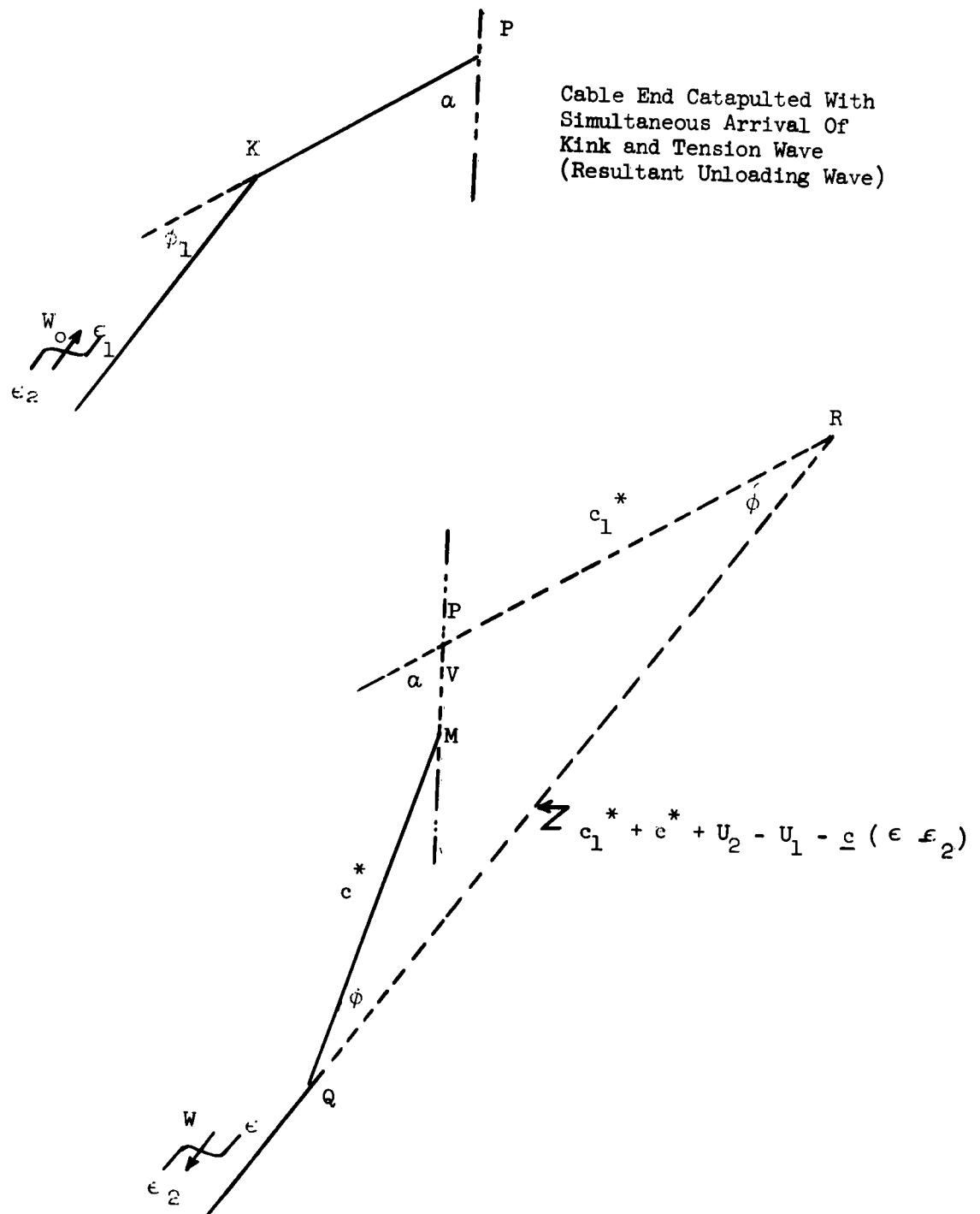


Figure 37

point Q separates from the projection R may be found by applying equation (4. 4) and equation (4. 5) across W_0 and W respectively. The resultant velocities are indicated in the velocity diagram of Figure 37.

From the diagram an equation may be obtained in terms of the single unknown strain ϵ :

$$(c^*)^2 = \{ [c_1^* + c^* + U_2 - U_1 - c(\epsilon - \epsilon_2)] \sin \phi_1 - V \sin \alpha \}^2 \\ + \{ [c_1^* - c^* + U_2 - U_1 - c(\epsilon - \epsilon_2)] \cos \phi_1 - V \cos \alpha - c_1^* \}^2$$

The new kink angle ϕ may also be found from the diagram as:

$$\tan (\phi + \phi_1) = \frac{[c_1^* + c^* + U_2 - U_1 - c(\epsilon - \epsilon_2)] \sin \phi_1 - V \sin \alpha}{[c_1^* + c^* + U_2 - U_1 - c(\epsilon - \epsilon_2)] \cos \phi_1 - V \cos \alpha - c_1^*}$$

For the case where $\epsilon_2 = \epsilon_1$, i.e., $W_0 = 0$, the above formulation is applicable to the case where kink impact occurs at a fixed wall.

4. 1. 8 Interaction of Two Kinks and Two Waves

With reference to Figure 38 suppose that two kinks K_1 and K_2 approach each other under a strain of ϵ_1 . Further suppose that behind each kink there approaches a loading wave such as W_0 and W_0' behind which the strains are ϵ_2 and ϵ_3 . The two kinks collide at the same time that the peak strains ϵ_2 and ϵ_3 meet. This procedure is used to determine the overall final strain distribution in the cable since in reality the longitudinal and transverse wave fronts are continuously distributed along a finite segment of the cable.

The large diagram of Figure 38 represents the situation in the cable after the wave interactions have occurred. Two new kinks and two new continuous and

Interaction of Two Kinks
and Two Waves

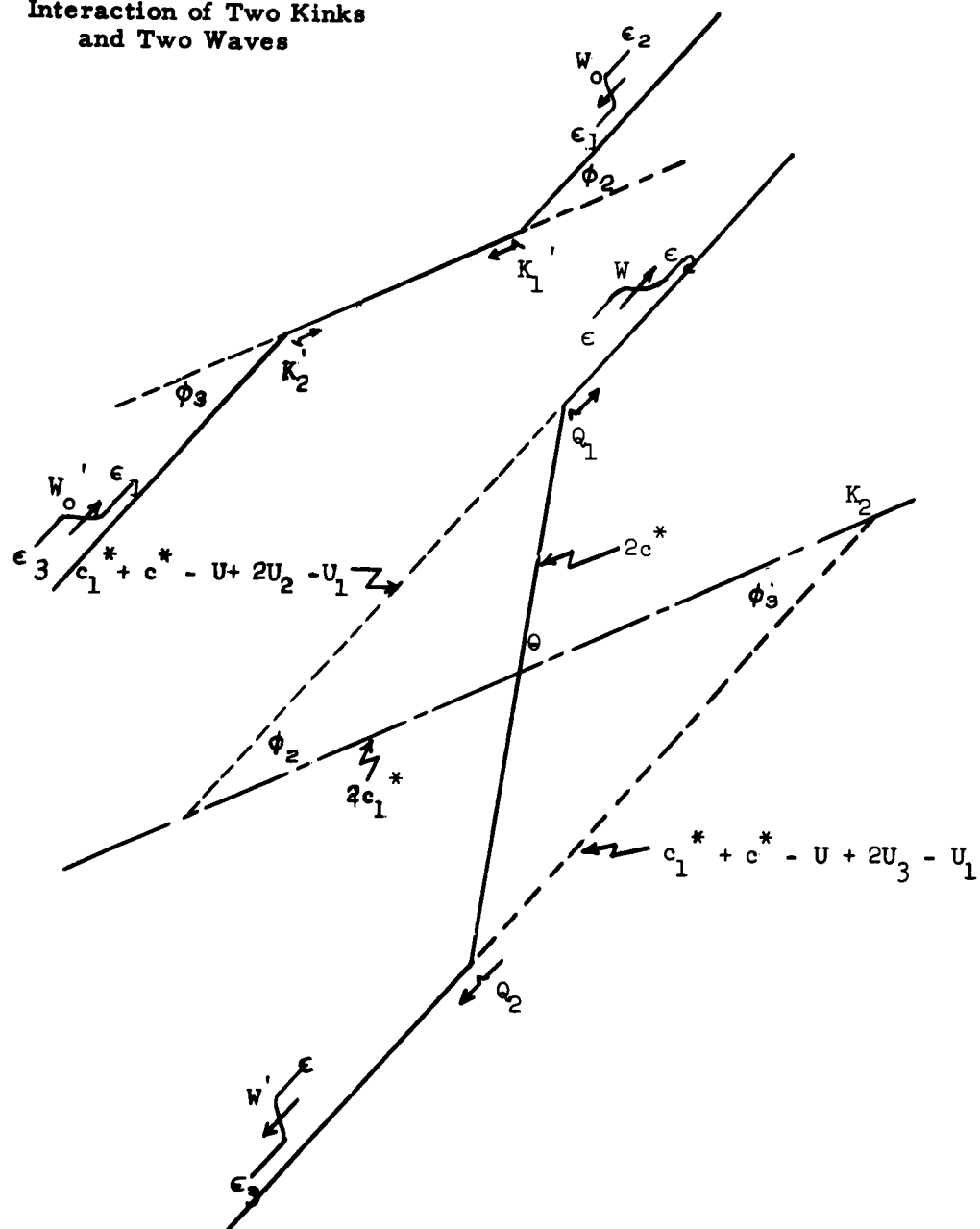


Figure 38

longitudinal strain waves are created. Ahead of the wave W and ahead of the wave W' the strains are ϵ_2 and ϵ_3 respectively. Behind each wave front the strain is designated by ϵ .

With the aid of equation (4.4) across W_0' , and with equation (4.3) across W' , and by relating the velocities of the kink Q_2 and the projection K_2 to points of the cable just ahead of W' , the separation velocity of Q_2 and K_2 can be determined as,

$$c_1^* + c^* - U + 2U_3 - U_1 \quad .$$

Since the strain behind each of the kinks is given by c , the two new kinks separate with velocity $2c^*$. The separation velocity of the projections K_1 and K_2 is given by $2c_1^*$. With the aid of equation (4.3) across W_0 and equation (4.4) across W, and by relating the velocities of projection K_1 and the kink Q_1 to unaffected points of the cable ahead of W, the separation velocity existing between K_1 and Q_1 can be determined as,

$$c_1^* + c^* - U + 2U_2 - U_1 \quad .$$

These velocities are shown in the velocity diagram of Figure 38.

From the diagram an equation can be obtained in terms of the single unknown strain ϵ :

$$\begin{aligned} (2c^*)^2 = & [(c_1^* + c^* - U + 2U_2 - U_1) \sin \phi_2 \\ & + (c_1^* + c^* - U + 2U_3 - U_1) \sin \phi_3]^2 + \\ & [(c_1^* + c^* - U + 2U_2 - U_1) \cos \phi_2 - 2c_1^* \\ & + (c_1^* + c^* - U + 2U_3 - U_1) \cos \phi_3]^2 \end{aligned}$$

The above equation may be solved for ϵ since U and c^* are known functions of ϵ .

The new orientation angle Θ may be found from the relation:

$$\tan \Theta = \frac{(c_1^* + c^* - U + 2U_2 - U_1) \sin \phi_2 + (c_1^* + c^* - U + 2U_3 - U_1) \sin \phi_3}{(c_1^* + c^* - U + 2U_2 - U_1) \cos \phi_2 - 2c_1^* + (c_1^* + c^* - U + 2U_3 - U_1) \cos \phi_3}$$

4.1.9 Plastic Loading Wave Overtaken by Unloading Wave

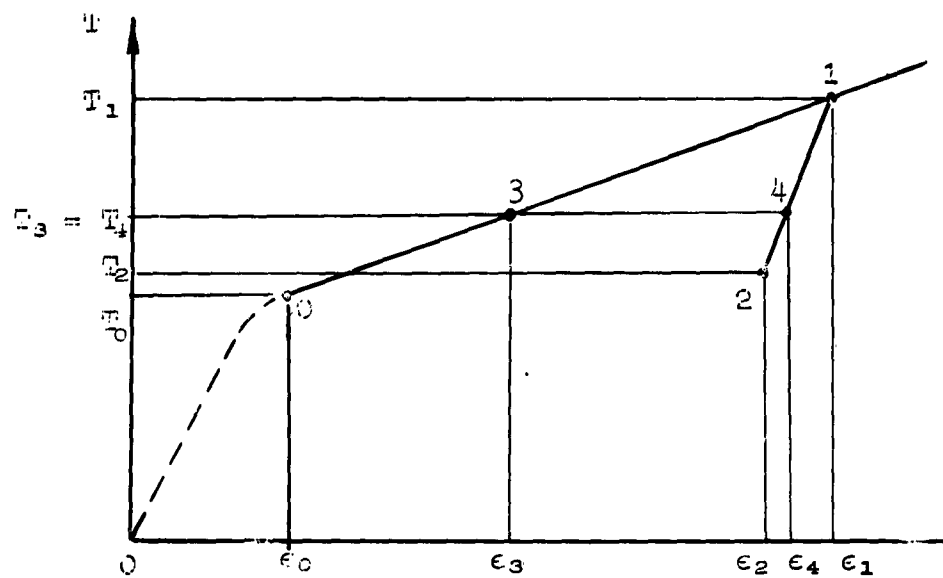
Consideration is here restricted to a material having a linear segment in the plastic region of its tension-strain curve, as shown in Figure 39a. The analysis then involves only singular waves and is thereby facilitated. The analysis can be made applicable to nonlinear tension-strain curves if the loading waves are first restricted to infinitesimal jumps, after which the effect of a finite dispersed loading wave can be obtained by integration.

Figure 39b shows a plastic strain jump just before it is overtaken at x_1 by an elastic unloading wave. Figure 39c shows the plastic strain jump emerging beyond x_1 substantially reduced by the interaction, and a small reflected elastic reloading wave. Five tension-strain states are involved, and are shown in Figure 39a as states 0, 1, 2, 3, 4. States 0, 3, 1 lie on the plastic loading curve having a tension-strain modulus of E_p , while states 1, 2, 4, lie on the elastic unloading and reloading curve having a modulus of E_e .

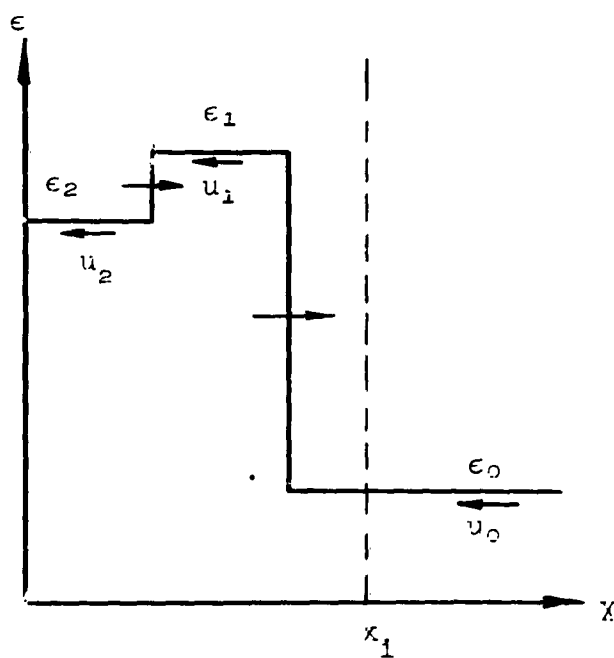
Given states 0, 1, 2, the problem is to find states 3, 4. Observe that equilibrium and continuity at x_1 require states 3, 4, to have equal tensions and equal particle velocities, although state 4 has more permanent plastic deformation than state 3. From Figure 39a the tension-strain relations are

$$\begin{aligned} T_1 - T_0 &= E_p (\epsilon_1 - \epsilon_0) \\ T_1 - T_2 &= E_e (\epsilon_1 - \epsilon_2) \\ T_3 - T_0 &= E_p (\epsilon_3 - \epsilon_0) \\ T_4 - T_2 &= E_e (\epsilon_4 - \epsilon_2) \\ T_3 - T_4 &= 0 \end{aligned}$$

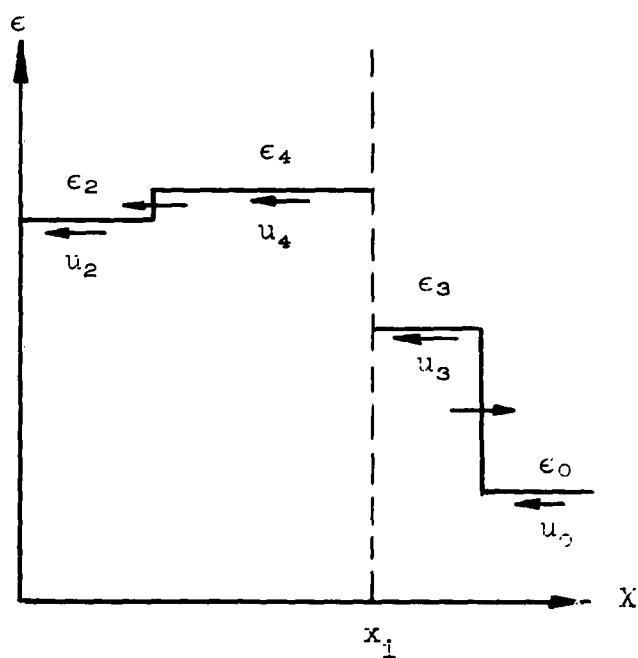
while, by equations (4.1) and (4.2), the velocity-strain relations are



(a) Tension-strain diagram



(b) Strain distribution before interaction



(c) Strain distribution after interaction

Figure 39

Loading Wave Overtaken by Unloading Wave

$$\begin{aligned}
u_1 - u_0 &= \sqrt{E_p/\mu} (\epsilon_1 - \epsilon_0) \\
u_1 - u_2 &= \sqrt{E_e/\mu} (\epsilon_1 - \epsilon_2) \\
u_3 - u_0 &= \sqrt{E_p/\mu} (\epsilon_3 - \epsilon_0) \\
u_2 - u_4 &= \sqrt{E_e/\mu} (\epsilon_4 - \epsilon_2) \\
u_3 - u_4 &= 0
\end{aligned}$$

After the foregoing equations are solved for the unknowns, the solutions can be expressed in the following convenient dimensionless form:

$$\begin{aligned}
\frac{T_1 - T_3}{T_1 - T_2} &= \frac{\epsilon_1 - \epsilon_4}{\epsilon_1 - \epsilon_2} = \frac{2}{1 + c_e/c_p} \\
\frac{u_1 - u_3}{u_1 - u_2} &= \frac{\epsilon_1 - \epsilon_3}{\epsilon_1 - \epsilon_2} = \frac{2}{1 + c_p/c_e}
\end{aligned}$$

where $c_e = \sqrt{E_e/\rho}$ and $c_p = \sqrt{E_p/\mu}$ are the respective elastic and plastic wave velocities. It is noteworthy that the solution is independent of the initial state 0 and, hence, of the magnitude $(\epsilon_1 - \epsilon_0)$ original plastic strain wave. Observe also that the plastic strain wave is reduced by an amount $(\epsilon_1 - \epsilon_3)$ which exceeds the original unloading $(\epsilon_1 - \epsilon_2)$.

4.2 Practicability of Specific Aircraft-Arresting Concepts

In an aircraft-arresting system which employs energy-absorbing material in the cable, a new cable must be installed for each arrest. This feature should not be regarded as impractical when it is realized that the aircraft to be arrested will be exotic by present standards. There is only one pertinent criterion in the evaluation of an arresting system for such an aircraft, and that is the success of the arrest.

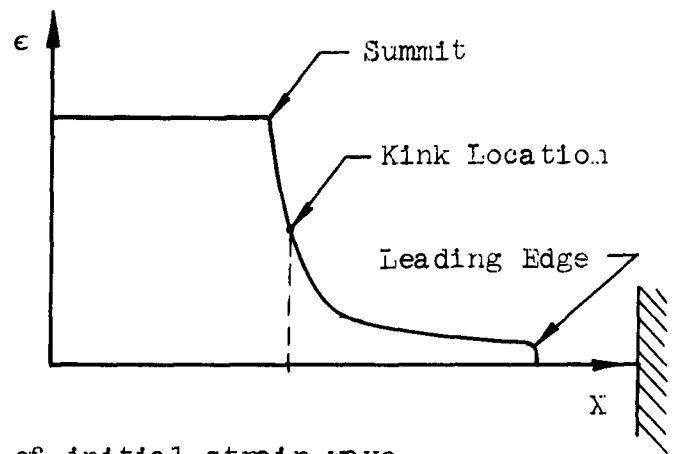
Consider an arresting system which has energy-absorbing material in the cable as the sole sink for the kinetic energy of the aircraft to be arrested. If after aircraft arrestment the final distribution of strain along the cable were uniform, such an arresting system could be designed merely by providing, in a cross section consistent with the maximum permissible aircraft deceleration, that volume of cable material whose strain-energy capacity is adequate to absorb the energy of the incoming aircraft. But the aircraft impact produces wave phenomena which introduce severe nonuniformities of strain distribution.

It is therefore necessary to analyze the wave phenomena to determine the extent to which the associated strain nonuniformities persist. If the final amount of nonuniformity can be ascertained, an allowance can be made for it simply by reduction of the usable strain-energy capacity on which the design is based.

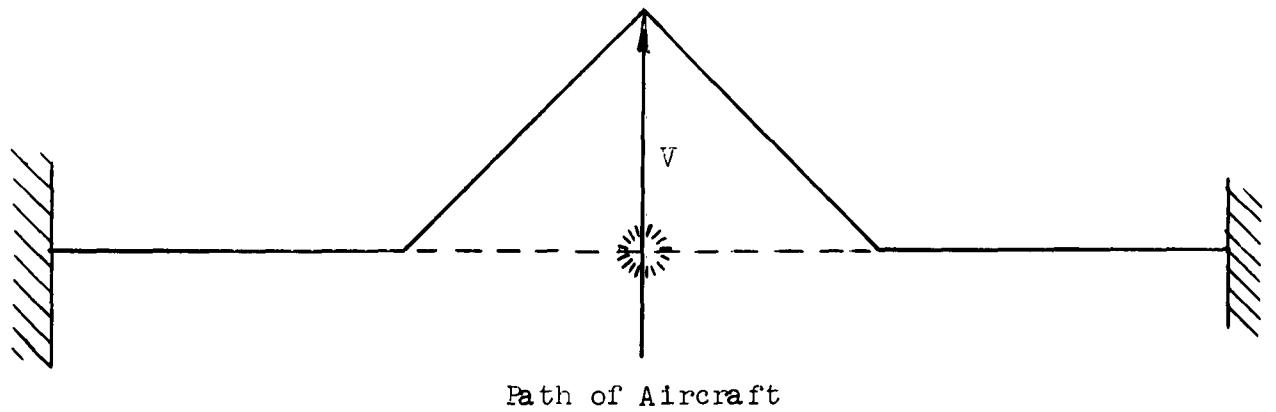
The following cases illustrate the method by which a particular design can be evaluated.

4.2.1 Case I: Energy-Absorbing Cable with Fixed Ends

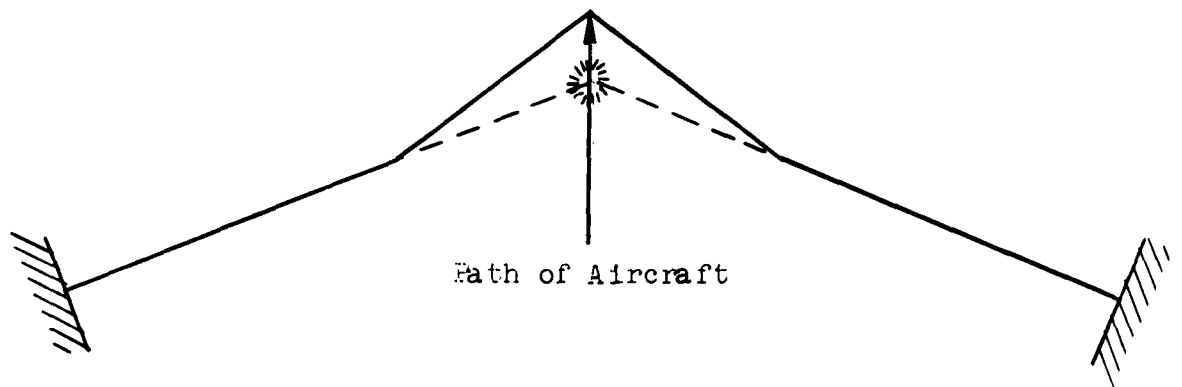
For an arresting system which consists simply of an energy-absorbing cable stretched across the runway between fixed ends (Figure 40b), it is possible



(a) Distribution of initial strain wave



(b) Plan View of Cable



(c) Plan View of Alternate Arrangement

Figure 40

Energy-absorbing Cable with Fixed Ends

to determine an upper bound on the nonuniformity of the final distribution of strain.

An example has been considered in which the ultimate strain of the material is 0.50. With an arbitrary design limit of 0.40, calculations of strain nonuniformity indicate that the design can be based on the strain energy associated with an average strain of 0.32.

Nonuniformity of strain distribution arises because the development of strain is essentially a process of propagation of two strain waves that reflect back and forth between the fixed end and the aircraft, increasing the general strain level with each passage.

The two strain waves that contribute significantly to the nonuniformity are (1) the strain wave generated upon impact by the aircraft and (2) the strain wave generated when the first transverse wave interacts with the fixed end. These two strain waves steadily increase their lengths because of the decrease of sonic velocity with increasing strain. At the same time, the amplitudes of these two major waves are diminished steadily by interaction with the many minor waves.

Minor waves will include both strain and transverse waves. They are generated by the continuous deceleration of the aircraft and by further interaction of both minor and major waves already present. The minor waves make no significant contribution to nonuniformity of strain distribution other than through their beneficial effects on the two major waves.

For example, the deceleration of the aircraft generates a continuous unloading wave which travels many times faster than any loading wave in the plastic region. This unloading wave is one of a relatively slight rate of decrease in strain but, as it overtakes a loading wave, the strain amplitude of the latter is

diminished at a rate nearly double that of the unloading wave itself. This effect is readily explained and calculated by Figure 39 and the formulas of Section 4.1.9.

With an energy-absorbing material such as fully annealed stainless steel, the dependence of sonic velocity on strain is such that the summit (see Figure 40a) of either major strain wave propagates at only a fraction of the velocity of the leading edge of the wave. By the time the summit has made one round trip from the aircraft to the fixed end and back, the leading edge will have traversed this path several times. Thus various portions of the wave will be in various stages of reflection, propagating in opposite directions, and superposed on each other, so that the nonuniformity of strain over the length of the cable will be only a fraction of the amplitude of the original wave. An estimate of this effect is readily computed with the aid of a sonic-velocity-versus-strain graph.

It remains to consider the history of the initial transverse wave, because this wave retains its identity as a kink during the early part of the arrest and therefore looms as a potential source of more than one major strain wave. The initial kink generates one major strain wave when it reaches the fixed end; when it returns to the aircraft, might it still have sufficient potency to generate another major strain wave? To answer this question, the stability of kinks must be examined.

A transverse wave can propagate stably as a kink when in, or when encountering, a wave of decreasing tension. In the latter instance there would be a transverse reflection and the kink angle would increase, yet the kink would be stable. But a transverse wave encountering continuously increasing strain would be unstable as a kink because, if the transverse wave is dispersed slightly,

the trailing part would be in a region of lower tension and so would fall further behind rather than catch up. In this instance the total angle of the transverse wave would decrease as reflection progresses.

In view of the continuous nature of the strain waves, it is apparent that the transverse wave will alternately disperse and condense (and at the same time dwindle and grow, respectively). But it would require an ideal set of circumstances for a kink to disperse and then condense back into a single kink. Before condensation is completed, further dispersion will generally occur. Since the strain is predominantly increasing, all transverse waves will predominantly disperse and dwindle.

Thus the nonuniformity of strain distribution generated by the interaction of the first kink against the fixed end may be regarded as a generous upper bound on strain nonuniformity originating from transverse waves. Note that, even before the first kink reaches the fixed end, it will encounter the reflection of the first major strain wave and will become a well distributed transverse wave by the time it reaches the fixed end. By the time it reflects back to the aircraft, its effects can be regarded as minor.

In view of the foregoing discussion, the steps in design of an arresting system comprised of a fixed-end energy-absorbing cable can be enumerated as follows:

1. Choose a maximum design strain safely below the ultimate strain of the energy-absorbing material.
2. Compute the cross-section of the cable.
3. Compute the strain and kink produced by the aircraft impact.
4. Make a preliminary estimate of the final amount of nonuniformity of strain distribution. Subtract half this estimate from the design strain

to get the final average strain. Compare the strain energy at this strain with the aircraft energy and compute the required length of cable. This preliminary design can now be evaluated, after which the preliminary estimate of nonuniformity can be revised if necessary.

5. Compute the rate of unloading due to aircraft deceleration. Compute the resulting decrease in the magnitude of the initial strain wave to the time its (now reduced) summit reaches the fixed end.
6. Compute the approximate strain when the first kink is about to reach the fixed end. Compute the additional strain produced by reflection of the kink from the fixed end.
7. Compute the approximate lengths of the two major strain waves at completion of the arrest. Compare each with the length of the cable to determine what fraction of each wave can contribute to final nonuniformity of strain distribution.
8. Compare the total final nonuniformity of strain distribution with the preliminary estimate of Step 4 and revise the latter if necessary.

A numerical example will now be given to illustrate a procedure by which the foregoing computations can be executed.

Suppose a fixed-ended 7 x 19 cable of fully annealed stainless steel is to be designed to arrest a 40,000-pound aircraft engaging at 675 ft/sec with a maximum permissible deceleration of 9g. Figure 25 gives curves for wave velocities in this material, Figure 27 gives a curve for particle velocity, and Figure 24 gives the tension-strain curve for a cross section of 2.61 in².

In view of the ultimate strain of 0.50 for this material, the maximum working strain or design strain may be chosen as 0.40.

With a 9g limit on aircraft deceleration, the force must not exceed 360,000 lb, which limits each side of the deck pendant to 180,000 lb. According to Figure 24, a tension of 180,000 lb will develop at 0.40 strain if the total steel area in the cross section is $2.61 \frac{180,000}{239,000} = 1.96 \text{ in}^2$; this size section should be used. Then the elastic modulus $AE_e = 15,700,000 \text{ lb}$ and the elastic wave velocity $c_e = 8690 \text{ ft/sec}$.

From the graphs of material properties and the formulas of Section 4.1.2.2, it is found that an impact at 675 ft/sec produces a strain of 0.178, a kink of 45.9° , and a tension of 155,000 lb. The kink travels at 930 ft/sec within the strain wave where the strain is 0.163. The initial summit (0.178) of the strain wave propagates at 890 ft/sec.

As a preliminary estimate, assume that 0.16 will be the final nonuniformity of strain. Then the final strain distribution will vary from 0.40 down to 0.24, with a probable average of about 0.32. According to Figure 24 the strain energy is $61,200 \frac{1.96}{2.61} = 46,000 \text{ ft-lb/ft}$ at 0.32 strain. Since the kinetic energy of the aircraft is $\frac{1}{2} \frac{40,000}{32.2} 675^2 = 283,000,000 \text{ ft-lb}$, the required length of cable is $\frac{283,000,000}{46,000} = 6150 \text{ ft}$. There will be about 3075 ft of cable on either side of the aircraft.

The initial deceleration of the aircraft will be $\frac{2 (155,000) \sin 45.9^\circ}{40,000/32.2} = 179 \text{ ft/sec}^2$ which, according to Section 4.1.7.2, will unload the cable strain at an initial rate of $\frac{179}{8690} \sin 45.9^\circ = 0.0148/\text{sec}$ and the tension will begin to unload at a rate of $0.0148 (15,700,000) = 232,000 \text{ lb/sec}$. As deceleration continues, all three rates will diminish roughly exponentially with a decay time of

$\frac{40,000 (8690)}{2(32.2) 15,700,000 \sin^2 45.9^\circ} = 0.667$ sec until the leading edge of the reflection of the initial tension wave returns to the aircraft about 2.1 sec after impact. The average summit velocity will be about 950 ft/sec, so from Section 4.1.9 both unloading rates are reduced upon interaction by the factor $\frac{2}{1 + \frac{8690}{950}} = 0.197$

while the summit strain will decay at the rate of $\frac{2}{1 + \frac{950}{8690}} (0.0148) = 0.0267/\text{sec.}$

In passing over the kink this rate will be reduced, according to Reference 2, by

the factor $\frac{2}{\sqrt{\frac{15,700,000}{155,000} \frac{1 - \cos 45.9^\circ}{2} + 1 + \cos 45.9^\circ}} = 0.62$ so that the net

rate of summit decay will be $0.0267 (0.62) = 0.0166/\text{sec}$ while the summit is ahead of the kink. Actually, the summit begins behind the kink, catches it after $\frac{0.178 - 0.163}{0.0267} = 0.56$ sec., then falls permanently behind the kink when the first reflection from the fixed end passes it at about $2.1/2 = 1.05$ sec. The summit will average about 950 ft/sec for the first 1.05 sec, then slow to about 750 ft/sec, reaching the fixed end (under superposed reflections) after $1.05 + \frac{3075 - 950(1.05)}{750} =$

3.82 sec. Neglecting the short-lived situation in which unloading waves must pass through the kink to reach the summit, the approximate magnitude of the summit upon reaching the fixed end will be $0.178 - 0.0267 \left[0.667 + (3.82 - 2.1) \right] = 0.114$ (Since aircraft deceleration acquires fresh vigor upon feeling the reflection of the major strain wave, it is assumed not to decay).

The kink will travel at an average velocity of about 1000 ft/sec after it meets the first tension reflection from the fixed end. Thus the kink will reach the fixed end after $1.05 + \frac{3075 - 950(1.05)}{1000} = 3.15$ sec. At this time the part

of the strain wave just arriving at the fixed end is that part whose initial velocity exceeded that of the 0.114 strain by a ratio of 3.82 to 3.15, and from Figure 25 its velocity is seen to be $\frac{3.82}{3.15}(1080) = 1310$ ft/sec corresponding to a strain of 0.072. The strain level at the fixed end, including all reflections, will be just over double this value or about 0.15. By Section 4.1.3.3, the new strain is found by solving

$$(u_2 - u_1 + c_1^*)^2 = c_1^{*2} + (2c_1^*)^2 - 2(c_1^*)(2c_1^*) \cos 45.9^\circ$$

for u_2 , in which c_1^* and u_1 are based on $\epsilon = 0.15$. Thus

$$\begin{aligned} c_1^* &= 900 \text{ ft/sec} & u_1 &= 256 \text{ ft/sec} \\ u_2 - u_1 &= 440 \text{ ft/sec} & u_2 &= 696 \text{ ft/sec} \end{aligned}$$

Inspection of Figure 25 reveals that no strain is high enough for $u_2 = 696$ ft/sec. The cable would break.

It is also noted from Figure 25 that the strain at time of kink impact would have to be practically down to zero to permit a value of $u_2 - u_1 = 440$ ft/sec. A basic problem with fully annealed stainless steel is that the transverse and strain waves propagate with nearly the same speed at the higher strains, so that the kink reaches the fixed end just when part of the strain wave has reflected and the impact of the large-angle kink is then too severe.

It is concluded that the only practical way to arrest an aircraft at this speed successfully with a fixed-ended rope of fully annealed stainless steel would be to use a configuration such as is shown in Figure 40c. The angle should be such that the initial impact produces the design strain at once. By this scheme a large share of the available strain-energy capacity can be utilized before the damaging kink reaches the fixed end. Also, the kink angle is considerably smaller. The cable length should be such that the aircraft would be arrested by the time the kink reached the fixed end. Some of the aircraft energy would be in the rope as kinetic rather than strain energy at completion of the arrest, but this would actually permit greater efficiency. A special case of this scheme is shown in Figure 41 and analyzed in the next section.

4.2.2 Case II - Energy Absorbing Rope Using a Series of Sheaves *)

At the outset, this system (Figure 41) appears to offer two possible advantages over Case I.

1. Physical arrangement of the cable along and parallel to the runway is possible.
2. Strain distribution in the cable may be more uniformly distributed by means of the sheaves interacting with the transverse waves.

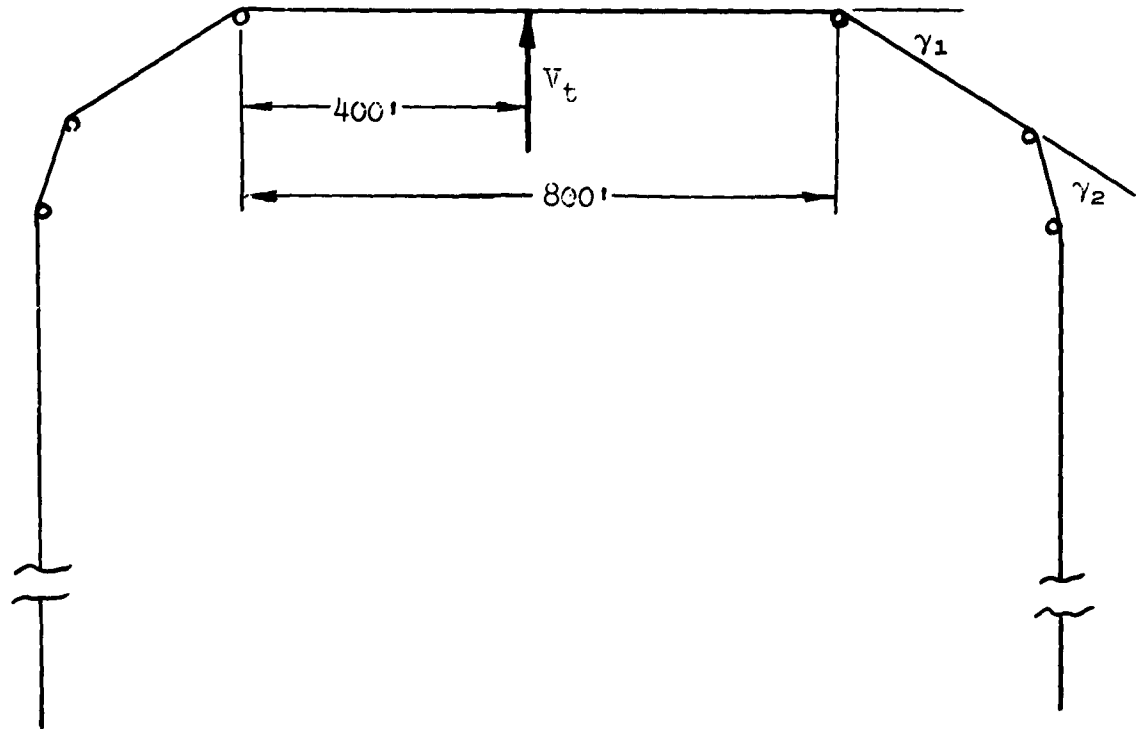
As in Case I the following parameter values will be used:

Plane Weight	= 40,000 pounds
Initial Plane Velocity	= 675 fps
Cable Material	= Stainless Steel
Cable Length	= 6150 ft.
Cable Area	= 1.96 in ²

As shown in Figure 41 the first sheave of the series is arbitrarily placed 400 feet from the point of impact of the hook against the cable. When the kink reaches the first sheave, two possibilities arise. Either the cable may remain in contact with the sheave after the kink reaches it or the cable may disengage from the sheave. Since the second alternative offers the desirable feature of pre-determining the resulting strain by adjusting the angle of wrap γ around the sheave, it is the case of greater interest and therefore will be investigated.

Not knowing at first how rapidly subsequent interactions will build up the level of strain and the rate at which these strains will decelerate the plane, thereby feeding slack into the system, a promising level of strain produced by

*) In all of the interactions subsequent to impact the principle of coincidence as stated in Reference 2 is used in order to facilitate computations.



Material: 7 x 19 Stainless Steel (50%) Cable
 Area of Metal: 1.96 in²
 Total Length of Cable in System: 6150 ft.

Figure 41

Energy Absorbing Rope Using a Series of Sheaves

the kink impact against the first sheave will be selected and the analysis continued on this basis. It is to be noted that the selection of strain at this stage of the analysis is a hit-or-miss situation and not until the analysis is carried further will it be known if the selection was correct. Clearly then the solution for the correct strain level produced by the interaction at the first sheave would involve numerous trials before the correct strain level is found. It will also be observed that a similar situation exists when the second and subsequent sheaves are encountered.

Selecting a level of strain of 35.0% to be produced by the kink impact against the first sheave and using the following input values which are determined by the method of Section 4.1.2.2 for impact

$$\begin{array}{ll} \epsilon = 16.3\% & \epsilon_1 = 17.8\% \\ u = 266 \text{ fps} & u_1 = 2.80 \text{ fps} \\ c = 925 \text{ fps} & \phi_1 = 45^\circ 41' \end{array}$$

the required angle of cable wrap can be determined. Using the method of Section 4.1.4 the angle of wrap of the cable is found to be $\gamma = 49^\circ 50'$. See Figure 42.

Kink K_3 and strain wave S_3 then interact with the hook. Taking into account the deceleration of the aircraft up to the time of the interaction with the hook, the method of Section 4.1.3.3 can be used. Figure 42 shows the resulting situation. The strain produced by the interaction is 35.4%. The small change in strain levels means that there is for all practical purposes no strain wave resulting from the interaction. Also the emerging kink is rather small being only 6.5° .

The deceleration of the aircraft up to the time of interaction of K_3 and S_3 at the hook is approximately 5.5 times that of gravity due only to energy absorp-

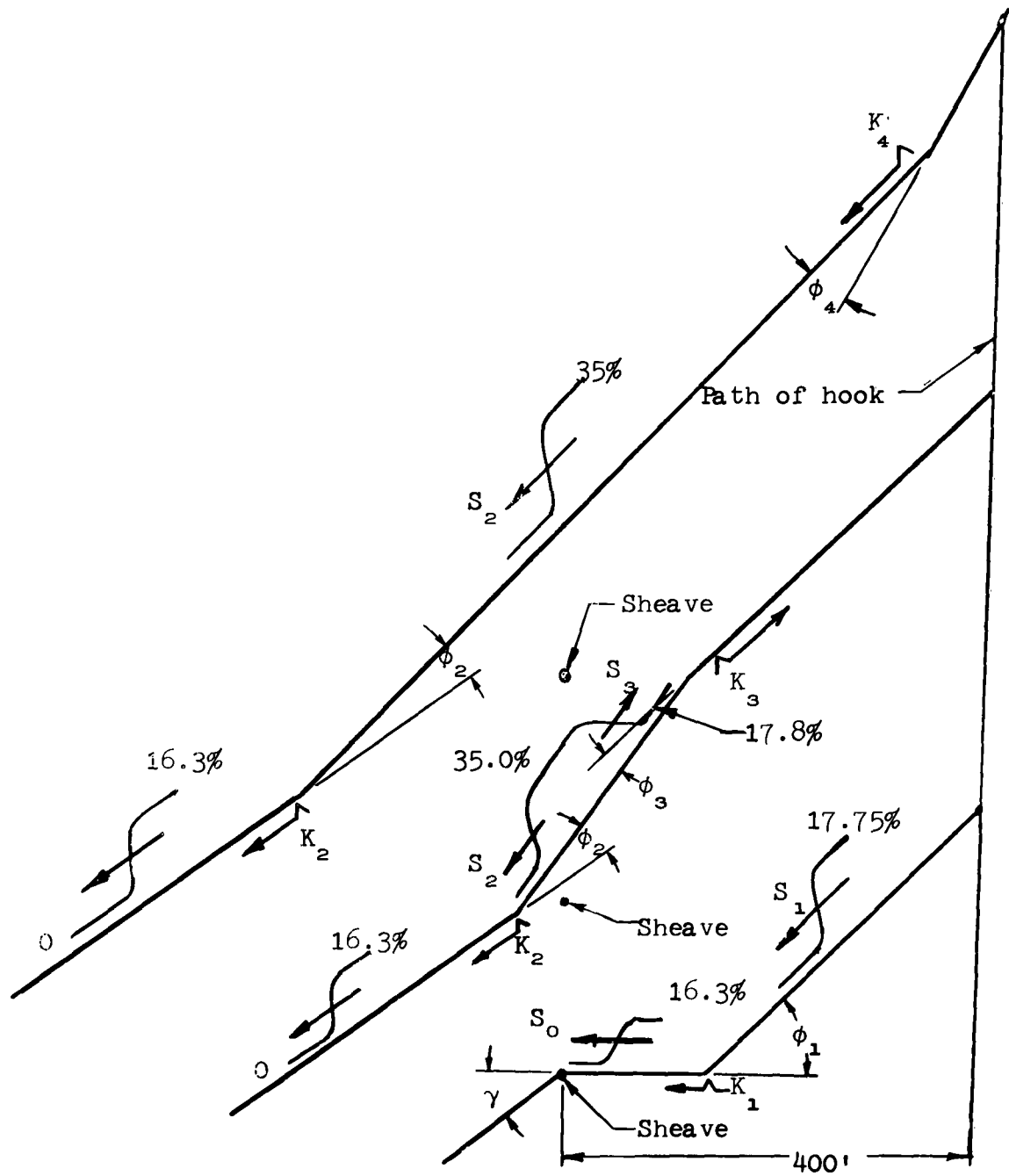


Figure 42

Sequence of Interactions for Case II

tion by strain placed in the cable. Additional kinetic energy of the aircraft will have been converted to kinetic of the cable and hence the aircraft velocity will be significantly lower than 490 feet per second.

The fact that the 35.0% strain is now essentially uniformly distributed from the hook out to the location of the S_2 wave front ensures a continued smooth deceleration of the aircraft at a slightly higher rate than before the interaction at the hook. If, after further deceleration of the aircraft and resulting slack feed into the system, it becomes necessary to raise the strain level, kink K_2 can be allowed to interact with a sheave at some later instant.

Clearly the above procedure is a very promising method for arrestment of high-speed aircraft. With several trial-and-error solutions similar to that presented above, an optimum location and angle of wrap for the first and any subsequent sheaves could be established such that an essentially uniform strain level equal to the working strain of the material would be attained. Hence very practical use of the energy-absorbing material would be achieved.

4.2.3 Case III - Energy-Absorbing Cable in Water Trough

In Section 4.2.1 it was found that an arresting system comprised simply of an energy-absorbing cable between fixed ends is inefficient. Strain decay due to aircraft deceleration results in continuous reduction of cable tension and aircraft deceleration. One way to compensate for this effect of aircraft deceleration was examined in Section 4.2.2.

Another way to compensate for aircraft deceleration is to submerge the cable in a water trough of suitably varying depth, as shown in Figure 43. Part of the

cable will be in longitudinal motion through the water, and part will be in transverse motion. Although only a short length will be in transverse motion, the transverse drag coefficient and the transverse velocity are far greater than their longitudinal counterparts. Therefore the effects of both transverse and longitudinal motion will be investigated.

The exact equation for longitudinal motion of a cable through a still fluid is

$$\mu \frac{\partial u}{\partial t} + \frac{\partial T}{\partial x} + \frac{1}{2} c_D (\pi d) \rho u |u| = 0$$

Since $u \geq 0$ in this application, the equation may be written as

$$\mu \frac{\partial u}{\partial t} + \frac{\partial T}{\partial x} + \frac{1}{2} c_D (\pi d) \rho u^2 = 0 \quad (4.9)$$

where

- u = cable particle velocity toward hook
- x = position coordinate along cable away from hook
- T = cable tension
- ρ = mass density of fluid

No analytic solution to Equation (4.9) is available.

However, an estimate of the longitudinal drag force can be made if we temporarily neglect the reduction of u due to reflection from the drag. This reduction cannot proceed much faster than the deceleration of the aircraft, or the cable would break between the aircraft and the kink. Neglecting this reduction, we find that the longitudinal drag is

$$\frac{1}{2} c_D (\pi d) \rho \int_{c_t}^{c_t} u^2 dx$$

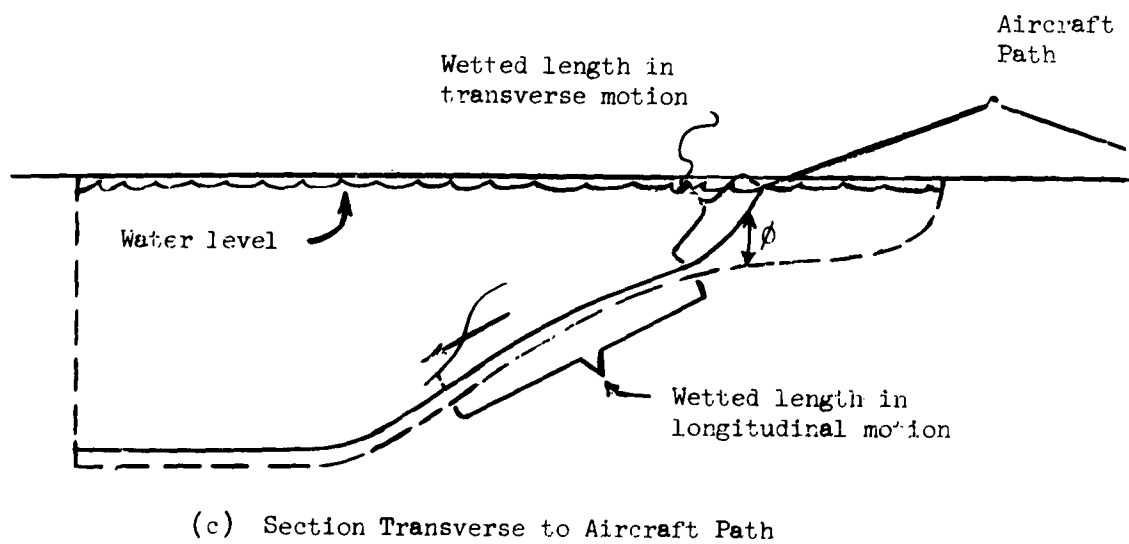
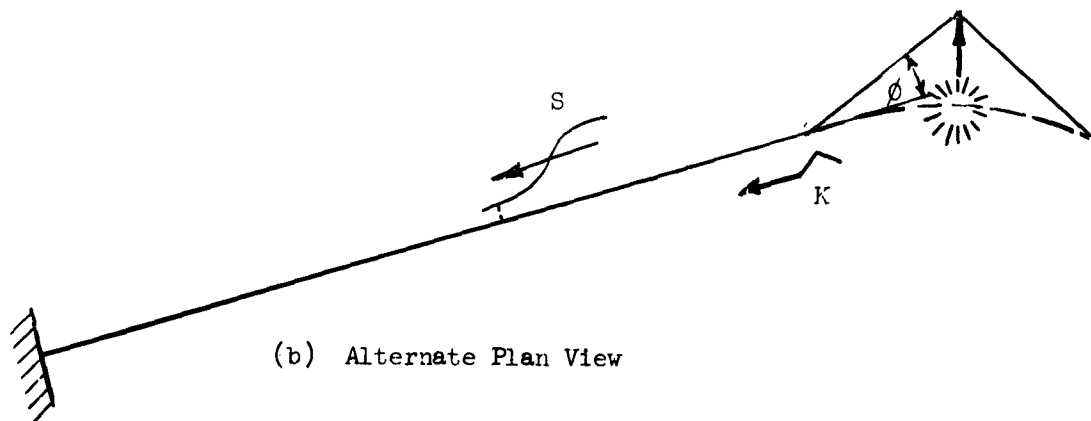
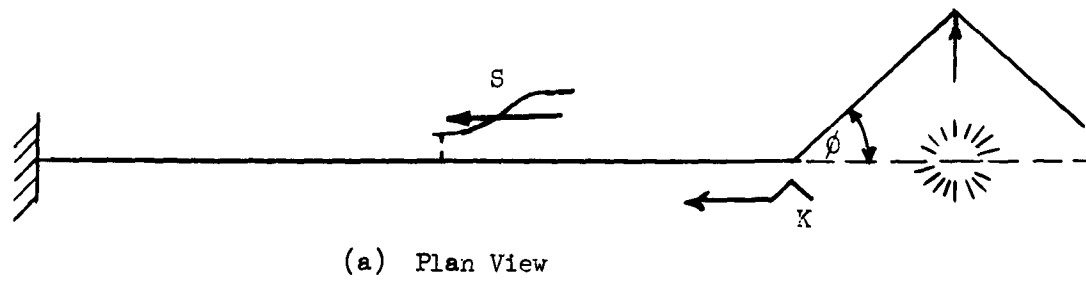


Figure 43

System Using Water Troughs

The lower limit of the integral indicates that, behind the kink, the cable is not in the water. Numerical integration based on Figures 25 and 26 shows that, for 7 x 19 stainless-steel rope,

$$\frac{1}{t} \int_{c \cdot t}^{c \cdot t} u^2 dx = 63,000,000 \text{ ft}^3/\text{sec}^3$$

with

$$c_D = 0.0135 \text{ (estimate based on limited data)}$$

$$d = 0.17 \text{ ft (corresponding to } 1.96 \text{ in}^2 \text{ metal area)}$$

$$\rho = 1.94 \text{ slugs/ft}^3 \text{ (for water)}$$

longitudinal drag develops at the rate of

$$\frac{1}{2} (0.0135) \pi (0.17) 1.94 (63,000,000) = 441,000 \text{ lb/sec}$$

until the leading edge of the strain wave reaches the fixed end. With a 40,000-lb aircraft at 675 ft/sec as in Section 4.2.1, and with the arrangement indicated in Figure 43a, about 3075 ft. of cable on each side of the runway would be required to absorb the kinetic energy of the aircraft (the energy absorbed by water is estimated to be less than 5% of the total, and is neglected). Thus the strain wave reaches the fixed end after $\frac{3075}{8690} = 0.354 \text{ sec}$, at which time the drag is $441,000 (0.354) = 156,000 \text{ lb}$.

As this drag force develops, approximately half of it serves to reduce the tension propagating ahead of it, while the other half is reflected back toward the hook. Thus, tension in the deck pendant would grow at the rate of 220,000 lb/sec due to longitudinal drag. But, according to Section 4.2.1, unloading due to

aircraft deceleration proceeds at the rate of 232,000 lb/sec. Therefore the deck-pendant tension remains nearly constant during the first 0.85 sec (it takes this long for the reflection from the fixed end, which essentially eliminates longitudinal motion, to reach the neighborhood of the kink and effectuate a substantial decrease in drag).

As the reflection from the fixed end passes the kink and eliminates much of the longitudinal drag, the reflection itself increases the deck-pendant tension and thereby compensates for further aircraft deceleration up to perhaps 1.5 sec after engagement. From 1.5 sec until the kink reaches the fixed end at 3.15 sec, there is nothing but transverse drag to compensate for tension decay due to aircraft deceleration.

Transverse velocity of the cable is approximately equal to aircraft velocity. Therefore the transverse drag is

$$\frac{1}{2} c_D (\pi d) l \rho v^2$$

where

$$c_D = 0.8 \text{ (estimate for transverse motion)}$$

$$l = \text{wetted length in transverse motion, projected normal to motion.}$$

Clearly l will be proportional to the depth of the trough. If we assume the kink angle in the trough (Figure 43c) to be equal to the kink angle ϕ in the plan view (Figure 43a), then the required depth is $l \tan \phi$ (not $l \sin \phi$, because l is the horizontal component of the actual wetted length). It remains to determine the l required for a desired drag force.

From 1.5 sec to 3.15 sec, the tension would decay perhaps 70,000 lb due to aircraft deceleration (the rate is less than the initial 232,000 lb/sec, because the aircraft is now much slower, making the cable orientation smaller at the hook). To compensate for this decay, a drag of 140,000 lb is needed because only half the drag is reflected. When the aircraft has slowed to 100 ft/sec, the required l is

$$l = \frac{2(140,000)}{0.8 \frac{(0.17)}{1.94} (100)^2} = 33.7 \text{ ft}$$

and if the kink angle is still 45.9° the required depth of the trough would be

$$33.7 \tan 45.9^\circ = 34.8 \text{ ft}$$

While this seems somewhat deep, it should be noted that full compensation for decelerative decay can be furnished down to 200 ft/sec with a trough depth of only 8.7 ft.

All computed drag forces compare favorably with the 180,000 lb which the cable can sustain at the design strain of 0.40. For other cable sizes, however, the drag force varies only as cable diameter while tension must vary as cable area; this would increase the relative magnitude of the drag forces on smaller cables.

4.3 Conclusion

A fixed-end energy-absorbing rope is feasible for arresting high-speed aircraft if the cable is so arranged that the design strain of the cable is reached during the early part of the first transit of the strain wave. A possible arrangement is shown in Figure 40(c), with the cable forming an angle at midspan. In actual practice the cable could be arranged in a straight or curved line across the runway to facilitate engagement. The angle between the aircraft path and the major portions of the cable should be made equal to that angle which would be required (according to Equation 4.7 or 4.8) to produce the design strain upon an oblique impact.

This arrangement can be refined with a series of sheaves (Figure 41) so arranged as to compensate for aircraft deceleration and thereby maintain approximately the design strain. With this refinement the final strain distribution will be comparatively uniform so that the energy-absorbing material is more economically utilized.

Submerging a fixed-end energy-absorbing rope in a water trough of suitably varying depth appears to be a feasible way of maintaining nearly uniform strain through most of the arrestment. However, experiments are needed to determine whether the effects which were assumed in Section 4.2.3 to predominate are truly the major effects in this type of arresting system.

Of the three cable arrangements considered, the energy-absorbing rope using a series of sheaves appears the most attractive because of its simplicity of operation and economical use of the energy-absorbing material.

REFERENCES

1. ASD TN 61-66, An Investigation of the Materials and Constructions of Tension Members For Use in Aircraft Arrestment Equipment, American Machine & Foundry Company, February 1961, Hausknecht, Kessler and Darienzo.
2. WADC TR 58-217, ASTIA Document No. AD 155542, An Analytical Approach to the Alleviation of Dynamic Tensions in Aircraft Arresting Gear Cables, American Machine & Foundry Company, May 1958, Neidhardt, Eslinger and Sasaki.
3. WADD TN 60-151, Tests of Major Components of an Arresting Cable "Pop-Up" System, Research, Incorporated, May 1960, J. A. Zdrazil.